University of Naples Federico II

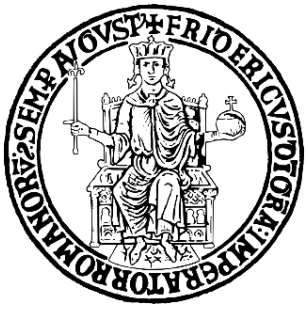

Sustainable PVA-based packaging films with starch and zeolite additives

Mattia Fornaro

PhD in Industrial Product and Process Engineering (XXXVIII Cycle)

Department of Chemical, Materials and Production Engineering

PhD Supervisors: Prof. Domenico Caputo

Prof. Barbara Liguori

PhD Coordinator: Prof. Andrea D'Anna

Abstract

Conventional polyolefin-based packaging films provide excellent mechanical strength and moisture barrier, but their fossil origin and persistence in the environment are increasingly incompatible with the transition toward a circular packaging economy. In parallel, the European Packaging and Packaging Waste Regulation (PPWR) is pushing the development of structures that are recyclable, material-efficient, and, where appropriate, biodegradable. In this framework, water-soluble poly(vinyl alcohol) (PVA) is an attractive candidate for thin functional layers thanks to its excellent film-forming ability, high dry oxygen barrier, and intrinsic biodegradability, but it remains limited by moisture sensitivity and by the need to tailor its end-of-life in real environments. At the same time, inorganic fillers such as zeolites and bio-based polymers such as starch offer opportunities to tune functional performance and environmental fate.

This dissertation investigates the combined effect of starch and synthetic zeolites (types 4A and 13X) on the properties and soil biodegradation of thin PVA-based films prepared from aqueous formulations by rod coating. First, the formulation and processing window required to obtain defect-free, highly transparent films with a homogeneous zeolite distribution was established, using an ATR-FTIR “up–down surface” method to monitor additive sedimentation during drying. Two families of films were then produced at constant overall polymer concentration (20% w/v): (i) plasticized PVA films (20P) and their zeolite-filled counterparts, and (ii) PVA/starch blend films (18P/2S) with and without embedded zeolites at 2 and 4 wt% with respect to total polymer. The pristine films were characterized in terms of surface morphology (optical microscopy and SEM), thermal stability (TGA/DTG), degree of crystallinity (XRD), water uptake, and water vapour transmission rate (WVTR). The environmental behaviour of the films was assessed by soil burial tests in a controlled, highly moist soil at 30 °C for 16 weeks. At each unburial, weight loss, surface morphology, and ATR-FTIR spectra were collected, while XRD was used to compare crystallinity before and after burial. Finally, the metabolic activity of the soil microbiota was quantified by an AlamarBlue® assay on liquid extracts of the test soils and appropriate references.

The results show that the optimized 18P/2S formulations allow for industrially relevant rod-coating viscosities and, when dried at 105 °C, yield a nearly uniform zeolite distribution throughout the film thickness. Starch addition and zeolite loading both influence film microstructure: starch introduces additional surface defects but also markedly increases the thermal stability of plasticized PVA, while zeolites—especially type 13X at 4 wt%—further shift the main degradation peak to higher temperatures. All PVA-based films remain highly hydrophilic, with water uptake above 130% and WVTR of the order of 10^3 g m^{-2} d^{-1}, and zeolite addition at the tested loadings has limited impact on moisture barrier.

Under soil burial, neat 20P films undergo primarily an initial loss associated with plasticizer leaching and show limited further mass loss, whereas starch-containing films exhibit significantly higher weight loss and more severe surface erosion, consistent with preferential starch biodegradation and a modest enhancement of PVA degradation. Zeolites do not hinder soil biodegradation; on the contrary, both 4A and 13X slightly increase the overall mass loss, likely by favouring water retention and micro-erosion around filler domains. FTIR and XRD analyses confirm the disappearance of glycerol and starch bands, moderate reduction of PVA crystallinity and the persistence of the inorganic phases. Soil bacterial activity is comparable across all films and higher than in the bare reference soil, essentially reflecting the availability of readily metabolizable carbon.

Overall, the study provides a coherent picture of how starch and zeolite microfillers can be combined with fully hydrolysed PVA to obtain rod-coatable, thin films with tailored thermal response and controlled biodegradation in soil. These results support the future design of PVA-based, zeolite-modified coatings as functional layers in recyclable packaging structures in line with emerging PPWR requirements, and they delineate the key trade-offs and open questions that must be addressed for industrial implementation.

Contents

List of tables

List of figures

List of abbreviations

	Abbreviation	Definition
A	A	Zeolite 4A *(%w/w of polymer blend)*
	ATR	Attenuated total reflectance
D	DI	Deionized
	DTG	Derivative thermogravimetry
F	FAU	Faujasite
	FTIR	Fourier-transform infrared spectroscopy
H	HDPE	High-density polyethylene
L	LDPE	Low-density polyethylene
	LLDPE	Linear low-density polyethylene
	LTA	Linde Type A
M	MW	Molecular weight
O	OTR	Oxygen transmission rate
P	P	Polyvinyl alcohol *(%w/v of formulation)*
	PE	Polyethylene
	PLA	Polylactic acid
	PP	Polypropylene
	PTFE	Polytetrafluoroethylene (Teflon)
	PVA	Polyvinyl alcohol
R	RFU	Relative fluorescence units
	RH	Relative humidity
S	S	Starch *(%w/v of formulation)*
	SEM	Scanning electron microscopy

T	TGA	Thermogravimetric analysis
	$T_{initial}$	Initial degradation temperature
	T_{max}	Peak degradation temperature
	TPS	Thermoplastic starch
V	VOC	Volatile organic compound
W	WU	Water uptake
	WVP	Water vapor permeability
	WVTR	Water vapor transmission rate
X	X	Zeolite 13X *(%w/w of polymer blend)*
	XRD	X-ray diffraction

Introduction

Aim of the work

The overarching motivation of this work arises from the tension between the widespread use of flexible plastic packaging and the urgent need to reconcile performance with environmental sustainability and regulatory compliance. Flexible packages based on polyolefins such as PE and PP currently dominate the market because they combine low cost, processability, and excellent moisture barrier, but they are mainly fossil-based and intrinsically non-biodegradable. At the same time, the emerging European Packaging and Packaging Waste Regulation (PPWR) is reshaping the design space for packaging materials by imposing strict targets on recyclability, material minimisation, and, in selected cases, biodegradability and compostability. In this context, the use of ultra-thin functional coatings deposited from water-based formulations onto recyclable substrates (polyolefin films, paper, and paperboard) is one of the most promising strategies to add specific barrier or active functions while preserving mono-material architectures and the associated recycling routes.

Poly(vinyl alcohol) (PVA) is a key candidate for such coatings. It is a synthetic but water-soluble and ultimately biodegradable polymer, with excellent film-forming ability and outstanding oxygen barrier in the dry state. Its water processability enables the formulation of aqueous coating solutions without organic solvents, which is attractive from both environmental and industrial viewpoints. However, PVA-based films still suffer from intrinsic limitations: sensitivity to humidity, relatively poor water vapour barrier, and an environmental fate that strongly depends on grade, formulation, and disposal conditions. In addition, there is still a limited understanding of how thin PVA-based layers containing functional additives behave when exposed to realistic end-of-life scenarios such as moist soil.

At the same time, there is increasing interest in enriching PVA with bio-based and inorganic additives. Starch is a low-cost, renewable, biodegradable polysaccharide that can be blended with PVA to reduce the share of synthetic polymer, enhance biodegradability, and lower raw-material cost. Synthetic zeolites, on the other hand, are crystalline aluminosilicates with high internal surface area and tunable

adsorption properties. When embedded in polymer matrices, they can act as multi-functional fillers, potentially improving mechanical properties, thermal stability, and gas-barrier properties and serving as carriers of active species for antimicrobial or scavenging functions. Nevertheless, the combined use of starch and zeolites in thin PVA films processed by rod coating has not been systematically explored, especially with a focus on soil biodegradation.

This dissertation, therefore, aims at building a coherent experimental and interpretative framework for thin, water-based PVA films containing starch and zeolite additives, with particular attention to their potential role as functional coatings for sustainable packaging applications.

More specifically, the work pursues the following objectives:

• To design and optimise aqueous PVA-based formulations, with and without starch and synthetic zeolites, that are suitable for laboratory rod coating while being conceptually translatable to industrial coating processes. Particular emphasis is placed on achieving viscosities compatible with Mayer-bar application and on defining drying conditions that avoid severe film/coating defects.

• To develop and validate a rapid, spectroscopy-based methodology to assess the dispersion of micro-zeolite additives across the film thickness, using ATR-FTIR spectra collected on the “air side” and on the “plate side” of the films as a probe of additive sedimentation during film drying and formation.

• To prepare a controlled set of thin films based on a fully hydrolysed (99+%) PVA grade, differing only in the presence and amount of starch (PVA-only versus PVA/starch blend) and in the type and loading of synthetic zeolite (4A or 13X) while keeping the overall polymer concentration and the processing route constant.

• To characterise the pristine films in terms of surface morphology (optical microscopy and SEM), thermal stability (thermogravimetric analysis), crystalline structure (X-ray diffraction), water uptake, and water vapour barrier, in order to quantify the effect of starch and zeolite fillers on key technological properties relevant for packaging.

• To investigate the biodegradation behaviour of the different films in a moist soil environment, through a 3-month burial test at controlled temperature and humidity, monitoring weight loss, evolution of surface defects, chemical-structural changes

(with FTIR), and changes in crystallinity, and to relate these observations to the composition and microstructure of the films.

• To evaluate the response of soil microbiota in contact with the films and with zeolite-rich soils by means of an AlamarBlue® assay, in order to verify that the presence of PVA, starch, and zeolites does not inhibit, and possibly even stimulates, microbial activity under the conditions studied.

• To integrate the collected data into a critical discussion of how starch and zeolite additives influence the trade-off between functional performance (thermal stability, barrier properties) and environmental fate (biodegradation and soil response), and to outline design guidelines for PVA-based coating systems compatible with the PPWR framework.

By addressing these objectives, the thesis aims to clarify the role of starch and zeolite additives in tailoring, both individually and synergically, the properties and soil biodegradation behaviour of thin PVA films obtained by a scalable wet-processing technique. The ultimate goal is to provide scientifically grounded indications for the development of water-based, PVA coatings that could serve as functional layers in recyclable or partially biodegradable packaging laminates, offering an intermediate route between conventional non-biodegradable plastic films and thick, fully biobased alternatives.

Thesis organization

The dissertation is articulated into four main chapters to guide the reader from the general context to the specific experimental work and its implications.

Chapter 1 introduces the scientific and regulatory framework of the thesis. After a general overview of packaging plastics and the dominance of conventional polyolefins, it reviews the main families of biodegradable polymers and focuses on PVA as a water-soluble and biodegradable synthetic polymer of particular interest for packaging. The fundamentals of wet processing of thin polymer layers are summarised, with emphasis on solvent/water-based techniques such as casting and rod (Mayer-bar) coating. A dedicated section discusses the new EU Packaging and Packaging Waste Regulation (PPWR) and its consequences for packaging design, highlighting the opportunity offered by ultra-thin functional coatings on recyclable substrates. The chapter then presents zeolites as microporous aluminosilicate materials, their synthesis, structure and adsorption/ion-exchange properties, and their emerging use as multi-functional additives in polymer matrices. Finally, the mechanisms of polymer biodegradation in soil and the specific case of PVA, as well as the role of typical packaging additives, are reviewed, with a focus on starch and zeolites and on their potential synergistic effects in PVA-based films.

Chapter 2 describes the materials and methods. It details the PVA, glycerol, starch and zeolite grades employed and the preparation of aqueous film-forming formulations, including the definition of plasticiser content. The rod-coating procedure used to cast thin free-standing films and the drying/conditioning conditions are reported. The chapter then presents the characterisation techniques applied to both components and films: FT-IR spectroscopy in ATR and transmission modes, optical microscopy and SEM for surface morphology, thermogravimetric analysis for thermal stability, X-ray diffraction for phase identification and crystallinity, and water uptake and water vapour transmission rate tests for moisture-related properties. The design of soil burial tests is described in detail, together with the unburial protocol and weight-loss evaluation, and the use of the AlamarBlue® assay to assess the metabolic activity of soil bacteria. A final section explains the strategy used to select the optimised formulations and processing

conditions that ensure homogeneous zeolite dispersion, based on ATR-FTIR comparison of the two film faces.

Chapter 3 reports and discusses the experimental results on the final PVA-based films with different additives, object of this dissertation. The first part is devoted to the pristine films, analysing how starch and zeolite additives affect surface morphology, thermal degradation behaviour, crystalline structure, water uptake and water vapour barrier. The second part concentrates on the soil burial tests: it examines the evolution of weight loss and surface defects over 16 weeks, interprets FT-IR spectra to follow the disappearance of glycerol and starch and possible changes in PVA, quantifies changes in crystallinity after burial and discusses the AlamarBlue® assays data in terms of soil microbial activity in contact with the different films and with only zeolite-enriched soils.

Chapter 4 provides the overall conclusions of the work. The main findings are synthesised with reference to the objectives outlined earlier in the previous paragraph, and so the implications for the design of PVA-based, starch- and zeolite-containing films as potential functional coatings for sustainable packaging are discussed. The final part of this chapter includes possible future developments, including the translation of the present free-standing films onto industrial substrates and the exploration of natural or nano-structured zeolites and ion-exchanged systems for advanced active packaging applications.

1. State of the art

1.1 Packaging plastics

Packaging refers to any material used to contain and protect goods, to allow their handling and delivery from the producer to the consumer [1]. Packaging can be classified into primary (enveloping the single product and constituting a single sales unit), secondary (grouping multiple primary sales units), and tertiary (facilitating the handling and transport) [1]. Packaging can be further classified into rigid – thick, with high mechanical protection and strong barrier properties – and flexible – light, thin, and generally cheaper [2]. In 2022, rigid packages led the overall packaging market, whereas flexible packages led the food packaging market, and this latter segment is growing very fast [2,3]. Additionally, there is a strong interest in *active food packaging*, which involves interactions between the package and the internal gas atmosphere or directly with food, in order to extend the shelf life of the goods, inhibit the growth of pathogenic and spoilage microorganisms, prevent the migration of contaminants, and ensure overall food safety [4,5].

Materials that are generally used in packaging include paper/paperboard, plastics, glass, metal, or a combination of these as laminates. The final choice is driven by considering some material properties such as heat sealability, processability, strength, barrier properties (against O_2, water vapor, aromas), and printability, but also a certain inertness to fats, lights, acidic and alkaline media. Other factors include cost-effectiveness and sustainability as well [6,7]. Plastics are the most used materials for packaging, mainly for food and beverage applications. Globally, one-third of the total packaging market is represented by flexible plastics and one-fifth by rigid plastics, followed by paper/paperboard, metal, and glass. Interestingly, relative to the globally produced non-fiber plastics, it is worth noting that around 42% of them are used for packaging purposes – corresponding to more than double the plastics produced for the second biggest consuming sector, which is building and construction. Particularly, more than one-half of the total packaging plastics are destined for food and beverage applications. Plastics can be used as layers (cast or co-extruded) in flexible/rigid polylaminate packages and as flexible self-standing packaging films [2,3,8–10].

Nowadays, interesting sustainable materials are paper and paperboard, employed for rigid and semi-rigid packages, as in 2022 they represented about one-third of the total food packaging market [3]. These cellulosic recyclable materials, made from wood pulp, surely provide containment and protection by offering rigidity; furthermore, they are printable, lightweight, and cheap. However, plain paper alone is not ideal for food products mainly due to its inadequate barrier properties, heat sealability, and strength. To enhance these properties and also bypass their inherent wettability, paper-based packages are generally treated with additives or laminated, mainly with plastics as mentioned above [6,11]. Therefore, plastics (even as thin layers) are usually unavoidable in packaging applications. Enhancing their technological and barrier properties and thus valorizing their life cycle is crucial.

Conventional polyolefins

The largest market shares in packaging materials belong to low-cost, commodity thermoplastic polymers, especially polyolefins, such as polyethylene (PE) and polypropylene (PP). Polyolefins are particularly durable, with strong chemical and biological inertness, because of their high molecular weight, hydrophobicity, and absence of functional reactive groups. Furthermore, their properties can be easily adjusted (with processing and/or additives) to achieve the desired technological properties such as strength, permeability, porosity, opacity, and color [12,13].

PE represents the most produced polymer worldwide, mainly used for several packaging applications [10]. This class of polyolefins is very suitable for food packaging films: it has high processability and provides great water vapor barriers (but low O_2 barrier) [14]. PE needs to be classified into two main different polymeric structures that affect the final film performances: low-density polyethylene (LDPE), with many and long side-chain branches; high-density polyethylene (HDPE), linear with few and short side-chain branches. HDPE has higher crystallinity, better chemical resistance and barrier properties, a higher melting point, greater tensile strength, and hardness, and therefore it is ideal for industrial wrappings and films, mainly in food packaging. LDPE is softer, more flexible, and stretchable, with good clarity and heat sealability but worse oxygen barrier properties: it is a good choice for films (also food, better for bakery,

confectionery, frozen foods), bags and also sealant layers in polylaminate films [14–16]. Then, under the name linear low-density polyethylene (LLDPE), a family of ethylene-based copolymers is represented, consisting of long and linear PE chains with many short side-chain branches of other alkene co-monomers (1-10 mol%): they are excellent sealants with a melting point typically lower than that of LDPE, provided with the strength and toughness comparable to that of HDPE, and so they can be employed as strong bags and shipping sacks, too [14–17]. The structures of LDPE, HDPE, and LLDPE are schematized in Figure 1.1.

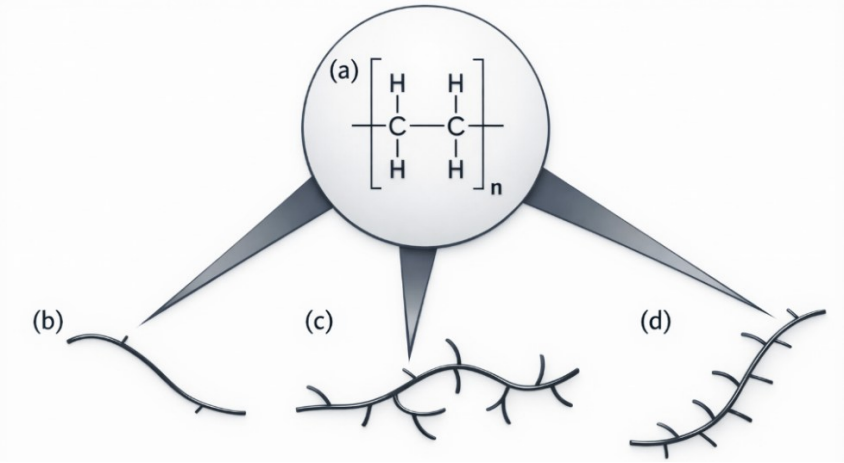

Figure 1.1. Scheme of (a) the repeating unit of PE; schemes of the main molecular structures of PE differing in linearity and branching: (b) HDPE, (c) LDPE, (d) LLDPE.

PP ranks as the second most widely produced polymer, primarily demanded for its applications in packaging [10]. It is semicrystalline, relatively stiff, with high chemical inertness and melting point, has good barrier properties (intermediate to those of LDPE and HDPE), and has high resistance to impacts. PP finds easy applications for both flexible and rigid packaging films in the cosmetics and food industry, including cold-chain food and heat-treated food, such as bakery products. Still, it is often combined with other materials to enhance performance, like gas barrier and heat sealability [14,18–20]. These commodity polymers are conventionally petroleum-based; still, bio-based alternatives exist – with "bio-based" meaning that these polymers can be obtained from either biomass or renewable resources [21]. However, in general, the production of these bio-based alternatives can be considered negligible compared to that of conventional petroleum-based polyolefins [22].

Since conventional petroleum-based polyolefins are strongly spread worldwide for packaging, these polymers – usually produced to be disposable – represent a major type of pollution among all types of plastics, with PE wastes that are a primary aware, mainly for the marine environment [23,24]. Still, mono-material PE and PP flexible packages can be easily and successfully mechanically recycled compared to multi-material polylaminate films [25,26], if end-of-life is correctly managed and a certain waste homogeneity is achieved [27].

Biodegradable bio-based polymers

Some polymers, regardless of their being petroleum- or bio-based, can also be biodegradable, meaning that environmental microorganisms can convert them into natural substances such as CO_2, H_2O, and CH_4, depending on whether the process is aerobic or anaerobic. Factors influencing biodegradation include environmental conditions, the chemistry of the polymer, and its specific application. The compliance with certain biodegradation rates under different specific conditions has to be certified using standardized test methods [28–31]. Some biodegradable polymers can further be classified as compostable, meaning they can fully degrade into the soil as compost according to standards [32]. Not all biodegradable plastics are compostable, as composting is not natural but a human-driven process under optimized conditions [33,34]. PE and PP, due to their chemistry, are not biodegradable [21]. Nevertheless, it is important to disclose that biodegradable polymers – generally protein-based or carbohydrate-based – have low physical barrier properties when compared to conventional petroleum-based polymers (such as PE and PP), and additionally, their sealability (a key step in packaging) is hard to achieve. However, research moves on to functionalizing these materials and valorizing their potential [11].

Polymers like chitosan, polylactic acid (PLA), and thermoplastic starch (TPS) belong to the class of bio-based biodegradable polymers and are of high interest for academic and industrial researchers as they can be potentially used for sustainable packaging applications, both as self-standing films and as coatings [35,36].

Starch is a polysaccharide found in many plants and is composed of two types of biopolymers, namely amylose and amylopectin. Amylose is a linear polymer of D-

anhydroglucose rings with α-1,4 linkages, making up to 15-20% of starch depending on the source, while amylopectin (the main crystalline component, with its clusters of short branches) is a branched polymer with side chains grafted to the linear chain by α-1,6 linkage [37–40]. Native starch, by the addition of plasticizers, can be transformed into thermoplastic starch (TPS), a biodegradable and compostable material. Despite its potential, TPS has limited applications due to high moisture sensitivity and aging issues [37,41–43]. Glycerol is the most widely used plasticizer for thermoplastic starch films. A minimum of 30% glycerol is needed for acceptable mechanical strength and heat sealability [44,45]. Starch is not soluble in water at room temperature: granules swell and form a gel when their outer membrane is broken. After treatment in warm water, however, the soluble part (basically amylose) can diffuse out, with the starch granules that swell and burst; therefore, a certain but limited solubility in water can be achieved [46–49].

PLA is a biodegradable and compostable thermoplastic polyester obtained by polymerization of lactic acid, which can be produced either via carbohydrate fermentation of starch or chemical synthesis [50]. It is provided with excellent thermoforming ability; its films have high mechanical strength, great optical properties and biocompatibility; still, its inherent rigidity and brittleness, along with high water vapor permeability, currently limit neat PLA applications, compared to conventional polyolefins [51–55]. Therefore, in order to improve the technological properties required for packaging applications, the employment of plasticizers is required for PLA to increase flexibility, ductility, and resistance to impacts [56].

Chitosan and chitosan oligomers are polysaccharides extracted from shrimp shells that are receiving much interest thanks to their biocompatibility, antimicrobial activity, and film-forming properties [57–60]. Chitosan films are transparent, possibly strong and flexible, and with low oxygen permeability. These films, however, have a certain permeability to water vapor, and since chitosan is not thermoplastic, it cannot be heat-sealed. Additionally, chitosan is generally obtained by solvent casting from an acid solution, as this polymer is poorly soluble in neutral media, and this may also limit its applications. Furthermore, properties like solubility and final mechanical properties are strongly affected by parameters like molecular weight and degree of deacetylation [61–63].

Nowadays, the majority of the globally produced biodegradable polymers are used for packaging, mostly PLA. It is worth saying that less than 0.3% of globally-produced plastic products are made of biodegradable polymers; still, sensible growth is expected in the next years [22,64].
Particularly, high interest in packaging applications is increasingly being given to polyvinyl alcohol due to its outstanding properties, despite its non-bio-based origin.

Polyvinyl alcohol

Polyvinyl alcohol (PVA) is a synthetic polymer distinguished by its water solubility and biodegradability – a rare combination for a vinyl polymer [65–68]. PVA is produced on a large scale and finds use in diverse sectors, including textiles, paper, construction, and especially packaging [69]. In the packaging industry, PVA has gained attention as an eco-friendly material due to its excellent film-forming ability, transparency, and gas barrier properties [70,71].
Chemically, PVA is a polymer composed of repeating vinyl alcohol units with the idealized formula $[–CH_2–CH(OH)–]_n$. In practice, pure vinyl alcohol monomer cannot be directly polymerized (as it tautomerizes to acetaldehyde), so PVA is manufactured by a two-step process. First, vinyl acetate monomer is polymerized to poly(vinyl acetate), and then the acetate groups are hydrolyzed (saponified) to hydroxyl groups to yield poly(vinyl alcohol) [66,72,73]. The extent of this hydrolysis can be controlled, producing grades of PVA that are partially hydrolyzed (with some residual acetate groups) or fully hydrolyzed (with >98–99% of acetate groups converted to alcohol) [66,74]. The scheme of the molecular formulas for both PVA and its precursor is reported in Figure 1.2. The degree of hydrolysis (DH) can be expressed as $DH = \frac{n}{n+m}\%$, with n and m being the average numbers respectively of new alcoholic groups and of residual acetate groups in PVA [75].
The polymer backbone of PVA is carbon-only (a saturated C–C chain with pendant –OH groups) and largely atactic in configuration. Despite the atacticity, PVA can crystallize due to regular hydrogen bonding between –OH groups [65,76]. This polymer exhibits a suite of useful properties – it is a tasteless, odorless, nontoxic polymer that forms clear, flexible films with high tensile strength. Many of these

properties can be tuned by adjusting the polymer's degree of hydrolysis and molecular weight, as discussed hereafter [66,76].

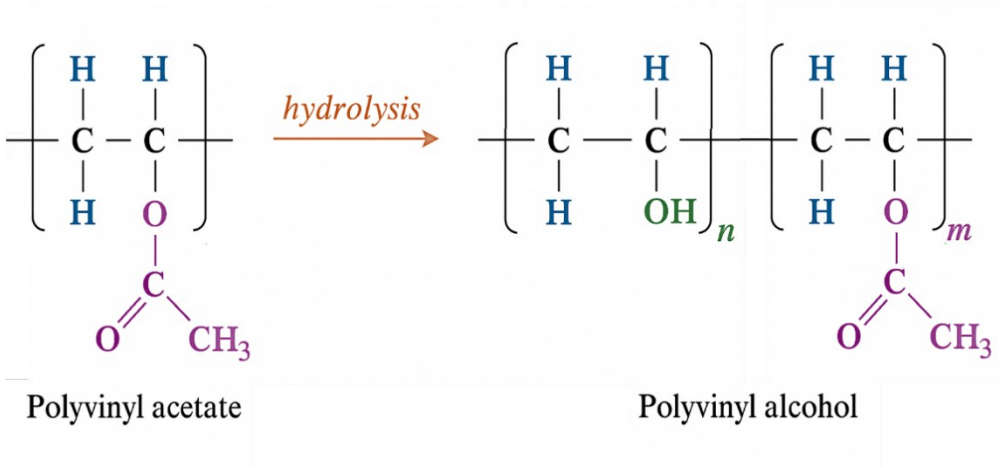

Figure 1.2. Representation of vinyl and alcoholic groups in PVA and its precursor.

The proportion of hydroxyl groups versus residual acetate groups profoundly influences PVA behavior. Fully hydrolyzed PVA (typically 98–99+% OH) has very strong intermolecular hydrogen bonding. As a result, it has a higher degree of crystallinity and is less water-soluble at room temperature – it will only dissolve in hot water (80 °C or above) [66,77,78]. Its melting point is also higher (around 230 °C for fully hydrolyzed grades) compared to partially hydrolyzed grades (180–190 °C) [76,77]. Fully hydrolyzed PVA films are relatively more rigid, with excellent oxygen and aroma barrier properties in dry conditions due to the dense hydrogen-bonded network. They also resist humidity and water to a greater extent; in fact, water resistance increases as the degree of hydrolysis increases [70,74,79]. These super-hydrolyzed grades are chosen when minimal water sensitivity is required.

By contrast, partially hydrolyzed PVA (e.g., 85–90% hydrolyzed) contains enough hydrophobic acetyl groups to disrupt some crystallinity and hydrogen bonding. This makes it more flexible and dramatically increases cold-water solubility [80]. In practice, PVA film used for quick-dissolving applications (such as detergent pods) is often 85–90% hydrolyzed, resulting in being strong in storage yet fully soluble even in cold water [66,81]. The retained acetate groups also make partially hydrolyzed PVA more adhesive to hydrophobic surfaces (useful in coatings or adhesives) [73]. However, partial hydrolysis increases the polymer's affinity for

moisture; water acts as a plasticizer, reducing tensile strength but increasing elongation and tear resistance when humidity is high [70]. Thus, partially hydrolyzed PVA grades are more flexible and easier to dissolve or process, but are less crystalline and have lower heat resistance and barrier performance than fully hydrolyzed grades [82].

The chain length (molecular weight) of PVA affects solution viscosity, film strength, and biodegradation [79,80,83,84]. Higher molecular weight PVA yields more viscous solutions (at a given concentration) and generally stronger, tougher films due to longer entangled chains [66,67,74,85]. For example, PVA with a high degree of polymerization forms very robust films and is often used when high mechanical strength is needed [86]. Lower molecular weight is much easier to dissolve and handle, but produces films of lower strength [66,87].

Molecular weight also influences biodegradation: shorter PVA chains are more readily metabolized by microbes, whereas extremely high molecular weight or highly crystalline PVA may degrade more slowly [65,84,88,89]. Chemically, the multitude of –OH groups makes PVA highly polar and capable of forming hydrogen bonds. This not only aids film formation and adhesion, but also gives PVA excellent resistance to oils, greases, and many organic solvents [66,90]. PVA is also intrinsically transparent and has no odor, and it is considered biocompatible and safe enough for food and pharmaceutical use [72,86,91,92]. These characteristics, combined with the tunability of water sensitivity, make PVA a unique polymer for packaging.

PVA is used in food packaging, often in a blend or coating form. PVA's high tensile strength and flexibility are attractive for load stabilization or wrapping. While not common yet (due to moisture sensitivity), research has looked at PVA blended films as sustainable alternatives to PE stretch wrap, especially for applications where the wrap can be dissolved off [93]. Pure PVA film by itself has the drawback of being water-sensitive (which is problematic for moist or liquid foods), but it boasts excellent oxygen barrier properties when dry. This has led to its use as an inner coating or barrier layer on multilayer food packaging films – for example, a thin coating of PVA on a biodegradable PLA film [70,94,95]. PVA is also utilized in edible packaging research: it can form edible films when mixed with plasticizers

and food polymers (though PVA itself is not digestible, it is at least safe if ingested in small quantities). However, regulatory approval may be needed depending on the region and PVA content for direct food contact use in edible form [81,91,92].

Wet processing of thin layers

Packaging applications often rely on polymer films or coatings to provide barriers, adhesives, and other functional layers. Unlike melt-processing, wet processing involves applying polymers from a liquid medium (solution or dispersion) onto a substrate and drying to form a solid film. This approach is common for coating paper, plastic, or foil in packaging to impart properties like moisture/oxygen barrier or sealability [96,97]. As the packaging industry moves toward sustainability, water-based formulation coatings are increasingly favored for applications like paperboard barriers, biodegradable packaging films, and sealable layers. PVA, being water-soluble, exemplifies both the strength and weakness of solution-based coatings: excellent dry oxygen barrier but humidity sensitivity, often remedied through multilayer designs [70,98]. Because fully hydrolyzed PVA dissolves rather than forms a stable latex, PVA is typically applied from aqueous solution; packaging practice often pairs an inner PVA barrier with a more hydrophobic overcoat for moisture protection [98,99]. For PVA specifically, solution-cast films exhibit exceptionally low OTR in dry conditions, with barrier depending strongly on crystallinity and degrading with humidity [70]. Wet processes range from small-scale laboratory methods to high-speed industrial coating techniques. Researchers have developed various lab techniques to create thin polymer films or coatings from liquid formulations, depending on the viscosity.

Solution casting (also called solvent casting) is one of the oldest and simplest wet processing techniques for polymers [100,101]. A polymer is dissolved in a solvent (aqueous or organic), and according to the viscosity of the film-forming formulation the process might involve pouring it into a Petri dish or onto a support substrate (such as PTFE) to form free-standing films after drying and peeling-off – or simply casting onto a test substrate like paperboard or aluminium foil for coating [102–104]. Indeed, as the solvent evaporates, polymer chains that were mixed in solution entangle into a continuous solid layer. The resulting film (if dried properly) is

typically homogeneous [97,102,105]. A great advantage is that solution casting does not require high temperatures, so it can be used for polymers that degrade upon heating [100]. Despite its simplicity, solution casting can be slow (depending on the amount of solvent to be evaporated) and sensitive to drying defects [105]. Thick single coats often develop drying stresses and may require replacing them with multiple thin layers; solvent handling raises flammability/VOC issues when organic solvents are used [100,106,107]. High-MW polymers may be difficult to dissolve at useful solids, driving viscosity too high for practical casting [104,108,109]. In general, solution casting is widely used in academia for characterizing polymer blends or composites, particularly to develop biodegradable films and coatings [97,102,110,111].

In spin coating, a small volume of polymer solution is deposited on a substrate, which is then rapidly spun. Centrifugal force spreads the liquid into a thin, uniform film [112]. However, it is not practical for large-area packaging films and surely not scalable at industrial levels [101,106,113]. In dip coating, a substrate is dipped into a polymer solution/dispersion and withdrawn, leaving a wet film that dries into a coating [114]. In spray coating, a polymer solution or latex is sprayed (e.g., with a nebulizer) onto a substrate, depositing a thin layer. Spray coating can cover large areas and irregular shapes [115]. For both of the last two methods, however, limited control on final thickness is achieved [106,116]. Doctor blade coating, also known as knife coating, uses a fixed-gap blade to spread a wet film of polymer solution on a substrate. By adjusting the blade height, a controlled thickness is obtained [101,113,117].

In Mayer rod (bar) coating, a wire-wound metal rod is drawn across the substrate, distributing the liquid into a thin wet film. Mayer rod coating is widely used in lab settings because it is simple, reproducible, with minimal equipment, good width uniformity, and easy thickness adjustment (by swapping rods with different wire sizes that control the wet thickness). It is also readily translatable to industrial continuous lines because the metering mechanism is the same. It is commonly used for solution/emulsion formulations (mainly adhesives), but generally limited to lower-viscosity formulations [96,113]. Solvent evaporation rate, sensitivity to viscosity, and surface tension are key parameters to consider for high-quality

coatings/films [105,118]. Generally, this method is extremely common in lab settings for reproducibly coating papers, films, or glass with polymer solutions or dispersions, obtaining thin polymer layers [96,106,119].
These simple wet-processing lab methods allow screening polymer formulations and are relatively low-cost, even if with slow production. On the other side, on an industrial level, continuous roll-to-roll coating techniques are employed to process packaging materials at high speeds (often 100-500 m/min or more) [106,118].

Processing PVA into usable forms can be done via wet or dry (melt) methods, with some special considerations due to its water sensitivity and thermal behavior. The most common approach for making PVA films is the wet processing, with the methods described earlier. Because PVA readily dissolves in water (especially if heated and for partially hydrolyzed grades), aqueous solutions can be prepared and then cast onto a surface and dried to form a film [80]. This method yields clear, uniform films and is also used industrially. Manufacturers often sell PVA as a dry powder/granulate that the end user dissolves at ~90 °C to make a 5–20% solution for casting or coating. Wet processing is also employed as it allows for to easy combination of PVA with other additives/polymers to create blend films or coatings [120]. While solution casting is prevalent, melt processing of PVA is possible under controlled conditions. Pure dry PVA has a tendency to thermally degrade around its melting point, but adding plasticizers or residual moisture can facilitate melt extrusion or injection molding at lower temperatures [121].

Implications of the PPWR

The European Union's Packaging and Packaging Waste Regulation (PPWR) represents a comprehensive overhaul of packaging legislation, aiming to drive a circular and sustainable economy for packaging. Adopted in late 2024 and entering into force in 2025, the PPWR replaces the older Packaging Waste Directive and sets ambitious targets across the packaging lifecycle [122,123]. Its core objectives include making all packaging recyclable in an economically viable way by 2030, increasing the use of recycled materials, and reducing dependence on virgin resources [124,125]. In practice, this means that by 2030 no packaging can be placed on the EU market unless it achieves at least 70% recyclability (a threshold

below which it would be barred) [126,127]. At the same time, packaging must be designed to minimize material volume and weight to the essential amount needed for functionality. This “minimal packaging” requirement is meant to eliminate excessive or overly thick packaging, aligning with the PPWR’s “Reuse – Reduce – Recycle” spirit [122]. Beyond recyclability and reduction, the regulation introduces new recycled-content mandates (for example, certain plastic packaging must contain 30% recycled polymer by 2030), reuse and refill targets for specific sectors, and bans on select single-use formats (such as small condiment sachets and certain single-use plastic packaging for food service) by 2030 [122,126]. These sweeping rules are expected to impact every packaging sector – mostly food packaging – by enforcing stricter standards for sustainability and waste reduction.

Given the PPWR’s stringent requirements, packaging engineers are turning toward innovative design solutions that comply with the new rules while maintaining product protection. A prominent strategy is the use of ultra-thin functional coatings on conventional packaging substrates as opposed to wholly replacing structures with thick bio-based plastics. This approach addresses a key challenge: balancing barrier performance (for shelf life and food safety) with recyclability [128]. Under the PPWR, packaging materials must often remain mono-material (to simplify recycling) or be easily separable; multi-layer or heavily composite films risk being non-recyclable. Thin coatings emerge as an elegant solution: a recyclable primary material (such as paper, cardboard, or a recyclable plastic film) can be augmented with a microscopically thin barrier layer that provides needed functionalities (e.g., moisture/oxygen barrier or grease resistance) without altering the overall recyclability of the item [128]. These coatings – often applied from water-based formulations – add only a few microns of material. Such minimal additional mass aligns perfectly with the PPWR mandate to reduce packaging weight to the necessary minimum [122]. Indeed, in regulatory terms, a very thin coating (often well under 5–10% of the total package weight) is typically designed to either dissolve or be easily removed in standard recycling processes or be so small that it does not impede material recovery [128,129]. This ensures that the coated packaging can still count as “recyclable” under the 2030 targets. Moreover, using water-based, bio-derived coatings helps avoid restricted substances [122].

In contrast, trying to replace entire conventional packages with thick bio-based films (e.g., fully compostable plastic laminates) is not the primary focus under the PPWR framework. The regulation is relatively cautious about compostable or biodegradable plastics – it supports their use only in specific applications with clear environmental benefit, to avoid "greenwashing" [125,130,131]. Simply swapping a traditional plastic package for a bulky bio-plastic alternative does not guarantee compliance, especially if that bio-material cannot be recycled or interferes with established waste streams. In fact, the PPWR specifies strict criteria for compostable packaging and generally prioritizes recycling and waste reduction over wholesale substitution with bio-materials [132]. Thus, a thin coating strategy – as a properly functionalized PVA-based layer can be – is viewed as more pragmatic and a regulatorily approach.

1.2 Zeolites: a microporous material

Zeolites are crystalline, microporous aluminosilicate minerals that are characterized by a three-dimensional framework of corner-sharing SiO_4 and AlO_4 tetrahedra [133–135]. Particularly, the substitution of Si^{4+} by Al^{3+} in the lattice creates a net negative charge, balanced by extra-framework cations (typically Na^+, K^+, Ca^{2+}) residing in the pores [136]. These charge-balancing cations and water molecules occupy the zeolite's internal channels and cavities and can move freely and reversibly – for instance, water can be adsorbed and desorbed up to ~30% of the zeolite's dry weight without disrupting the crystal structure [137]. This unique architecture of interconnected nanometer-scale pores results in zeolites having exceptionally high internal surface area and the ability to act as molecular sieves, selectively adsorbing molecules that fit within their pore apertures [134,138]. Because of their tunable composition and uniform porosity, zeolites have become indispensable in industrial catalysis, ion-exchange processes, and adsorption/ separation technologies [139]. There are roughly 50 naturally occurring zeolites (e.g., clinoptilolite, chabazite, mordenite) and over 150 synthetic zeolite types identified, with synthetic variants dominating industrial use due to their higher purity and tailored properties [140,141].

Synthesis and general properties

Natural zeolites typically form over geological time scales from the alteration of volcanic ash in alkaline groundwater, yielding deposits often intermixed with other minerals [133]. In contrast, synthetic zeolites are produced via hydrothermal crystallization of aluminosilicate gels under controlled conditions [142]. Conventional synthesis involves an alkaline aqueous medium heated to ~90–150 °C, in which silica and alumina sources react and crystallize into the zeolite framework over hours or days. By varying synthesis parameters (temperature, time, pH, etc.), chemists can obtain different zeolite structures or morphologies [143]. Synthetic zeolites often exhibit more uniform pore sizes and greater stability than natural ones, and they avoid the impurities found in mined zeolite ores [138]. Today, different synthetic zeolites are manufactured worldwide (by companies in the

chemical and petrochemical sector) to meet demands in catalysis, adsorption, and ion-exchange applications [139,144].

Zeolites possess a crystalline network of channels and cages on the molecular scale: pore openings are typically in the range of ~3 to 10 Å in diameter, classifying them as microporous materials [143,145]. These uniform pores create a high internal surface area and allow zeolites to admit certain molecules while excluding larger ones, giving rise to size- and shape-selective sorption and reaction – the hallmark "molecular sieve" behavior [136,146]. When extra-framework cations of a zeolite are replaced by protons (via ammonium exchange and calcination), the material becomes a solid Brønsted acid – the H^+ resides on framework oxygen, able to donate a proton. Such acid sites, together with Lewis acidic cation sites, make zeolites powerful solid acid catalysts [147]. The intracrystalline pores impose shape-selectivity, allowing specific reactions on accessible substrates. This combination of acidity and shape-selective confinement is exploited in petroleum refining and petrochemical processes: for instance, H–Y zeolite catalysts revolutionized fluid catalytic cracking in the 1960s by more efficiently cracking heavy oil into gasoline-range hydrocarbons [138,144]. Moreover, zeolites can incorporate redox-active metal ions ($Fe^{2+/3+}$, Cu^{2+}, etc.) or metal nanoparticles in their pores, imparting catalytic activity for oxidation, hydrogenation, and other reactions [136]. High-silica zeolites often exhibit greater thermal/hydrothermal stability (and also hydrophobicity), whereas low-silica zeolites (with more Al, hence more cations) are more hydrophilic and have higher ion-exchange capacity. By adjusting the Si/Al ratio and the identity of exchangeable cations, one can tailor a zeolite's affinity for polar vs. nonpolar molecules and its stability in various environments [134,143,148]. About some of the most used synthetic zeolites, zeolite 4A has a Si/Al=1, zeolite X has Si/Al~1.24, for zeolite Y the Si/Al ratio is around 2.5-2.8, meanwhile, for ZSM-5 the Si/Al ratio is in a broad range with sensibly higher values (at least one order of magnitude bigger) [149–151].

Zeolites are excellent sorbents for gases and liquids. Their internal voids can adsorb a significant volume of guest molecules – for example, dehydrated zeolites can take up water or other polar molecules strongly via ion-dipole interactions [134]. Notably, as said, zeolites are often highly hydrophilic if they have low Si/Al.

Conversely, high-silica or purely siliceous zeolites preferentially adsorb organic molecules; this principle is applied in scenarios like volatile organic compound (VOC) capture [152,153]. The heat of adsorption on zeolites is also appreciable for polar molecules, meaning adsorption is exothermic, and regenerating (desorbing) the zeolite may require heating [154].

A defining feature of zeolites is their high cation-exchange capacity, arising from the anionic aluminosilicate framework. The loosely bound extra-framework cations within the pores can be readily replaced by other cations when the zeolite is contacted with a solution, without altering the crystal structure [155]. This versatile ion-exchange capability is central to many environmental applications of zeolites (e.g., pollutant remediation, soil conditioning) and also allows post-synthetic modification of zeolites to tune their catalytic and antimicrobial properties [133,134,142].

Among the many zeolite types, 4A and 13X are two of the most commercially important, often serving as reference materials for small-pore and large-pore zeolites, respectively. Their framework can be observed in Figure 1.3.

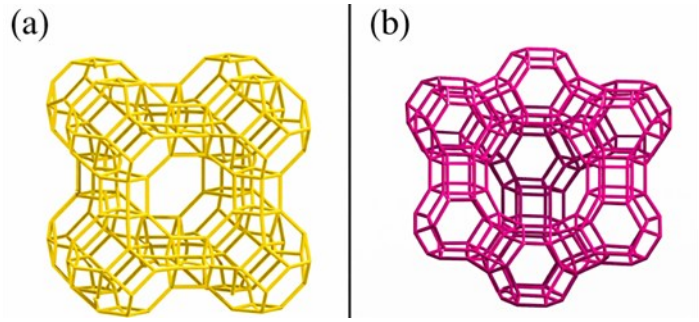

Figure 1.3. Frameworks of (a) Zeolite A (LTA) and (b) Zeolites X and Y (FAU) [145].

Zeolite 4A is the common name for the sodium form of Linde Type A (LTA), with an effective pore aperture of 4 Å [145,156]. Its formula reflects a 1:1 Si/Al ratio, meaning a high density of charge-balancing Na^+ cations is present in its cavities. Zeolite 4A's restricted cavities limit access to small molecules (H_2O, NH_3, CO_2, etc.), and it is highly hydrophilic due to the many cationic sites [150,151]. In contrast, Zeolite 13X, belonging to the framework type FAU, has larger pore openings connecting spacious supercages, which can accommodate bigger molecules than LTA can [135,145,157,158]. The Si/Al ratio of 13X is around 1.25

[150,151,159]. The higher aluminum content gives 13X a high CO_2 and N_2 adsorption capacity, and indeed 13X has long been a standard adsorbent for gas separation [144,160].

Major industrial applications

Thanks to the properties described earlier, zeolites are employed across a wide range of industrial and environmental applications.

Zeolites are prominent solid catalysts in oil refining and petrochemistry. They catalyze cracking, isomerization, and alkylation reactions with high efficiency and product selectivity [161]. Zeolites also serve as desiccants and molecular sieves in gas purification and separation. Type A and type X zeolites are widely used to dry gases and liquids by selectively adsorbing water and other small polar molecules [134,162–164]. The ion-exchange capabilities of zeolites can be employed in water treatment and pollution control. Zeolite minerals can be packed in filters to extract ammonium from municipal or aquaculture wastewater and to capture heavy metals (Pb^{2+}, Cu^{2+}, Cs^{+}, Sr^{2+}) from industrial effluents [154,165–168]. Natural zeolites find extensive use in agriculture, too. In soil, zeolite's cation exchange and water retention help regulate nutrient release and moisture, improving fertilizer efficiency and soil quality. They are added to animal feed or litter to adsorb ammonia; also, encapsulation of agrochemicals (herbicides, pesticides) in zeolite matrices has been explored [134,153].

1.3 Biodegradability in soil

Different biodegradable polymers exhibit very different behaviors in soil, and these can be understood based on their chemical structure and physical properties [13,21,169]. A general trend is that polymers resembling natural biopolymers or containing hydrolyzable linkages degrade more readily in soil, whereas polymers with very stable backbones or high crystallinity tend to degrade slowly [13,21,170]. Overall, the structural factors that favor soil biodegradation include: the presence of hydrolyzable or oxidizable bonds, a polymer chain structure that leads to low crystallinity or easy hydration, lower molecular weight (polymers or oligomers below a certain size may even be directly assimilated by microbes), and chemical similarity to natural substrates (so that existing microbial enzymes can act on them) [21,169]. Conversely, factors that hinder biodegradation are strong C–C backbones, high crystallinity or cross-linking, and inclusion of aromatic structures that many microbes have difficulty breaking [13,21,171]. These principles explain why, for example, polyhydroxybutyrate – a linear aliphatic polyester – degrades quickly, but polyethylene terephthalate (PET) – an aromatic polyester – tends not to biodegrade in soil at all: PET is essentially inert due to its aromatic rings and high crystallinity – unless ultra-specialized enzymes are present [171–174].

Soil burial tests

Soil burial tests are a common method to evaluate the biodegradability of polymers under realistic soil conditions. In a typical soil burial assay, samples of a polymer (often films or molded pieces) are buried in natural soil and incubated under controlled conditions for an extended period. Standardized methods provide guidelines for these tests [30,175,176]. The test duration is usually at least 90 days and up to 6 months, or until a plateau in biodegradation is observed [175]. Throughout the burial period, environmental variables like temperature, moisture content, soil pH, oxygen availability, and native microbial community composition are critical factors that can greatly influence the degradation rate [175,177].

In soil burial tests, respirometric measurements (CO_2 evolution or O_2 consumption) as direct evidence of microbial mineralization of the carbon in the polymer are needed to assess the effective biodegradation of the polymers [30,175,177]. Another

method consists of samples being periodically exhumed from the soil and weighed to determine mass loss over time, indicating degradation or disintegration. Other analytical techniques are routinely employed, such as Fourier-transform infrared spectroscopy to detect changes in chemical functional groups; tests of molecular weight and mechanical properties are also telling indicators of degradation progress [169,177]. The detailed mechanisms of polymer biodegradation will be discussed in the next paragraph.

Typical soil burial tests last on the order of a few months to a year. Many studies run ~90–180 days in the lab, while field burial trials may extend 6–12 months or more to capture slow-degrading materials. Importantly, microbial diversity in soil is generally very high – on the order of 10^9 bacteria per gram, plus fungi, etc. – providing a broad enzymatic capability to attack polymers [175,177–179]. This richness means that soil burial tests can, under favorable conditions, reveal biodegradation for a wide range of polymers, but the trade-off is that soil tests are inherently variable and non-accelerated compared to industrial composting. Factors like insufficient moisture, low nutrients, or suboptimal temperature can slow the process in a given soil [176].

The AlamarBlue® (resazurin) assay is a widely used method to measure the metabolic activity and viability of microorganisms. It relies on a redox indicator dye, resazurin, which living cells (including bacteria and fungi) reduce to resorufin, a highly fluorescent product. Because only metabolically active (viable) microbes can perform this reduction, the resulting fluorescence (measured at appropriate excitation/emission wavelengths) correlates with the number and activity of viable bacteria in the sample [180–182]. Higher fluorescence means more active, viable bacteria in that soil under the given conditions. Using a reference soil (with the same initial soil composition and moisture conditions) as a control is important to establish a baseline for comparison [181].

Mechanisms of polymer biodegradation

Biodegradation of polymers in soil is a multi-step process involving mechanisms that ultimately lead to the polymer's breakdown and mineralization. Broadly, the biodegradation proceeds in four overlapping stages: (1) physical and chemical

deterioration, (2) depolymerization, (3) microbial assimilation, (4) mineralization to inorganic end-products. Each of the four stages involves distinct mechanisms [13,169,183,184].

(Bio)deterioration is the initial stage that refers to any physical or chemical weathering of the polymer that makes it more accessible to microbes. In soil, environmental factors can cause polymer deterioration – often visible as surface erosion, discoloration, loss of mechanical integrity, and formation of micro-cracks. Also, the growth of fungi and other microorganisms on the polymer's surface can produce localized pitting and weaken the material. This stage does not yet break the polymer into monomers. Instead, it reduces the polymer's molecular weight to some extent and creates more surface area, making the polymer chains more accessible to enzymatic attack. Weight loss and deformation can begin in this stage [169,185].

(Bio)fragmentation and depolymerization is a critical stage in which microbial enzymes actively cleave the polymer's long chains into shorter oligomers, dimers, and monomers. Soil microorganisms (bacteria and fungi) secrete a variety of extracellular enzymes that can attack susceptible bonds in the polymer; the exact mechanism depends on the polymer's chemistry: polysaccharides like starch by amylases, PVA by specialized oxidases/dehydrogenases, etc. [89,169,186,187]. During biofragmentation, the polymer's molecular weight drops rapidly as covalent bonds in the backbone are broken. Importantly, the chemical structure of the repeat unit is not necessarily altered in this step; rather, the polymer is simply cut into its constituent monomer or oligomer units. Enzymatic fragmentation is often the rate-limiting step of biodegradation because long, insoluble polymer chains need to be broken down into water-soluble or small enough units that microbes can actually take up. Some polymers also undergo abiotic fragmentation in parallel, which assists the overall depolymerization process [13,21,169,185,187].

Assimilation is the third stage. In soil, countless microorganisms are competing to consume available carbon sources. Once the polymer has been depolymerized to monomeric or other small organic molecules, the degradation products can be assimilated by microbial cells as nutrients. For example, many bacteria can take up lactic acid, glycerol, etc., and catabolize them for energy and growth. Assimilation can occur via aerobic respiration, anaerobic respiration, or fermentation. Successful

assimilation is often confirmed by an increase in microbial population in soil containing the polymer, or by intermediate metabolites unique to the polymer's degradation [169,183,184].

The final stage, mineralization, is the complete conversion of the organic carbon of the polymer into inorganic constituents – primarily carbon dioxide, water, and, depending on elements present, mineral salts. Mineralization occurs concomitantly with assimilation: as microbes metabolize the polymer's carbon for energy, that carbon is oxidized to CO_2 or to a mix of CO_2 and CH_4, which are released into the environment. Likewise, any nitrogen or other heteroatoms in the polymer may be mineralized to ammonia, nitrate, or other inorganic forms. Full mineralization is the ultimate proof of biodegradation, as it demonstrates the polymer no longer exists in any organic form. Standard respirometric tests for biodegradability (like measuring CO_2 evolution) are essentially tracking this mineralization stage [13,30,175]. It is worth noting that not all of the polymer carbon necessarily mineralizes; some fraction is converted into new microbial biomass. Over longer timescales, however, that biomass will die and its carbon may also eventually mineralize or be incorporated into humic substances in soil. The consortium of soil microbes often works synergistically in this final stage: for example, one species might specialize in depolymerization but not metabolize the monomers, whereas another species will consume those monomers and release CO_2. Ultimately, mineralization confirms that a polymer has been biodegraded to completion (aside from any inert traces like inorganic filler residues) [13,169].

Therefore, for proper biodegradation, it has to be verified that the polymer does not just disintegrate, but actually gets assimilated and mineralized [13,169,188]. Environmental conditions in soil also modulate each stage: for instance, low moisture or low temperature can halt microbial activity even if the polymer is chemically susceptible, while pH extremes can denature enzymes [177,188].

Biodegradability of PVA

PVA is unusual among carbon chain plastics because microorganisms can mineralize it – often in both aerobic and anaerobic settings – ultimately converting it to CO_2, water, and biomass [65,73]. This capacity derives from its polyhydroxy

backbone $[–CH_2–CH(OH)–]_n$, which resembles natural polyalcohols and can serve as a carbon source once appropriate enzymes are present. However, the extent and rate of PVA biodegradation depend strongly on environmental conditions, the presence of specialized microbes, and the polymer characteristics (molecular weight, degree of hydrolysis, formulation) [187]. PVA that is highly water-soluble (e.g., lower hydrolysis grades) tends to be readily bio-assimilated, whereas high-hydrolysis PVA may require more specialized microbes and time [189]. Partially hydrolyzed or lower molecular weight grades are more amorphous and soluble, giving microbes easier access; fully hydrolyzed, high molecular weight, highly crystalline PVA degrades more slowly, and crosslinking further retards breakdown [65]. So, fully hydrolyzed PVA formulations with very high MW can be more of an environmental pollutant concern if the end-of-life is not properly managed (similar to other plastics) until eventually some degradation occurs [187,190–194]. Generally, leading agencies like the U.S. EPA, European Chemicals Agency, and independent ecolabels classify the PVA used in pods (with a lower hydrolysis degree and high solubility) as readily biodegradable [73]. In other words, under favorable conditions (such as those in wastewater treatment plant effluents or compost), PVA films are expected to break down efficiently [195–197]. Enzymes such as PVA-specific dehydrogenases and oxidases can oxidize the secondary –OH groups on the PVA backbone, generating intermediates that are subsequently cleaved into smaller fragments (e.g., acetic acid) [187,198]. These intermediates are then funneled into common metabolic pathways, ultimately yielding CO_2, H_2O, and biomass. Documented degraders include *Pseudomonas* and Gram-positive *Bacillus* [89,192,198–200]. Adequate water swells or dissolves PVA into the soil/aqueous phase, where microbes can act. Context strongly governs persistence. Cold, arid, or otherwise microbially inactive environments similarly slow breakdown [69,89,187,194,201].

However, practically, PVA-based packaging should be routed to opportune biological treatment for proper biodegradation/composting. Ongoing research is refining real-world fate estimates, strongly depending on the specific PVA grade (i.e., hydrolysis degree and molecular weight) and on the environment employed for the expected biodegradation, in terms of soil media and its conditions [202].

1.4 Additives in packaging polymers

Additives are used to enhance the performance of polymer films and coatings and possibly enrich them with new, interesting technological properties. Increasing the performance and durability of these polymers may also reduce the overall request for virgin polymers by valorizing them [203].

Commonly used additives in packaging are plasticizers (e.g., phthalates, improving flexibility and processability), antioxidants (e.g., phenols and phosphites, retarding the aging of polymers), stabilizers (against thermal and UV degradation), colorants (e.g., pigments, giving color to materials), flame retardants (e.g., metallic oxides, improving fire resistance), biocides (granting antimicrobial activity), anti-fogs (avoiding water vapor droplets onto inner packaging surface), and fillers. Organic or inorganic fillers, such as clay, talc, wood flour, chalk, and sand, are commonly employed to improve polymeric film properties like mechanical strength, stiffness, and gas barrier, addressing their inherent limitations [38,204]. The additive/matrix interfacial adhesion surely has an important influence in terms of the final mechanical properties of the composite film [205,206]. Incorporating fillers – mainly if nanostructured – can be a cost-effective way to improve gas barrier performances, to which factors like dispersion levels and nano-filler orientations contribute [207]. A key challenge generally is in effectively dispersing the additives within the matrix, mainly in common melt compounding with viscous polymers [208]. In this way, employing additives and fillers, the life cycle may also be extended, leading to minor wastes. The additive concentration to increase the recycling value is also required to be relatively low, possibly below 10wt% according to some guidelines [209]. In the case of food packaging, a final consideration is related to the migration of additives into the products, for which specific national or international regulations exist. If the risk of migration of a certain additive is low, approved additives might be used without the imposition of specific restrictions, as is instead the case for potentially harmful migrating substances, for which maximum limits are imposed [204].

Zeolites as a multi-functional additive

Incorporation of active agents into PVA packaging is another area of development. For instance, PVA films have been loaded with nanosilver, essential oils, other functional compounds, or other antimicrobials to create active packaging that can extend food shelf life by reducing bacterial contamination [110,210,211].

Beyond traditional uses in catalysis and chemical processing, zeolites are increasingly explored as active packaging additives to extend the shelf life of food or pharmaceuticals by controlling the package atmosphere and microbial load. Zeolite-based composites have been developed to scavenge oxygen from food packages: in some systems, faujasite-type zeolites loaded with oxidizable organic compounds serve to absorb and chemically consume O_2 within the package, thereby inhibiting oxidative spoilage [212,213]. Another important target gas is ethylene, a plant hormone that accelerates ripening and senescence of fruits and vegetables, and that can be strongly bonded to zeolites, capturing it [214–216]. By scavenging oxygen, moisture, and ethylene (as well as other odors or volatiles), zeolite-based inserts or coatings act to maintain product quality in a controlled atmosphere – an attractive approach in active food packaging [4,5,217,218].

Ion-exchanged zeolites can serve as inorganic antimicrobial agents in packaging materials. The typical strategy is to load the zeolite with ions known for their biocidal properties – most commonly silver (Ag^+), but also copper (Cu^{2+}) or zinc (Zn^{2+}) – and then either incorporate the treated zeolite into polymer films or use it as a coating on surfaces [219,220]. The zeolite acts as a reservoir that slowly releases metal ions (or keeps them available at the contact surface) to inhibit microbial growth. Studies have shown that even a few weight-percent of silver-exchanged zeolite in a plastic film can provide significant antibacterial activity, suppressing pathogens like *E. coli* and *S. aureus* on the food contact surface [221–225]. Importantly, regulatory considerations come into play: for food packaging uses, the migration of silver or other ions from the zeolite into the food must remain below strict limits for safety [92]. Researchers noted that achieving the right balance between ion release (for antimicrobial efficacy) and minimal migration is critical. Nonetheless, such Ag-zeolite additives are already in use, and they offer a more stable, high-temperature-tolerant alternative to organic biocides

[226]. Additionally, ZnO-decorated zeolite composites can improve UV resistance and inhibit microbial growth [227,228].

Inorganic additives can have an impact on polymer biodegradation, as well. Silica particles in PVA/starch matrices have been linked to slower soil degradation, likely via reduced water uptake/diffusion [229,230]. Montmorillonite clays have been reported to reduce aerobic biodegradation of PVA – e.g., Jurča et al. observed up to 40–45% of PVA sorbing onto clay and a 58–71% decrease in CO_2 evolution vs. neat PVA [231]. By contrast, synthetic zeolites can be comparatively benign: in the previous study, PVA+zeolite films mineralized slightly more than neat PVA under respirometric testing, consistent with zeolites not strongly adsorbing PVA nor releasing toxic modifiers [231].

Talking about possible additive migration towards the packaged product, it is worth noting that the natural zeolite Clinoptilolite is the only one to have a general recognition as completely safe and non-toxic among all zeolites, actually being widely and commonly used for applications that involve both animals and humans. Still, considering the very small amounts required for packaging films, other zeolites may potentially be viable as well; surely, biological studies are required, case by case, to certify a possible application [232,233].

Differently to similar other works that either are outdated and do not include recent trends in biodegradable polymers or they discuss zeolites as active additives without a detailed study of mechanical, barrier, and thermal properties as well [234–236], a review article was published reporting all these effect in recent literature related to the employment of zeolites additives in both conventional and biodegradable films for packaging applications (excluding polymer blends) [237].

High interest in literature has been given to PE composites functionalized with zeolites, as reported in Table 1.1.

Table 1.1. Studies on the effects of zeolite additives in PE films, in chronological order for LDPE and HDPE matrices. The optimal zeolite concentrations are reported.

Matrix	**Zeolite additive**	**(%)**	**Effects**
LDPE	Clinoptilolite	4 wt%	Tensile strength, Barrier to O_2 and CO_2 ↑

			Elongation at break	↓
LDPE	Mordenite	10 wt%	Ethylene adsorption (up to 5.4 µl g^{-1})	↑
LDPE	Natural zeolite exch. with Ag^+	2 wt%	Antimicrobial activity Tensile strength, Elongation at break	↑ ↓
LDPE	Zeolite A exch. with Ag^+	<5 wt%	Antimicrobial activity	↑
LDPE	Natural zeolite	5 wt%	Elastic modulus, O_2 barrier, Antioxidant H_2O barrier	↑ ↓
Bio-HDPE	Chabazite exch. with Ag-Cu-Zn	<5 wt%	Antimicrobial activity, Tensile modulus Elongation at break, Tensile strength	↑ ↓
HDPE	Zeolite 4A	0.5wt%	Flame retardancy (synergistic)	↑

Literature interest in the application of zeolites as additives in PP film was instead limited (Table 1.2).

Table 1.2. Studies on the effects of zeolite additives in PP films, in chronological order. The optimal zeolite concentrations are reported.

Matrix	**Zeolite additive**	**(%)**	**Effects**	
PP	Zeolite 13X (ZnO-supported)	10 wt%	UV resistance, antimicrobial activity	↑
PP	Zeolite A, neat & exch. with Ag^+	2.5 wt%	Antimicrobial activity, Crystallinity Elongation at break, Elastic modulus	↑ ↓
PP	Natural zeolite exch. with Ag^+	1 wt%	Antimicrobial activity, Tensile strength, Elongation at break, Thermal stability	↑
PP	Zeolite 4A w/ ZnO NPs clusters	6 wt%	Antimicrobial activity (synergistic effect)	↑

High interest is given to papers in which zeolites led to enhancements in mechanical performance, thermal stability, and barriers to gases, additionally with scavenging

properties and antimicrobial activity in the case of cation-exchanged zeolites. It is worth noticing that, according to its physicochemical structure, each polymer has a certain compatibility with given zeolites (whose polarity increases with Si/Al ratio), and this compatibility affects the matrix-additive adhesion and so the final composite properties as well [238]. Improvements and new functionalities derived from zeolite addition, along with technological limits, with respect to neat polymers (excluding polymer blends) have been highlighted in Table 1.3.

Table 1.3. Studies on the effects of zeolite additives in biodegradable polymer films, in chronological order for each considered matrix. The optimal zeolite concentrations are reported. Blended polymer matrices have not been considered.

Matrix	**Zeolite**	**(%)**	**Effects**	
Chitosan	Natural Zeolite exch. with Ag^+	< 2 wt%	Antimicrobial activity, Biocompatibility	↑
Chitosan	Clinoptilolite	3.5 wt%	Resistance to water solubility Tensile strength	↑ ↓
Chitosan	Clinoptilolite	33 wt%	C_2H_4 adsorption H_2O barrier	↑ ↓
Chitosan	Zeolite Y exch. with Ag^+	10-20 wt%	C_2H_4 adsorption	↑
Gelatin	Zeolite A exch. with Zn^{2+}	4-6 wt%	Antioxidant and Antibacterial activity, Thermal stability, Resistance to solubility	↑
PBS	Zeolites exch. with Ag^+	0.5 wt%	Antibacterial activity, Thermal stability Biodegradability	↑ ↓
Pectin	Zeolite Y	0.2 wt%	Tensile strength, H_2O barrier, Thermal stability	↑
PLA	Micro-zeolites exch. with Cu	4 wt%	Barrier to O_2 and H_2O, Elastic modulus, Antimicrobial activity	↑

PLA	Lactide-grafted zeolite 3A	2 wt%	Crystallinity, Elongation at break, Tensile strength, Thermal stability, Barrier to gas	↑
TPS	Zeolite ZSM-5	4 wt%	Elastic modulus, Ultimate tensile strength, H_2O barrier Elongation at break	↑ ↓
TPS	Zeolite A	4 wt%	Tensile strength, Young modulus, Elongation at break, Tenacity	↑

Therefore, incorporating zeolites into flexible packaging formulations can boost the performance of PE, PP, and certain biodegradable polymers (Figure 1.4). These enhancements include antimicrobial or scavenging effects that can arise from zeolites' intrinsic ion-exchange and adsorption capabilities. The resulting films and coatings exhibit generally superior gas-barrier properties, higher stiffness and strength, improved thermal stability [237].

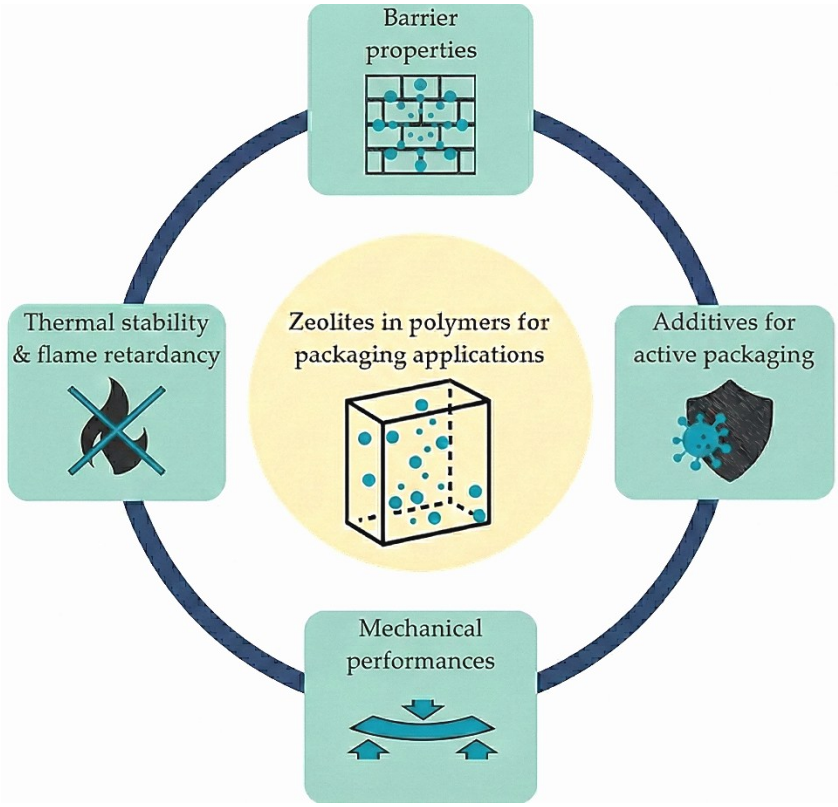

Figure 1.4. Scheme of the beneficial effects of zeolite additives on the properties of packaging polymers reported in literature [237].

Starch as a sustainable additive for PVA

Biodegradable polymer blends are actively being explored as sustainable packaging to reduce reliance on conventional plastics. Blends of PVA and starch are promising candidates [239,240]. The blend of PVA with natural polymers, such as starch, often improves biodegradability and may reduce the cost, all while maintaining adequate strength and flexibility for packaging use [241].

Solution casting is the most common method to prepare PVA/starch blend films in laboratory research [242]. In this technique, both polymers are dissolved or dispersed in a solvent (typically water) to form a homogeneous film-forming solution. PVA, which is water-soluble, is first dissolved in distilled water by heating and stirring until fully dissolved [242]. Starch is insoluble in cold water, so it is usually gelatinized by heating in water until its granules swell and dissolve [242]. Starch and PVA can also be mixed in powder form and dissolved together in water under heat, which ensures simultaneous gelatinization of starch and dissolution of PVA [243]. Both components are hydrophilic, so they tend to mix uniformly in water at the molecular or fine-particle level [242]. To improve the processing and uniformity of PVA/starch films, plasticizers are almost always added to the film-forming solutions to prevent brittleness and to enhance compatibility between the two polymers. Common plasticizers include polyhydric alcohols like glycerol, sorbitol, and glycol derivatives, which integrate into the polymer matrix and increase flexibility [242]. Plasticizers disrupt intermolecular interactions, making the blend more pliable and often improving transparency, but they can also increase water affinity and should be optimized [244]. After casting the solution onto a flat substrate and further drying at an opportune temperature, the resulting thin, continuous films are typically peeled off once dry and conditioned (often in a desiccator or at a set humidity) before testing [242,243]. While solution casting is prevalent in research, PVA/starch films can also be produced by melt processing (extrusion or compression molding), although this is less common in practice due to PVA's thermal characteristics [243]. However, careful control of temperature and moisture is required to avoid degradation. In general, solvent casting yields films with more homogeneous microstructure compared to direct melt blends [243,245].

Adding starch to PVA films markedly alters several key properties of the material.

Neat PVA films are usually strong and flexible, whereas pure starch films (especially unmodified starch) are stiff and brittle. Blending starch with PVA tends to produce a film that is mechanically intermediate between these two extremes [246]. This is because starch's molecular structure disrupts the uniform, flexible network of PVA. At higher loadings, starch can form dispersed domains or even agglomerates within the PVA matrix, which act as stress concentrators and weak points under tension. Beyond certain starch proportions, phase separation occurs – for instance, in a study, above roughly one-third starch in the blend, starch-rich regions and micro-voids were visible in the film, correlating with a sharp decline in mechanical performance [246]. On the other hand, small amounts of starch (with good dispersion) can sometimes be accommodated in the PVA matrix with only minor loss of strength. PVA and starch are reasonably compatible (both have hydroxyl groups that can hydrogen-bond), so at low starch content the blend can maintain continuity. Some studies even report that adding a little starch may maintain or slightly increase the tensile strength of PVA films, due to enhanced hydrogen bonding between starch and PVA chains that reinforces the structure [240]. However, this effect is very composition-dependent and often requires starch to be well gelatinized and perhaps chemically modified for optimal interaction. The use of plasticizer (e.g., glycerol) mitigates brittleness by making both phases more flexible, at the cost of lowering overall strength [245].

Blending starch with PVA also influences the thermal behavior of the film. The thermal stability of PVA/starch films is often slightly lower than that of pure PVA [247]. Nonetheless, the difference is usually not dramatic – the blend remains sufficiently stable for typical food packaging usage (which rarely involves high temperatures. Furthermore, good miscibility tends to produce a single glass transition temperature (T_g) intermediate between that of pure PVA and pure starch [244]. However, when plasticizers are present, they lower the T_g significantly for both components, making the blend softer at lower temperatures [244].

Barrier properties are critical for packaging. PVA films are known for their exceptionally low oxygen permeability because the polar OH groups create a tortuous path for oxygen molecules [242]. Starch films likewise have low oxygen permeability when dry. Therefore, a well-dried PVA–starch blend film retains a high

oxygen barrier performance, provided humidity is low [242]. The flip side is that PVA/starch films allow water vapor to transmit relatively readily. Both components contain many hydroxyl groups and readily interact with water molecules. Starch, in particular, is highly hydrophilic and can swell with water. Adding starch to PVA tends to worsen the moisture barrier of the films unless steps are taken to reduce hydrophilicity [239]. Therefore, a PVA-rich blend is preferable for a better moisture barrier. To address water vapor permeability in starch/PVA films, researchers often incorporate hydrophobic additives or create cross-links. Chemical cross-linking reduces the number of free hydrophilic groups and stiffens the network, which can cut down water uptake and slow vapor diffusion [242]. Another strategy has been to chemically modify starch to reduce its hydrophilicity, significantly lowering water absorption and vapor transmission [248]. Despite these improvements, PVA–starch films in general cannot match the water vapor barrier of truly hydrophobic plastics, limiting their applications: a separate water-impermeable overwrap layer may be employed, for instance.

On the other hand, PVA/starch films are usually impermeable to oils and fats, since both polymers are polar and not swollen by nonpolar substances. They can thus serve as effective grease barriers for dry or fatty foods [119,249–251].

The optical clarity of packaging films is important for product visibility. Pure PVA films are typically clear and transparent, often with very low haze (especially when fully hydrolyzed grades are used). When starch is added to PVA, the blend films tend to become more opaque or hazy as the starch content rises. This is because any phase separation or starch-rich microdomains in the film will scatter light [243,246]. That said, PVA–starch films can still be reasonably transparent at moderate starch loadings. If the starch is thoroughly gelatinized and molecularly dispersed in the PVA, the film may appear with only a slight reduction in transparency compared to neat PVA. For applications that require see-through packaging, a low starch content and good dispersion are preferred so that the film remains as transparent as possible [242,252]. Despite some trade-offs in properties, there are strong motivations for adding starch to PVA films for packaging.

Incorporating starch into PVA films enhances their overall biodegradability, since the starch portion will quickly degrade and leave behind a more porous PVA

structure that is easier for microbes to attack. PVA itself is one of the few synthetic polymers that is completely biodegradable under the right conditions, but its degradation in the environment can be slow [239,243]. Studies have confirmed that the biodegradation rate of starch/PVA films can rise with increasing starch content [253]. Also, replacing a portion of PVA with starch reduces the carbon footprint of the packaging film; in addition, starch is considerably cheaper than high-grade PVA resin, lowering the production cost of PVA, which is relatively high [239].

Synergistic effects of starch and zeolites

To fill the gap in literature, the present research is focused on a rigorous investigation into the resulting effects from the incorporation of specific additives – namely starch, zeolite 4A/13X, and their combined synergistic influence – on the characteristics of thin PVA-based films. First, this study examines changes in physical properties and functional properties; finally, and with a view toward environmental responsibility, the research thoroughly characterizes the biodegradation properties of the modified PVA-based films, determining how the inclusion of these additives impacts the material's environmental fate in soil.

2. Experimental section

2.1 Characterization methods

Tests for components and pristine films

Fourier-transform infrared (FT-IR) spectroscopy is indispensable for characterizing the chemical structure of polymer-based films and of their components, and also identifying functional groups that may be impacted by biodegradability tests [254–257]. In transmission FTIR, the beam traverses the specimen, so utility favors bulk analysis and rigorous quantitation when a known, uniform pathlength – such as a film sample – is set, but very thin films are required to avoid strong absorbance [255]. By contrast, ATR-FTIR requires minimal preparation, works also on opaque/thick solids and coatings, but probes only the near-surface (~0.5–5 μm) via an evanescent field, so it reports surface composition rather than true bulk [255,256,258]. In practice, transmission spectra map directly onto Lambert-Beer behavior, whereas ATR spectra exhibit wavenumber-dependent effective pathlength and intensity/position distortions that do not easily allow for identification or quantitative analysis [255,256]. In ATR, the exact penetration depth (d_p) varies with wavelength, incidence angle, and refractive indices [256,258]. For a single-bounce ATR at 45° on typical polymers (n≈1.5), diamond or ZnSe crystals give $d_p \approx 1.6–2.0$ μm at 1000 cm^{-1}; d_p increases toward lower wavenumber and decreases toward higher wavenumber, still being in the mentioned micro-range [255,256,258].

FT-IR analyses for chemical characterization have been carried out using a PerkinElmer Spectrum™ 3 spectrometer, in Attenuated Total Reflectance (ATR) modes, with 16 scans at a resolution of 4 cm^{-1} in the IR range 4000-700 cm^{-1}, with an analysis focus in the range 1550-850 cm^{-1}. This instrument was preliminarily employed to monitor the final additive dispersions in the films for preliminary characterizations, and therefore to assess the real stability of the aqueous formulations to be eventually used for the study. Particularly, ATR spectra of both sides of peeled films were recorded: different spectra would imply different compositions on the two sides, while similar spectra would indicate a good overall additive dispersion in the final dried films, as it will be discussed. A Vertex V70 FT-

IR spectrometer (Bruker Optik GmbH, Leipzig, Germany) was employed to record spectra in transmission mode as well for the thin reference films to underline the differences in chemical structures derived by starch addition in PVA formulations. The scanned IR range was 4000-600 cm^{-1} with 32 scans and a resolution of 4 cm^{-1}.

Optical microscopy is an important tool that enables rapid inspection of films' surface morphology. Optical micrographs of the films were taken after each unburial as well, using a Keyence VHX-7000 digital microscope (Osaka, Japan) equipped with a VH-Z20R swing-head zoom lens (providing a 200× maximum magnification). Particularly, both 50× and 200× magnifications were employed to assess visual differences in surface morphology among samples. Complementary, scanning electron microscopy (SEM), with its superior resolution, provides detailed visualization of microstructural features, such as porosity or microcracks. SEM images were recorded using a JSM-7001 with a maximum accelerating voltage of 10 kV and with magnifications up to x1000. Particularly, a Backscattered Electrons detector was combined with the apparatus so that the resulting image contrast is highly sensitive to the atomic number of the elements in the sample, in order to highlight the compositional differences within the sample [259]. Due to the high amount of samples that were obtained, SEM micrographs were recorded just to exemplify films containing all components; particularly, the SEM micrographs of the pristine films were studied mostly in comparison with those of soil-buried films.

Thermogravimetric analysis (TGA) offers insights into the thermal stability and decomposition mechanisms of biodegradable polymers [260,261]. Understanding the degradation onset and multi-step decomposition behavior is essential for establishing safe processing temperatures and predicting performance during use, especially for applications that involve heat exposure [261,262].
Thermogravimetric analysis in N_2 (Netzsch, model 409ST Luxx) in the temperature range of 20 to 900 °C with a heating rate of 10 °C/min was employed to understand the thermal stability of the components, and then of the different films. Specifically, for the films, a preliminary intermediate isotherm at 110°C for 30 minutes was included to remove excess humidity from the films, as it will be highlighted in the next paragraphs. The upper limit of the analysis range was then restricted to 600 °C

due to the low residual weights remaining constant after that temperature. The derivative thermogravimetric (DTG) curves, obtained as the first derivative of the TGA mass loss curves, were used to identify the main thermal decomposition stages and their corresponding peak degradation temperatures (T_{max}) [261,262].

X-ray diffraction (XRD) can offer insights into the degree of crystallinity, polymorphic phases, and molecular orientation – factors that significantly influence mechanical strength, thermal stability, barrier performance, and biodegradation kinetics. Crystallinity affects polymer packing density, which in turn governs properties such as oxygen and water vapor permeability. For instance, films with higher crystallinity typically exhibit lower water vapor transmission rates and slower degradation profiles compared to their amorphous counterparts [119]. XRD analysis of films processed via wet techniques (e.g., solution casting or rod coating) can also reveal the impact of solvent evaporation rate, film drying conditions, or annealing on the crystalline domain growth. Furthermore, blending, plasticization, or nanoparticle incorporation often alters crystalline packing, which can be efficiently monitored using shifts or broadening in XRD peak patterns [263].
XRD analyses were carried out with a wide-angle X-ray scattering XRD (Rigaku, Tokyo, Japan), with CuKα radiation at 40 kV and 30 mA anode excitation, and patterns recorded for 2θ angles from 5 to 40° using a high-speed one-dimensional silicon strip detector (D/teX Ultra 250 T) (Rigaku, Tokyo, Japan).
First, all the pristine solid reagents (both organic and inorganic) were characterized to assess their typical crystalline behaviour, in order to later study the prepared films. PVA diffractogram is of major interest due to its being the main component of the blend films. XRD analysis on starch also allows for investigating its nature (A-, B-, or C-type), since the supply of soluble starch powder does not include this kind of information [264]. Finally, the crystalline peaks of the supplied 4A and 13X zeolite powders were determined. After this, XRD analysis was employed to characterise both the overall crystallinity and the different crystalline phases of the films – particularly, both the reference original films and the biodegraded ones at the end of the experimental campaign. The diffraction profile of each sample typically consisted of one or more sharp crystalline peaks superimposed on a broad amorphous halo. The crystallinity index (X_c) of PVA was determined by

decomposing the XRD pattern into its crystalline and amorphous components, evaluating one characteristic crystalline peak. The area under the crystalline peaks (A_c) and the area of the amorphous halo (A_a) were calculated separately employing ImageJ. The relative degree of non-isothermal crystallinity was then calculated using the following equation [264,265]:

$$X_c(\%) = \frac{A_c}{A_a + A_c}$$

Besides comparing the original films, the changes in crystallinity after the biodegradation experimental campaign were assessed.

Water Vapor Transmission Rates (WVTR) of the different films were assessed with the Cup Method, as described by the ASTM E96. Specifically, in this home-made setup, the lids of Falcon® 15 mL plastic conical centrifuge tubes were removed, and each test tube was half-filled with DI water (wet method). For each film, circle-shaped specimens, bigger than the tubes' section, were cut out and opportunely parafilmed/wrapped onto test tubes, in order to make the thin films the only water vapor exchange surface for the water inside the tubes. The cups were conditioned for 1 day and inserted into a climatic chamber (MSL Humichamber, mod. EC 125) at 40°C and 40% RH. Daily, weight measurements were carried out to assess the moisture loss from the tubes due to an outer RH being lower than the inner RH. The tests were carried out for 5 days to ensure a certain linearity of the recorded weight loss as a function of time. Given Δm the change in mass of the test cup (g), A the test area of the exposed film (m^2) – equivalently, the section of the test tubes –, and Δt the time interval (d), the WVTR can be expressed in linearity conditions as [266]:

$$WVTR\ (g\ m^{-2}\ d^{-1}) = A \cdot \Delta t\ /\ \Delta m$$

Lower values of WVTR indicate better intrinsic water vapor barrier properties of the average films. PP films of comparable thickness and no-film open cups (named Control) were also tested under the same conditions, as 'boundary' references.

Additionally, water uptake tests are highly significant for biodegradable films, which frequently contain polar groups that readily absorb moisture, potentially accelerating hydrolytic degradation or plasticization. Measuring water uptake kinetics enables researchers to predict film behavior in humid conditions, guide the

selection of additives to mitigate moisture sensitivity, and assess the impact of water absorption on mechanical and barrier properties. Water uptake (WU) tests were conducted as complementary to biodegradation tests, in order to evaluate the films' affinity to water in soil, which is the main medium for biodegradation. A weighted quantity (W_i) of each specimen was immersed in 50mL DI water for 1 hour at room temperature. Then, the specimens were extracted, gently dried with a paper towel to remove only external surface water, and finally weighed (W_f). The WU was determined by the formula :

$$WU(\%) = \frac{(W_f - W_i)}{W_i}\ x\ 100$$

Studies related to soil buried films

The biodegradation of the films was assessed with soil burial tests. A rigid plastic plug tray (with 6x10 trays) and a commercial peat-based horticultural soil were supplied. The soil (a universal garden soil purchased from Zielona Oaza, Brzozów, Poland) had the following characteristics: balanced composition of high peat, low peat with sand, bark, dolomite, perlite, and micro- and macroelements (according to the producer statement), pH 5.5–6.5, ready to use (no mixing required). Three film specimens per sample (with similar weight and shape) were chosen for soil burial, for a total of 3x10 biodegradability plugs. For each plug, the procedure consisted of burying the specimens in the soil at half-height. Additionally, a row of 10 corresponding plugs filled with just soil was employed as a reference. The tray was then covered with aluminium foil and kept in a conditioned room at 30°C. Preliminarily, and repeated every two weeks, each plug was added with 10mL DI water; the relative humidity (RH) of the soils was measured and monitored (along with the pH). Particularly, the soils (both the test and reference ones) were ensured to be highly wet (RH>90%) throughout the entire experimental campaign. The described procedure is schematically represented in Figure 2.1.

Therefore, to evaluate the ongoing biodegradability, the buried films were periodically characterised using the following procedure. First, the films were unburied and mechanically cleaned to remove as much soil as possible. Then, each film was left air-drying for 24 hours, then characterised, and finally re-buried in the soil. Organic solvents and high drying temperatures were not employed to avoid

undesirable surface effects related to the tolerance of biodegradation micro-organisms, possibly still present on the films. The films were unburied a total of six times: every two weeks until the 8th week, then directly at the 12th week, and finally at the 16th week. This means that the experimental campaign for soil burial tests presented in this study lasted for 3.5 months. The main characterizations on biodegrading films consisted of weight measurements after each unburial, along with optical microscopy and FT-IR analyses for a better comprehensive study of the biodegradation phenomena.

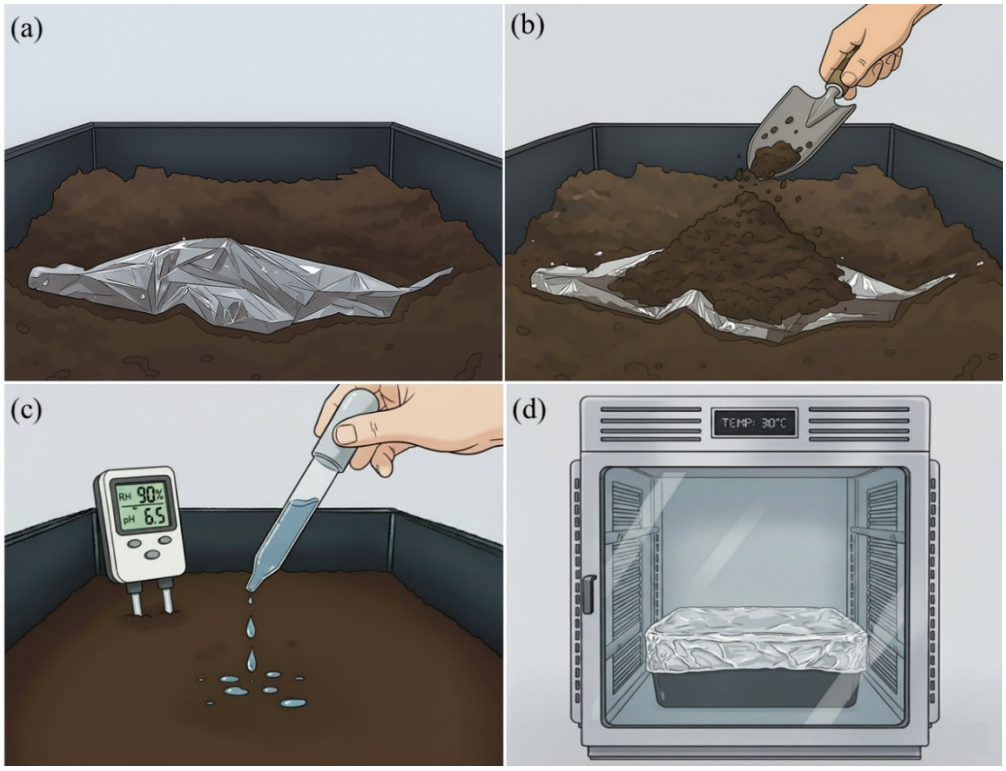

Figure 2.1. Experimental setup for soil burial biodegradability tests: (a) films are put into plugs half-filled with soil and then (b) covered entirely with other soil; (c) DI water is added to wet the soils, monitoring RH and pH; (d) the tray, covered with aluminum foil, is then stored at controlled temperature (30°C) until films unburial and new tests.

Weight measurements were carried out on the three replicates for each sample film after every unburial (and eventual air-drying), to estimate the weight loss after a certain test period (W_t) compared to the initial films' weight (W_{t0}), due to biodegradation phenomena:

$$Weight\ Loss\ (\%) = \frac{(W_t - W_{t0})}{W_t}\ x\ 100$$

Regarding this method, it is worth making two considerations. Despite most of the soil being removed from the films' surface after unburial, very little residue was indeed still trapped onto the films, mainly the 18P/2S-series. This would mean an additional weight that effectively returns a recorded weight loss lower than the real one. However, this effect is considered negligible due to the residual soil size and concentration, as it will be described in the next section. In second place, the air-drying for 1 day after unburial from wet soils cannot remove the entire water from the films; still, the drying procedures and conditions were consistent with each specimen. Moreover, it was granted that the weight of the films became very stable after already 1 day of air-drying. Indeed, negligible differences in weights occurred after a second day of air-drying, as can be observed in Figure 2.2. So, 1 day of air drying is definitely enough. Nevertheless, little humidity would be present as well on the initial reference films due to the intrinsic materials' hygroscopicity.

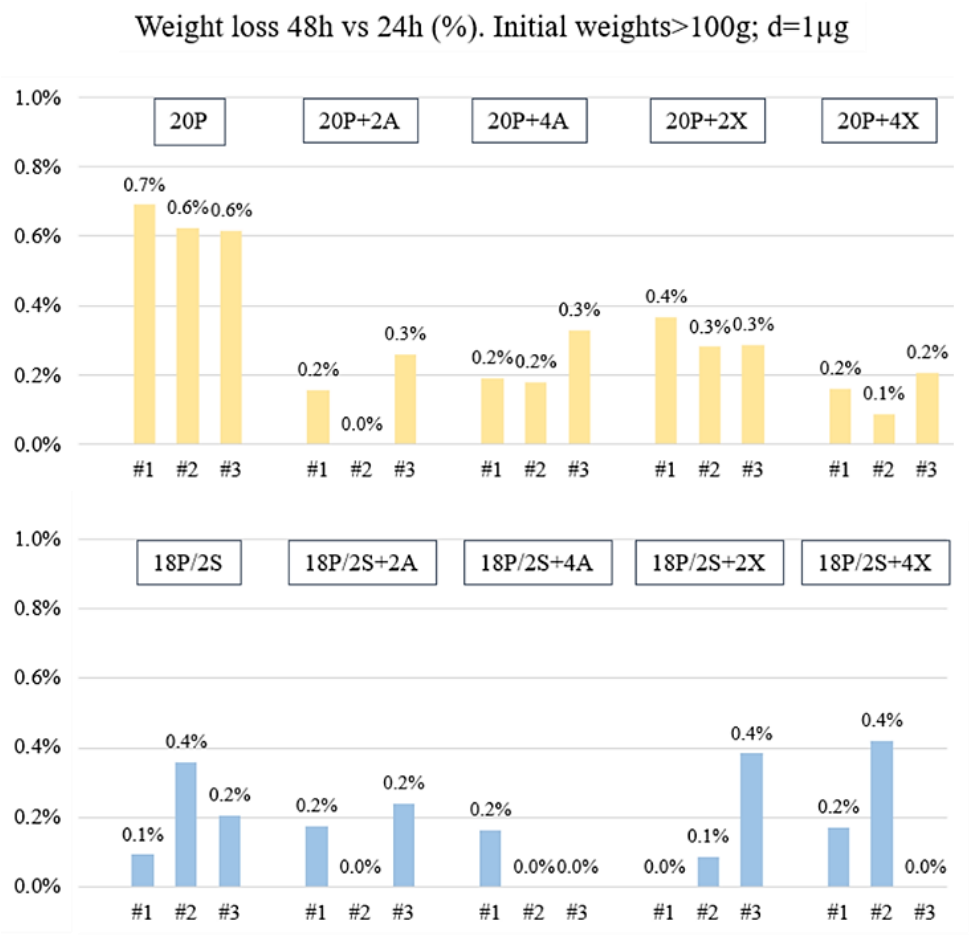

Figure 2.2. Relative weight losses of the films between 48 hours and 24 hours of air drying following unburials: the weights essentially stabilize already after 24 hours.

Optical micrographs were also taken after drying of the films to investigate phenomena such as defect formation, which are often exacerbated in biodegradable systems due to water absorption or hydrolysis. SEM further allowed better visualization of samples' surface for evidence of biodegradation, such as increased roughness and pits at higher magnification (up to x1500) – although, as explained earlier, only exemplifying films were considered and tested. The instruments used for optical micrographs and SEM, to assess the overall progress in biodegradation related to each film sample, are the same in the previous section for pristine films.

The Vertex V70 FT-IR spectrometer equipped with a Platinum-ATR unit (Bruker Optik GmbH, Leipzig, Germany) was further employed to carry out the comparisons in both reference and biodegraded films by characterizing chemical-structural changes during biodegradability tests. The scanned IR range was 4000-600 cm^{-1} with 32 scans and a resolution of 4 cm^{-1} (focusing on the fingerprint region). Additionally, FT-IR spectra in transmission mode were also recorded for the biodegraded thin films at the end of the experimental campaign.

The metabolic activity of bacteria inside the biodegradability test soils was evaluated using the AlamarBlue® assay (Thermo Fisher Scientific, Waltham, MA, USA) at the end of the soil burial experimental campaign. Particularly, three groups of samples were analysed: the biodegradation test soils of the 10 different film formulations; reference soils – that were kept at the same RH and temperature conditions of the test soils from the begin to the end of the experimental campaign – to assess the impact of the films; the same reference soils but with a final addition of either zeolite 4A or 13X raw powders at 10wt%, to understand the influence of more abundant zeolite presence inside the soils – since their concentration in the biodegradability test soils would be quite less. Therefore, for each condition, 0.5 g of soil (if need be, +10wt% zeolites) was suspended in 5.0 mL of phosphate-buffered saline (PBS) and incubated in conical Eppendorf tubes under agitation (vortex) for 1 minute to promote bacterial resuspension. After this homogenization, the samples were stored for 2 days to allow proper bacterial diffusion and resuspension from the soil to the liquid medium. Later, 100 μL of the supernatant was carefully withdrawn from each tube and transferred to a microplate well.

Subsequently, 10 µL of AlamarBlue® reagent was added to each aliquot. Samples were prepared in triplicate. The microplate was incubated in the dark for 3 hours at 30°C, allowing sufficient time for the redox indicator to change color in response to bacterial metabolic activity. After incubation, fluorescence intensity was measured using a GloMax microplate reader (Promega, Walldorf, Germany) at an excitation/ emission wavelength range of 580–640 nm. The fluorescence signal, in terms of Relative Fluorescence Units (RFU), was used as an indicator of bacterial viability in the presence of different soil conditions or additives [267].

As disclosed, the pH of the soils was measured as well after each film unburial, along with the RH. Changes in the pH are very important to consider and monitor: bacteria need a certain pH range, as microbial growth rates are slow in low pH soils, specifically below pH 5, which would lead to a direct negative effect on bacteria and on biodegradation itself [268].

2.2 Components' analysis

In this study, five different components were combined to obtain aqueous formulations, from which the final films were later obtained. Particularly, PVA (powder, Mw 89,000-98,000, 99+% hydrolyzed, SigmaAldrich) was employed as the main polymer material of the formulations – and of the final films. Anhydrous glycerol (AppliChem) acted as a film plasticizer. Soluble starch powder was supplied by Carlo Erba; similarly, for the 4A zeolite molecular sieves (fine powder, avg. 2µm). Instead, 13X zeolite molecular sieves (fine powder, avg. 3µm) were supplied by AlfaAesar.

Thermal behaviour

- *Polymeric components*

TGA/DTG tests for both pristine PVA and starch powders are shown in Figure 2.3. PVA exhibits a modest initial mass loss, roughly 3% at ~120 °C, attributable to the release of adsorbed moisture. This reflects PVA's limited hygroscopicity [269–271]. After this dehydration stage, the curve remains stable until decomposition begins, with the DTG revealing a two-step degradation. A first peak in the derivative weight loss rate appears around 280–290 °C, followed by a larger, global DTG maximum near 330–340 °C, corresponding to the main chain pyrolysis [270]. These two DTG peaks indicate a multi-stage thermal degradation mechanism: initial elimination reactions (e.g., OH group dehydration), then rapid polymer backbone breakdown at the higher temperature [272,273]. By 600 °C, only a ~4 wt% residue remains, demonstrating that PVA's organic content is almost entirely volatilized under nitrogen. This minimal char yield is consistent with literature for pure PVA (roughly 3% residue at 600 °C): this aliphatic vinyl polymer lacks aromatic content and tends to volatilize almost completely, producing very little char [274,275].

Starch shows a more pronounced early weight loss due to its greater hygroscopicity. About 10% of the mass is lost by ~150 °C. Starch's abundant hydroxyl groups readily absorb moisture, so this initial TG drop (with a DTG peak often around 120–130 °C) is directly related to its water content [276,277]. Once dried, starch undergoes a single dominant decomposition event: the DTG curve exhibits a sharp

global peak at approximately 300 °C as T_{max}, corresponding to rapid thermal depolymerization and degradation of the polysaccharide chains [276,278], and reflects the conversion of starch into volatiles (e.g., pyrolysis gases) and char. This peak is nearly twice the magnitude of PVA's, reflecting very rapid devolatilization, and then quickly subsides, indicating a more abrupt breakdown of its glucose polymer backbone. Above ~400 °C, the rate of weight loss diminishes markedly, indicating that the remaining material has carbonized. Notably, a substantial residual char (~20 wt%) persists at 600 °C [279]. Such a high residue is characteristic of starch and other carbohydrate polymers, which form a stabilizing carbonaceous char via dehydration and cross-linking at elevated temperatures. Indeed, beyond ~500 °C, starch's structure reorganizes into aromatic charred frameworks, accounting for the significant inert residue observed. This behavior signifies starch's higher char-forming propensity and lower volatility compared to purely aliphatic polymers [276].

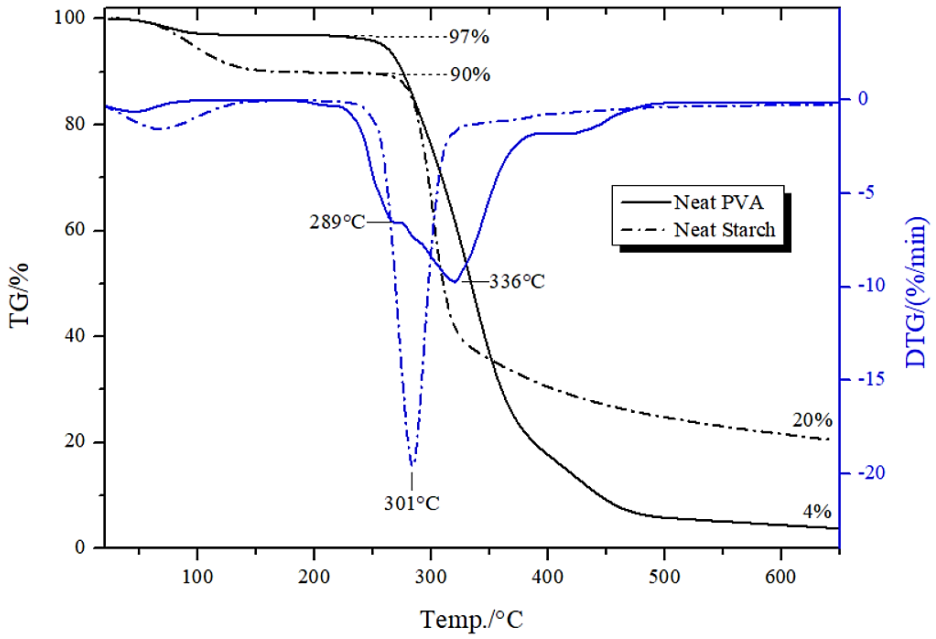

Figure 2.3. TGA/DTG tests for pristine PVA and starch powders in N_2.

The thermal stability of anhydrous glycerol was not tested, as the literature supplies consistent results for this plasticizer. Indeed, across several thermogravimetric studies using N2 and a heating rate of 10 °C/min, the reported temperatures of maximum degradation for anhydrous or pure glycerol are consistently reported around 240 °C. This single-step degradation, with the onset at 156 °C [280], is

mainly attributed to intramolecular dehydration followed by the breakdown of glycerol into acetol and formaldehyde-like intermediates before complete volatilization [281,282].

- *Zeolites*

TGA/DTG tests for the two different zeolite powders are shown in Figure 2.4.
The thermogravimetric profile of zeolite 4A is dominated by dehydration, as this aluminosilicate contains no combustible matter [283]. Only a gradual weight loss is observed from room temperature up to about 400 °C, corresponding entirely to the release of water from the zeolite's pores. An initial minor mass loss occurs below ~150–180 °C (removal of surface adsorbed and loosely bound water), followed by a slower ongoing water loss extending to approximately 350–400 °C as more strongly held intra-cage water is evacuated [284]. The DTG curve may show a broad peak in the vicinity of 150–180 °C, marking the highest rate of water desorption, and a secondary, smaller peak at a higher temperature. By 600 °C, zeolite 4A has lost about 18% of its initial mass, leaving a solid residue of ~83–85% which represents the dehydrated aluminosilicate framework. This final residue at 600 °C is slightly lower than the theoretical anhydrous framework mass: a fully hydrated 4A can contain ~20–22% water by weight, so the TG result suggests the sample was not completely saturated initially (or not all water escaped by 600 °C) [284]. Crucially, no additional weight loss occurs beyond dehydration – the curve flattens after ~400 °C – indicating excellent thermal stability of the inorganic lattice. The high 600 °C residue confirms zeolite 4A's purely inorganic nature and the absence of any organic or decomposable components; only water is removed, with the aluminosilicate skeleton remaining intact up to and beyond 600 °C [149].
Zeolite 13X likewise undergoes weight loss solely from dewatering, but it initially contains a larger amount of water than 4A. The TG data show a more substantial total moisture loss of about 22% by 600 °C, consistent with the high water adsorption capacity of type 13X molecular sieves [285]. Water evolution in 13X occurs in stages: a major fraction of the water is released at relatively lower temperatures (many pores empty by ~200–300 °C). The DTG profile features a prominent dehydration peak typically around 170–180 °C, indicating rapid removal

of loosely bound water in the large supercages. Beyond this, a tail of slower weight loss persists up to ~300 °C as residual water from tighter binding sites is gradually desorbed. By roughly 300–350 °C, the material is essentially dry, and the TG curve levels off. The residual mass (~78–80%) at 600 °C corresponds to the anhydrous zeolite framework, in line with expectations for a fully inorganic NaX zeolite. Notably, 13X's total water content is higher and released at slightly lower temperature compared to 4A, reflecting its greater pore volume and high-affinity hydration capacity [286]. After dehydration, there is no further mass loss up to 600 °C, underscoring that zeolite 13X's aluminosilicate framework remains thermally stable. As with 4A, no decomposition is observed apart from water removal; the remaining ~78% at 600 °C represents the dry material [149].

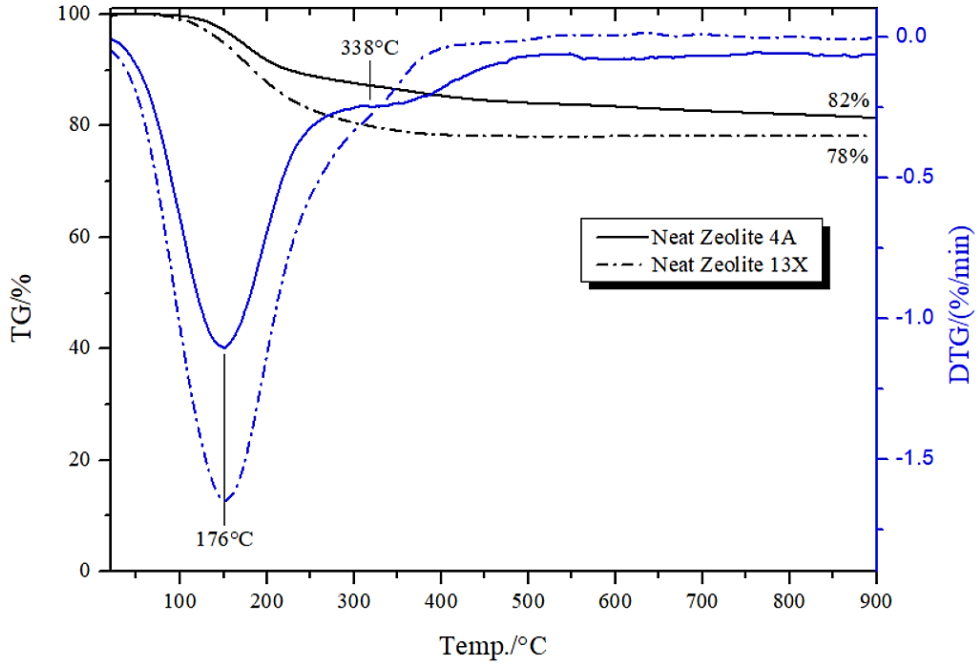

Figure 2.4. TGA/DTG tests for pristine zeolite 4A and 13X powders in N_2.

Crystallinity studies

- *PVA powder*

The XRD pattern of the PVA powder, which can be observed in Figure 2.5, reveals the typical semi-crystalline fingerprint of this polymer. Notably, a broad but discernible peak appears at $2\theta \approx 19.5°$. This diffraction peak is the hallmark of

PVA's crystalline regions [287]. The prominence of this peak indicates that the PVA has a high crystalline microstructure (due to strong intermolecular O–H bonding). The ~11.5° and ~22.5° peaks are characteristic secondary reflections of well-ordered PVA crystals. It is worth noting that fully or near-fully hydrolyzed PVA (98–99+%, as in this case) crystallizes more readily and shows sharper, more numerous peaks. In contrast, partially hydrolyzed PVA (with residual acetate side-groups) tends to have disrupted hydrogen bonding and lower crystallinity – often showing only a broad amorphous halo or a single weak peak around 19–22° [70,274,288,289].

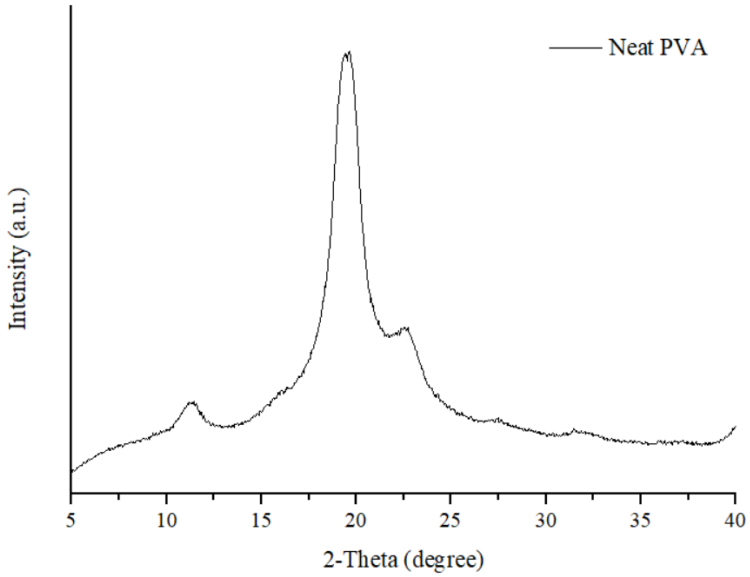

Figure 2.5. XRD pattern of pristine PVA powder.

The crystallinity index for these PVA powders, calculated as discussed by dividing the area of the total crystalline phase by the total area of the crystalline and amorphous phase, was estimated at 28.6 ± 0.7%. The broad diffuse halo is related to the amorphous regions of PVA, where polymer chains lack long-range order.

- *Starch powder*

Regarding the XRD pattern of the supplied starch powder (shown in Figure 2.6), a sharp main peak appears at approximately 17°, with shoulders near 15°, 22°, and 24°, and a (weak) peak around ~5.6° 2θ [290]. This profile best matches the characteristic B-type starch crystallinity, typical of potato starch. In contrast, an A-type starch (typical of cereal sources like maize or wheat) would lack the ~5° peak

and instead show major peaks at ~15°, 17–18°, and 23° 2θ. Commercial "soluble starch" for lab use is often potato starch (or a mixture) that has been partially modified for solubility [291–293]. Additionally, the B-type assignment indicates the sample is partially crystalline in the native granular form rather than fully gelatinized. If the starch had been heavily pre-processed (e.g., fully gelatinized and retrograded in a different form), one might expect either a V-type pattern or nearly amorphous behavior. However, the clear B-type XRD signals here imply the material still retains the native-like B-polymorph crystallites [294]. After calculations of crystalline and amorphous areas, the XRD crystallinity index for the supplied soluble starch powders was estimated at 26.5 ± 1.5 %. The potato starch provided in this study is acid-converted to a lower molecular weight for improved hot-water solubility. Acid hydrolysis preferentially erodes amorphous growth rings, which can raise the relative crystallinity compared to native starches.

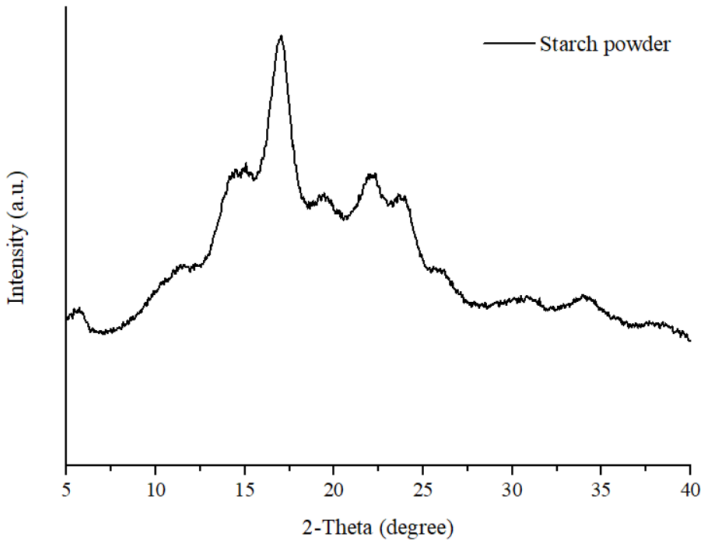

Figure 2.6. XRD pattern of pristine starch powder.

- *Zeolite powders*

The XRD patterns of pristine zeolite 4A and 13X powders are shown in Figure 2.7. The position and origin of the XRD peaks for both zeolites are consistent with values reported in the literature [295]. Zeolite 4A exhibits its strongest reflections at 2θ ≈ 7.2°, plus other peaks (10.2°, 12.5°, etc.), which are the characteristic peaks of the LTA-type zeolite framework [149,296,297]. The sharpness and intensity of the peaks indicate that the zeolite 4A powder is highly crystalline. Notably, no extra

diffraction peaks are observed, which suggests high phase purity. Zeolite 13X shows a distinct XRD pattern with its first intense peak at low angle $2\theta \approx 6.1°$, characteristic of the FAU zeolite framework [297,298]. In addition, multiple higher-angle peaks appear, all of which are recognized as the signature diffraction peaks of FAU 13X zeolite [149,298]. The absence of any extra/unindexed peaks implies the zeolite 13X powder is phase-pure and highly crystalline.

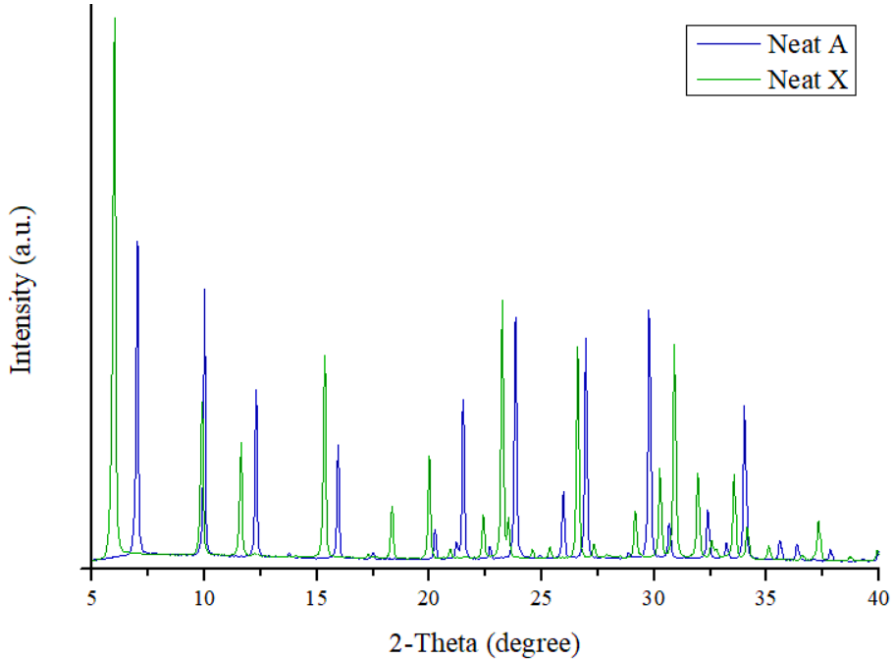

Figure 2.7. XRD patterns of pristine zeolite 4A and 13X powders.

Chemical-structural analysis

- *Organic components*

Because all three organic substances (glycerol, PVA, and starch) of the formulations contain hydroxyl functional groups and aliphatic CH bonds, their FTIR spectra share several common peaks, as can be observed in Figure 2.8.

In particular, O–H stretching is a feature present in all three, appearing as a broad band in the 3200–3400 cm^{-1} range for each. In PVA, the O–H stretch tends to be especially intense and very broad, reflecting the polymer's high density of –OH groups and extensive intermolecular hydrogen bonding [289,299,300]. Glycerol, a small molecule, appears to have a less intense band compared to the polymeric substances [277–279]. All three compounds also share aliphatic C–H stretching

bands in the 2850–2950 cm^{-1} region, arising from –CH_2– and –CH– groups. In PVA, the C–H stretching peak is fairly evident because the polymer has a hydrocarbon backbone. In starch, which has a lower proportion of C–H, the band tends to be relatively weak [301]. In glycerol, the stretches are of moderate intensity: it has a higher C–H/OH ratio than glucose units, so its C–H bands are more noticeable. Another common functional group in all three compounds is the C–O single bond; each spectrum shows one or more of them, though the exact positions differ due to the nature of the C–O bonds and the molecular context. Glycerol's primary C–O stretches appear around 1030 cm^{-1}. PVA, with secondary alcohols, has a strong C–O band near 1080–1095 cm^{-1}. Starch, containing C–O in both secondary alcohols and glycosidic ethers, shows multiple C–O stretching peaks (for example, a peak near 1155 cm^{-1} and another around 1078 cm^{-1} among others) [299–303]. Finally, some other bands can be noted for completeness. A broad band around 1400-1200 cm^{-1} appears in all compounds (attributed to –CH2 scissor bending). All three materials lack any intrinsic C=O stretch around ~1700 cm^{-1} due to no carbonyl groups. Particularly, this confirms the almost total hydrolysis of PVA: if a fraction of vinyl acetate remains unhydrolyzed, a very faint carbonyl band would appear. Last, a band around 1645 cm^{-1} related to H–O–H bending vibration of absorbed water can be observed, mostly for starch, due to its hygroscopic nature [299–303].

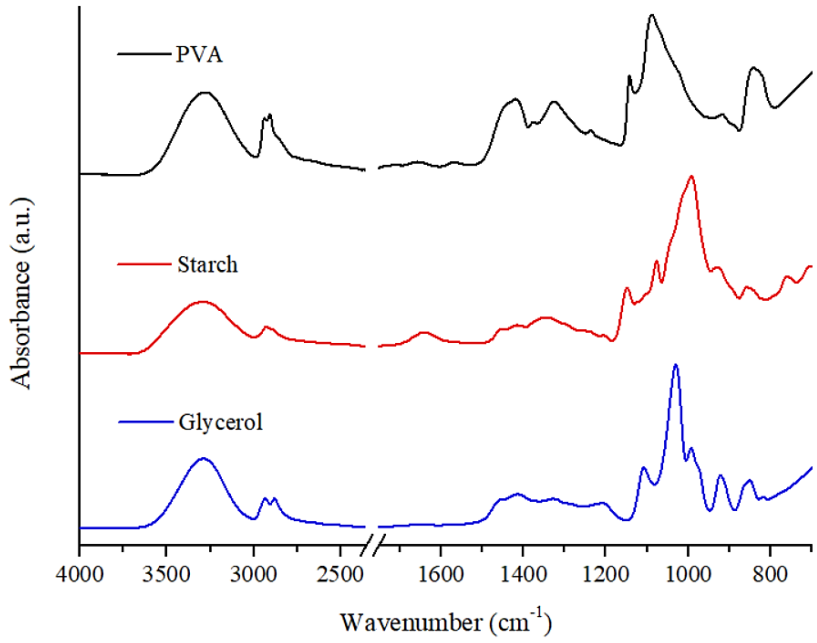

Figure 2.8. ATR-FTIR spectra of pristine PVA, Starch, and Glycerol.

Interestingly, the FT-IR spectra effectively align with the outcomes of the XRD analysis, confirming that the supplied starch is plausibly extracted from potato due to characteristic B-type peaks [303,304].

- *Zeolites powders*

The ATR-FTIR spectra of the two different zeolites, in their pristine powder form, are reported in Figure 2.9.

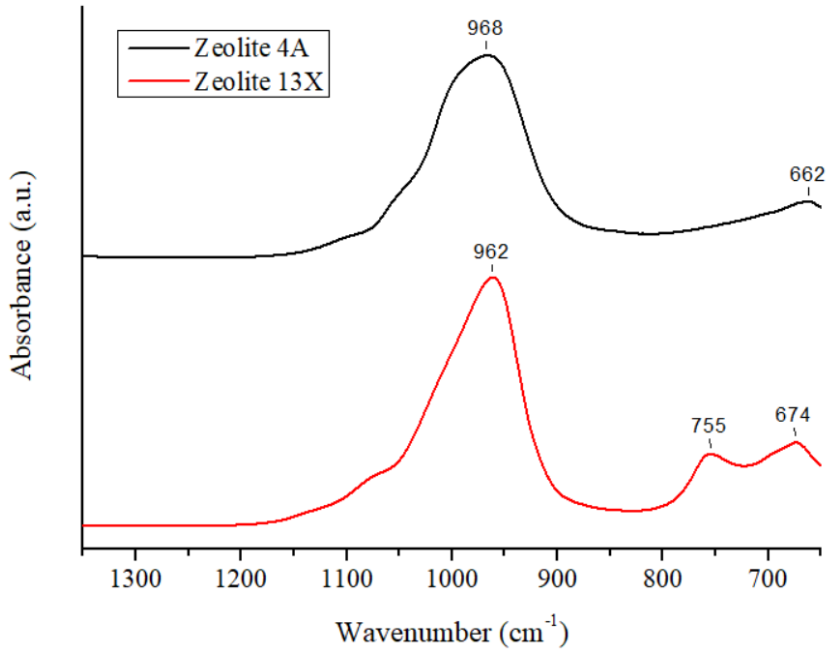

Figure 2.9. ATR-FTIR spectra of pristine zeolite 4A and 13X powders (focus on the 1300-650 cm^{-1} fingerprint region).

Both zeolites share a high-frequency T–O–T asymmetric stretch (~960–970 cm^{-1}) due to their aluminosilicate frameworks. The precise position can differ slightly (e.g., 968 cm^{-1} in 4A vs 962 cm^{-1} in 13X) because of framework geometry and Si/Al ratio. Zeolite X (FAU) tends to show its main asymmetric stretch band ~970–980 cm^{-1}, while zeolite A (LTA) is often ~990–1000 cm^{-1}. Both frameworks also display a tetrahedral symmetric stretch at ~660–670 cm^{-1}. The FAU structure additionally shows a characteristic vibration at ~755 cm^{-1}, which is absent in LTA, specific to its framework ring structure [305–308].

The O–H stretching region for physisorbed water (around 3400-3300 cm^{-1}) is broad in both zeolites, but the band centers differ slightly. This shift can reflect the

different pore sizes and hydrogen-bonding environments: water in smaller 4A cages is more tightly bound, often showing O–H stretches at slightly lower frequencies. Both materials exhibit the water bending vibration around 1640–1650 cm^{-1} with similar positions and intensity, indicating the presence of coordinated water in the pores [305–308].

It is worth noting that the 968/962 cm^{-1} (zeolites' main peak) region corresponds to a local minimum in the spectra of any organic compound, as can be seen in Figure 2.9. This will be strongly highlighted in the next paragraph, as it will be the basis for an easy and fast identification method of polymer formulations, providing the best zeolite dispersion in the film.

2.3 Preparation of the films

Film-forming PVA/starch aqueous formulations were prepared as follows. PVA (P) at different concentrations up to 20%w/v, starch (S) 2%w/v, and glycerol (G) as a plasticizer were added to a glass bottle in which an amount of pre-heated DI water was poured. The bottle was then put inside a beaker of a boiling water bath. So, each aqueous system inside the bottle was magnetically stirred for 4 hours at ~100°C, within the bottle was sealed to prevent water from leaving the system at high temperature. A scheme of the film-forming formulation preparation is shown in Figure 2.10. The blends were then cooled down at room temperature while still being stirred. Light-white viscous formulations were obtained and kept under stirring before further processing. For each formulation, the final plasticizer content was determined by the sum of glycerol contents required for each polymer of the blend, namely 10%w/w of PVA and 30%w/w of starch, as suggested in literature [44,45,309–311].

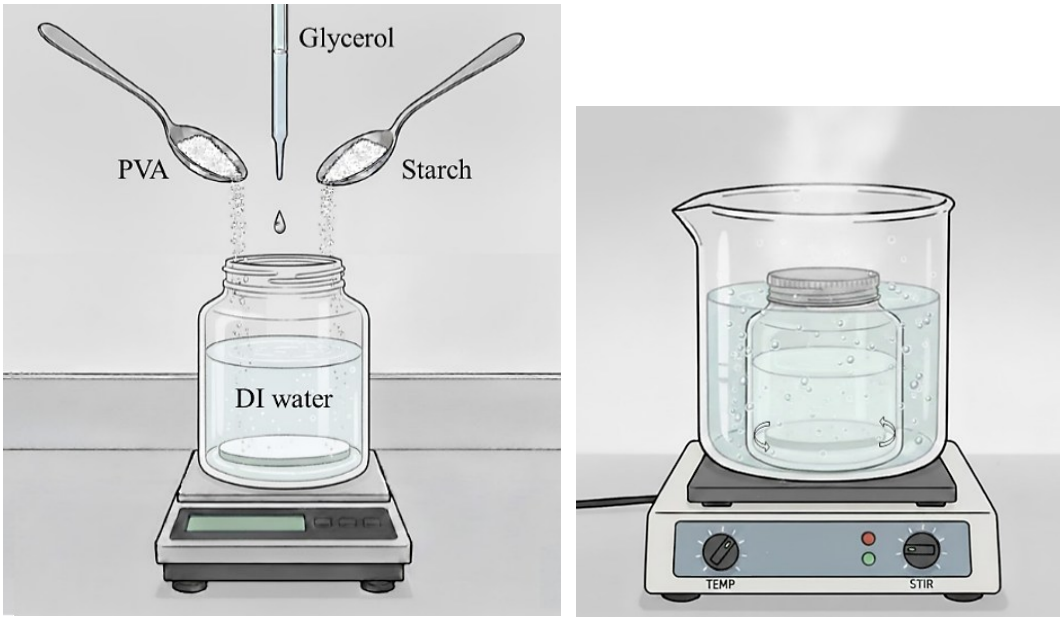

Figure 2.10. Preparation of the film-forming aqueous formulations: (left) the organic components are added to the glass bottle with DI water and a magnetic stirrer that allows (right) blending of the components inside the sealed bottle, put in a boiling water bath.

To prepare the zeolite-additivated films, either 4A zeolite (A) or 13X zeolite (X) powders at two different concentrations, namely 2 and 4%w/w of polymeric blend, were first added to PVA-based formulations (Figure 2.11) – prepared as previously

discussed. After 3 hours of magnetic stirring in the boiling water bath and subsequent cooling, white viscous formulations were finally obtained, either comprising A or X inorganic additive. Later, the viscous aqueous formulations were coated onto a PETG (Teflon) film – which was properly taped to a rigid support – particularly employing the rod coating method (rod provided by RK Print Coat Instrument, Royston, UK), as shown in Figure 2.12.

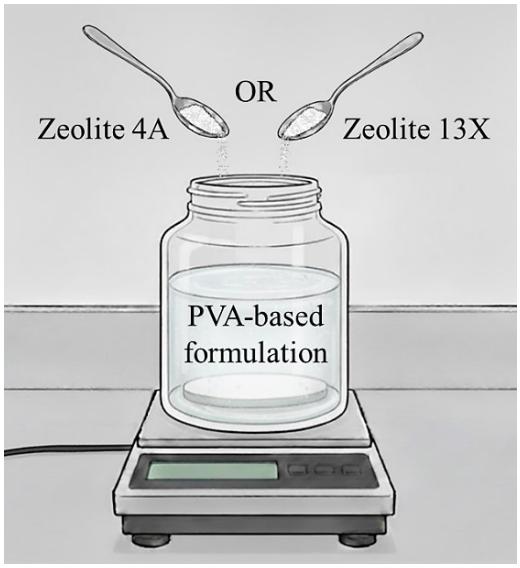

Figure 2.11. Preparation of PVA-based formulations additivated with zeolite powders.

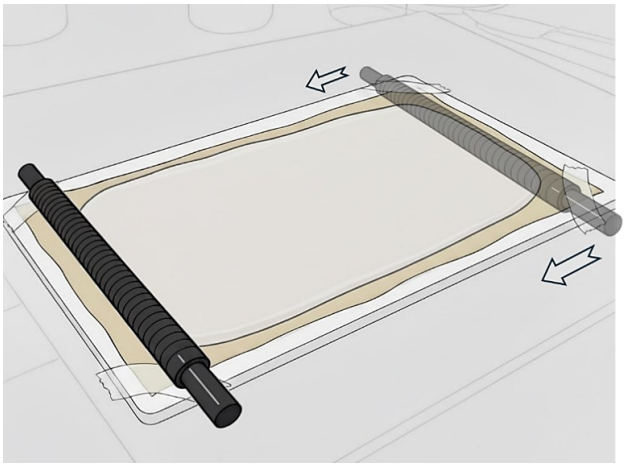

Figure 2.12. Rod-coating process of the film-forming formulations on a PTFE substrate.

Then, the whole system was put in a ventilated oven, set at maximum to 105°C, to allow the drying of the formulations and the obtainment of solid films on the PTFE substrate; finally, after proper drying, the PVA-based films were carefully peeled off the coated substrate. These last procedural steps are illustrated in Figure 2.13.

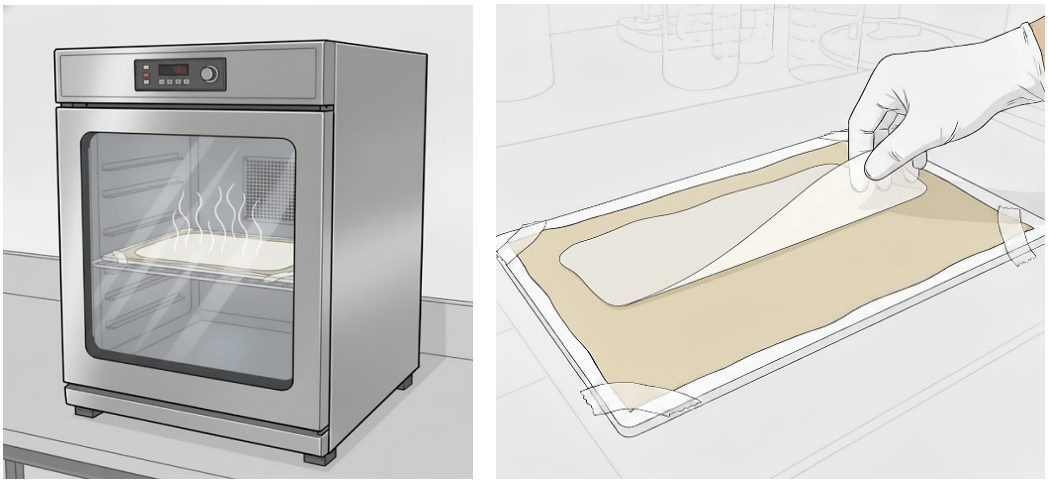

Figure 2.13. After rod-coating, (left) the rigid support with PTFE and the wet film is put into a ventilated oven; later, (right) the dried film is peeled off the PTFE substrate.

The films with only organic content were named as aP/bS, with a and b being respectively the %w/v of P and S in the neat aqueous formulations. Instead, the films with zeolite additives were named as aP/bS+cA or aP/bS+dX, with c and d being respectively the A content and the X content, both %w/w of total polymer blend, in the PVA-based aqueous formulations comprising zeolite additives. Before further characterizations, all films were stored in a desiccator at room temperature for some days. Using a digital micrometer, provided with a 1µm resolution, the films' average thickness was measured to be 20 µm for each film.

Selection of the optimized formulations

The core aim of this section was to rationally choose the PVA-based aqueous formulations that would have been suitable for a homogeneous dispersion of zeolite additives inside the organic matrix. Uniform dispersion of inorganic micro-fillers in polymer films increases stiffness and can maintain or tune toughness by improving stress transfer at the matrix–filler interface [312]. It reduces shrinkage and lowers the coefficient of thermal expansion, improving dimensional stability in service [313]. Also, gas and vapor permeability can be cut by one or more orders of magnitude when filler orientation is good [314]. Therefore, preliminarily, it is needed to understand what the physics is behind the additivated film formation.
The kinetics of two concurring phenomena determine the final dispersion of micro-zeolite fillers in the processing of the PVA-based films produced via casting: zeolite

sedimentation; drying along with film formation [101,105]. Zeolites, due to their unsolubility and to their higher density, will tend to sediment in the water-based additivated formulations, which are indeed unstable dispersions after mixing. The kinetics of zeolite sedimentation are determined essentially by the viscosity of the aqueous formulation (directly related to the polymer concentration) and the particle size of zeolites [315]. Particularly, the sedimentation rate of insoluble inorganic additives in aqueous polymer formulations can be described by Stokes' law, here shortly reported as $v \propto r^2 \eta^{-1}$, where v is the terminal settling velocity, r is the effective hydrodynamic radius of the additive (it can be related to the additive particle size), and η here is the dynamic viscosity of the polymer formulation. Because η appears in the denominator, the lower the formulation viscosity, the faster zeolites will then sediment to the bottom; any elevation in polymer concentration that raises the viscosity produces a decrease in v, thereby prolonging the residence time of the particulate phase in suspension and retarding observable sedimentation [316,317]. Nevertheless, operating on the viscosity of the formulation is something also needed on a practical level in general, even without zeolite additives that may sediment. A very low-viscous, water-like formulation cannot be appliable for rod-coating as it would easily slip away of the substrate with just a minimum slope, and the only way to apply it would be for simple pouring on either an open substrate (like a PTFE film) or a confined substrate (such as a PTFE evaporating dish), with sequent little control on the thickness, and just permitting film production [101,113]. In this study, thin films are produced after peeling off from PTFE; still, it was thought that these formulations could have been employed also as coatings on films such as polyolefins or paperboard, therefore it is wanted to grant a formulation provided with high viscosity, which is suitable for rod-coating, giving reliable and repetible results, both for film and coating applications.

Before going on, it was worth discussing briefly the parameter *r*. The average particle sizes of the supplied zeolites 4A and 13X are comparable (2-3 μm), and none of them was ground further to reduce the particle sizes: this would have surely allowed for lower polymer concentration in the final formulation, but it was chosen to use each zeolite as-is to ensure the same or comparable initial granulometry. Therefore, *r* is not an operational parameter here to slow down sedimentation; the

zeolite dispersion in the films was improved by only increasing the viscosity of the formulation, and so increasing the PVA concentration in the aqueous formulation. The other aspect to consider, in order to achieve a homogeneous zeolite dispersion in the film, is related to the process itself of rod-coating, along with drying and film formation. Working on the formulation itself, indeed, is not enough: it is obviously required that the zeolite sedimentation is slower, much slower, than the film formation after rod-coating [101]. This is surely achieved by increasing the viscosity of the formulation (and so the polymer concentration), as already discussed, but also allowing for a fast drying process, to let the film form rapidly in time before zeolite sedimentation, keeping the initial homogeneity obtained after mixing the formulation. Two main parameters are involved in the kinetics of film formation with the rod-coating on PTFE: wet thickness (directly related to the final dry film thickness) and drying temperature of the film. Besides valid motivations that regard material saving, low wet thickness allows for fast drying and so fast film formation [101,105,318]. Thin polymer films (and layers in general) are something that rod-coating easily allows to obtain in a controlled manner, compared to casting of liquid-like formulations. The wet thickness, fixed by a specific coating bar, was not a parameter for this study. Finally, drying temperatures of the wet film are important as well: a higher temperature in the oven means shorter evaporation time and faster film formation. It is, however, crucial to pay attention at very high temperatures that may impact on the final properties, as the film will tend to have more surface defects [118,319]. Vacuum-drying would be a valid method to avoid high temperatures and still have films with good quality; however, this would be limited to a lab-scale level [320]. Instead, in the present study, the aim was to actually emulate (at best) the film processing at an industrial scale, in which packaging substrates are coated at high rates, high temperatures, and, of course, in an open environment.

PVA-based aqueous formulations with zeolite additives were prepared by changing different parameters in order to optimize material usage and the processing conditions. In other words, it means finding the combination of the minimum amount of polymer basis in the formulations (linked to the minimum viscosity required to make zeolite sedimentation much slower than film formation), the

minimum drying temperature, and the maximum film thickness (to speed up drying), in order to grant a homogeneous dispersion of zeolite additives inside the PVA-based films. The goodness of the additive dispersion was evaluated, as already disclosed, by means of ATR-FTIR. Particularly, after a film with specific formulation and processing conditions was prepared and peeled off the PTFE substrate, ATR spectra were recorded for both sides of the film. The method demanded that the spectra for both the face touching the plate (hereafter called 'down') and the face exposed to direct air drying (hereafter called 'up') had to be as coincident as possible. The focus was particularly on the region around 968/962 cm^{-1} (corresponding to the main zeolites' characteristic peak and a local minimum absorbance for the organic materials). After spectra normalization, it can be predicted (and then tested) that the absorbance of the 'down' side of a certain film has to be either higher than to that of the 'up' side in that region, due to higher presence of zeolites at the bottom if a certain level of sedimentation occurs, or tending to be comparable, if film formation is much faster and this allows to original dispersion of the aqueous formulation to be preserved in the final dried product all over the film thickness. The aim was then to get spectra for 'up' and 'down' sides the most similar possible, by optimizing conditions – taking spectra on more points, even if not shown hereafter, to ensure the goodness of the test. The proposed method represents a very fast, reliable, easy, and repeatable way to assess the additive dispersion in the film.

Due to the high amount of parameters, these preparatory tests were conducted by fixing the coating bar – and so, the wet thickness linked to the bar thread. The starch concentration (2%w/v), the glycerol plasticizer relative contents (10%w/w of PVA + 10%w/w of starch), and the inorganic additive conditions were fixed as well. Particularly, only 13X zeolite was employed, assuming a similar behaviour for 4A zeolite – considering overall comparable densities and particle sizes; also, in order to be on the safe side and ensure a good dispersion also for lower concentrations, the additive concentration in this study was 5 wt%, a little higher than the 2 and 4 wt% of the final films to be produced. Therefore, only the PVA content and the drying temperature as parameters were changed to achieve a film with sufficient zeolite dispersion. Although the ATR-FTIR spectra were recorded for the whole

medium infra-red spectrum from 4000 to 600 cm^{-1}, the following analyses have focused on a narrower wavenumber range in the fingerprint region, since the most important region is related to the zeolite's peak at around 950 cm^{-1}. To highlight its contribution, the 13X spectrum is going to be shown as well in all the next analyses. First attempts, therefore, focused on increasing the concentration of PVA in water, starting from 10%w/v – which appeared to be the one that allowed for a minimum viscosity to be useful for rod-coating, whereas lower concentrations were too liquid-like; the films were instead initially drying with an oven temperature of 65°C, keeping them in the oven for almost one hour to grant full evaporation. In Figure 2.14, the spectra for both 'down' and 'up' sides of films obtained by formulations with 10%w/v, 12%w/v, and 15%w/v are reported. Big differences can be noted in the region around 950 cm^{-1} due to zeolite 13X. Particularly, as expected, at lower PVA concentrations – and so at lower formulation viscosities – the two sides of the films tend to be more different, with the 'down' side presenting a higher zeolite content. As PVA content and viscosity increase, the two sides tend to be much more similar, reducing the differences in zeolite contents, for the reasons described earlier that predicted this behaviour.

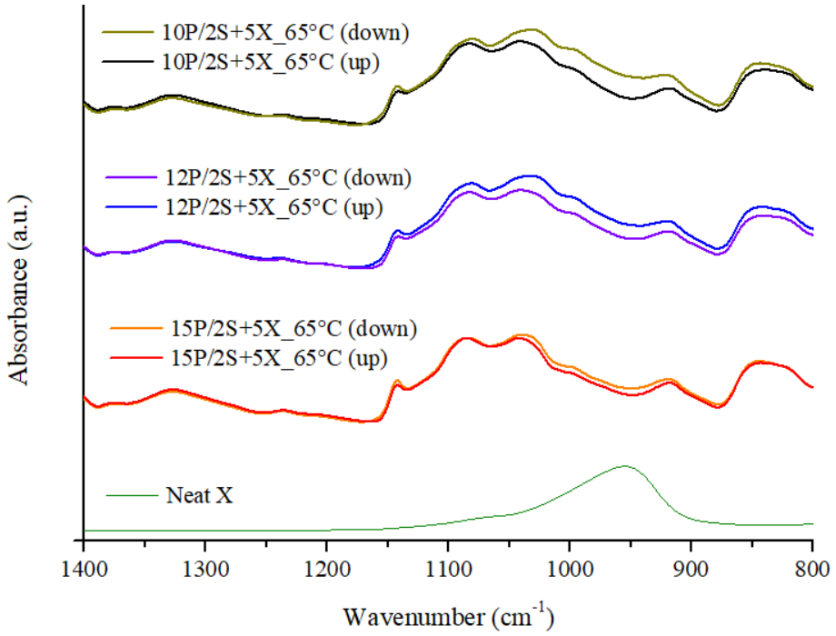

Figure 2.14. ATR-FTIR spectra on both sides of the following films after drying in an oven at 65 °C: 10P/2S+5X, 12P/2S+5X, 15P/2S+5X – same zeolite concentration in the formulations but different PVA content and viscosity. The spectrum of the pristine zeolite X powder is also added as a reference to highlight its contribution at 950 cm^{-1}.

The spectra of the two sides of the films become even more similar with a further increase in PVA, particularly for the formulation 18P/2S+5X. This is shown in Figure 2.15, along with a reference spectrum of a neat film obtained by the same polymer formulation but without zeolite to underline the impact of the additive on that specific region of the FTIR spectrum. It is worth noting that the mentioned PVA-based aqueous formulation showed both a good mixability (even at room temperature) and an excellent spreadability for rod-coating applications, which means its viscosity was balanced.

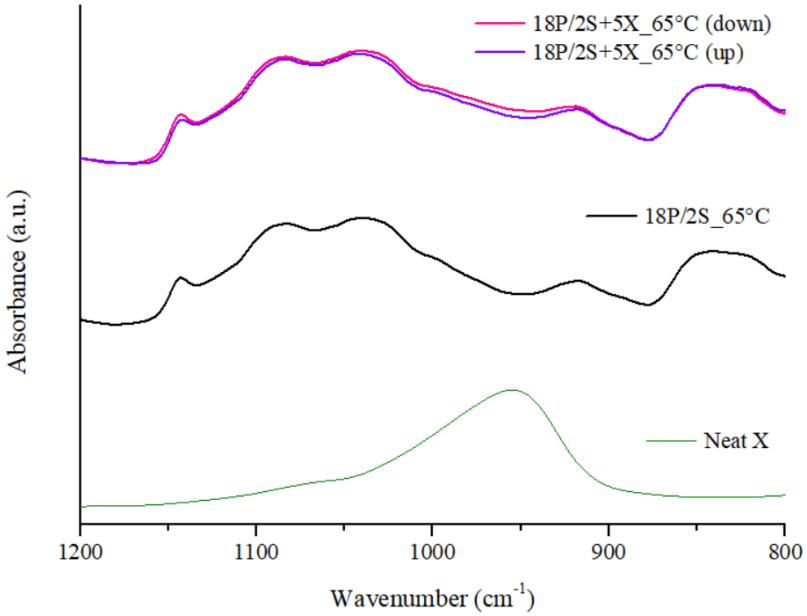

Figure 2.15. ATR-FTIR spectra of the following films after drying in an oven at 65 °C: 18P/2S (only one side is shown), 18P/2S+5X on both sides. The spectrum of the pristine zeolite X powder is also added as a reference to highlight its contribution at 950 cm^{-1}.

Since the spectra do not tend to overlap yet, the dispersion can further be enhanced. Still, the total polymer content in the aqueous formulation cannot be increased arbitrarily for two operational reasons. First, PVA is surface-active; its aqueous formulations trap air during mixing/stirring: hydrogen bonding between chains increases solution elasticity, which slows bubble coalescence and rise. The relatively high viscosity at useful concentrations further stabilizes entrapped air. Therefore, the bubble formation during the preparation of the formulations strongly increases with higher polymer content, and this would have required other methods for degassing. Second, at very low concentrations, the formulations behave close to

a Newtonian fluid, with viscosity growing roughly linearly with polymer concentration. In concentrated or gel-like regimes – as the ones described up to now – flow becomes strongly non-Newtonian and the viscosity grows rapidly with even small concentration increases. So, the viscosity of the formulation also dramatically increases at very high polymer concentration, making the mixing difficult and unreliable even at high temperatures, but also returning a PVA-based formulation that, even without zeolite, cannot be properly managed once cold.

Starting from the previous formulation, the other process parameter was changed: the oven temperature was increased from 65°C to 100°C, in order to speed up water evaporation and consequent film formation. It is worth noting that the set temperature inside the oven does not surely represent the temperature at which the film gets at completely dries; in other words, the ventilated oven may be set at 100°C, but water evaporates before the final films can reach said temperature. The PTFE substrate's low thermal effusivity also prevents the bottom interface from rising quickly, so the temperature gradient across the liquid relaxes on a timescale that is comparable to the evaporative mass-loss rate. Under these conditions, the water phase disappears completely in a matter of 1-2 minutes, while the volume-averaged temperature is still considerably below the surrounding air temperature; thus, the phase-change process and the film formation are concluded before the sensible energy required for boiling water can be delivered. This means that the process is surely sped up under these conditions, still with the risk of reducing the quality of the films compared to a process in which film formation occurs slowly; still, water is not allowed to boil, and this prevents the formation of visible bubbles on the surface of the films.

In Figure 2.16, it is possible to highlight the combined effect of chosen formulation/ viscosity and drying temperature on the film properties: the differences between the 'up' and 'down' spectra have been practically flattened. This suggests that the composition of both surface sides is essentially the same (besides statistical errors on a micron-scale), and so it has to be along the film thickness: a certain homogeneous dispersion of the zeolite additive was finally achieved. In the graph, also in this case, the spectrum of the film obtained from an analogous polymer formulation but without zeolite additive can be observed as a reference.

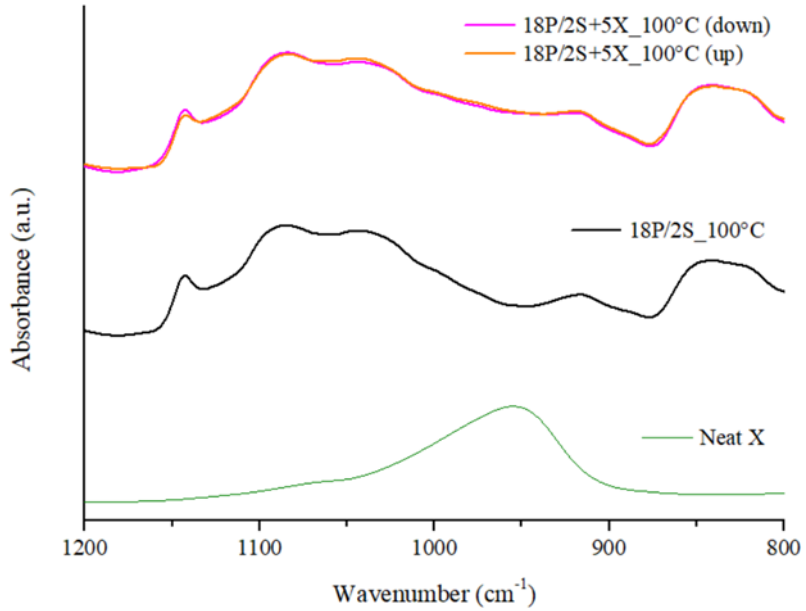

Figure 2.16. ATR-FTIR spectra of the following films after drying in an oven at 100 °C: 18P/2S (only one side is shown), 18P/2S+5X on both sides. The spectrum of the pristine zeolite X powder is also added as a reference to highlight its contribution at 950 cm^{-1}.

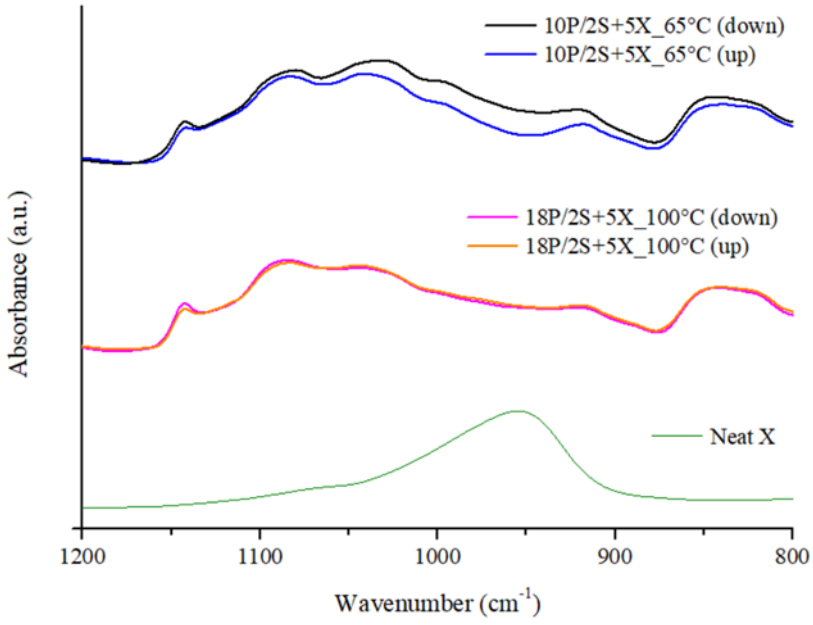

Figure 2.17. ATR-FTIR spectra on both sides of the following films after drying in oven: 10P/2S+5X at 65 °C, 18P/2S+5X at 100 °C. The spectrum of the pristine zeolite X powder is also added as a reference to highlight its contribution at 950 cm^{-1}.

The starting and ending point of the followed trial-and-error route is shown in Figure 2.17, which allows for a final recap. It is possible to appreciate the impact of the chosen combination of formulation viscosity and drying temperature on the achievement of the filler dispersion. Nevertheless, the processability of the formulations was increased from the 10P/2S to the 18P/2S polymer composition.

Overall, fixed all the other parameters, the optimized combination of formulation and processing conditions that allowed for a homogeneous dispersion of zeolite additives in the films was therefore established to be an 18P/2S organic basis in the aqueous formulation, to be then additivated with either 13X zeolite or 4A zeolite at 2-4%w/w with regard to polymer content, and employing a 105°C ventilated oven for the drying of the wet films after rod-coating. For the upcoming studies, it is worth noticing that the same drying conditions have also been employed for the analogous neat formulations without zeolite, in order to have a fair comparison under the same processing conditions. Besides zeolites, in order to better evaluate the impact of starch additive as well, formulations comprising only PVA and glycerol as organic content were prepared. The choice was to keep the same global polymer concentration in water, namely 20%w/v, for coherent comparison, which implies, in the present study, preparing film formulations with either 20P or 18P/2S as polymer bases, with or without zeolite additives.
A summary of the nomenclature for the films that have been studied henceforth is reported in Table 2.1.

4A

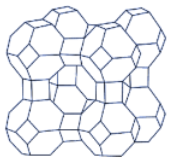

13X

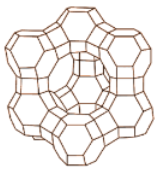

P/S / Zeo	100% P	90% P / 10% S
0%	20P	18P/2S
2%	20P + 2A 20P + 2X	18P/2S + 2A 18P/2S + 2X
4%	20P + 4A 20P + 4X	18P/2S + 4A 18P/2S + 4X

Table 2.1. Nomenclature of the PVA-based films according to their solid content. Zeolite is expressed as wt. % of total polymer basis, which is the same for 20P and 18P/2S films.

Photographs of the ten different thin PVA-based films (with a common background) are finally shown in Figure 2.18. It can be appreciated that all thin films are highly transparent regardless of the presence of starch and zeolite additives. Still, 18P/2S+4A and 18P/2S+4X films have a slightly lower transparency than others: this behaviour could be expected as these films both comprise starch presence and the highest zeolite concentrations.

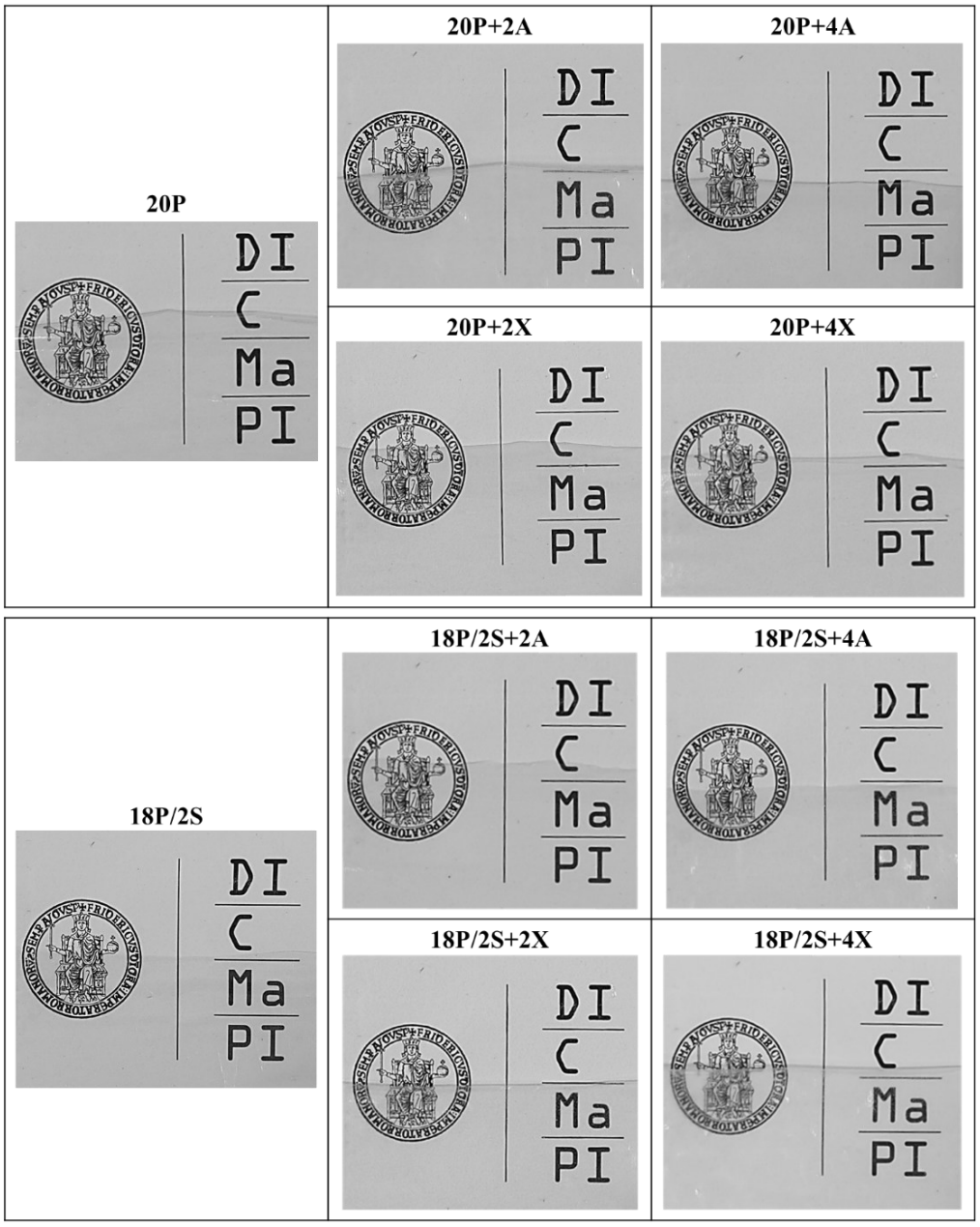

Figure 2.18. Photographs of the ten different thin PVA-based films.

A comparative study on the transmission FT-IR spectra of 20P and 18P/2S thin films (Figure 2.19, limited to the fingerprint region) is now presented to highlight the interactions among the different organic components.

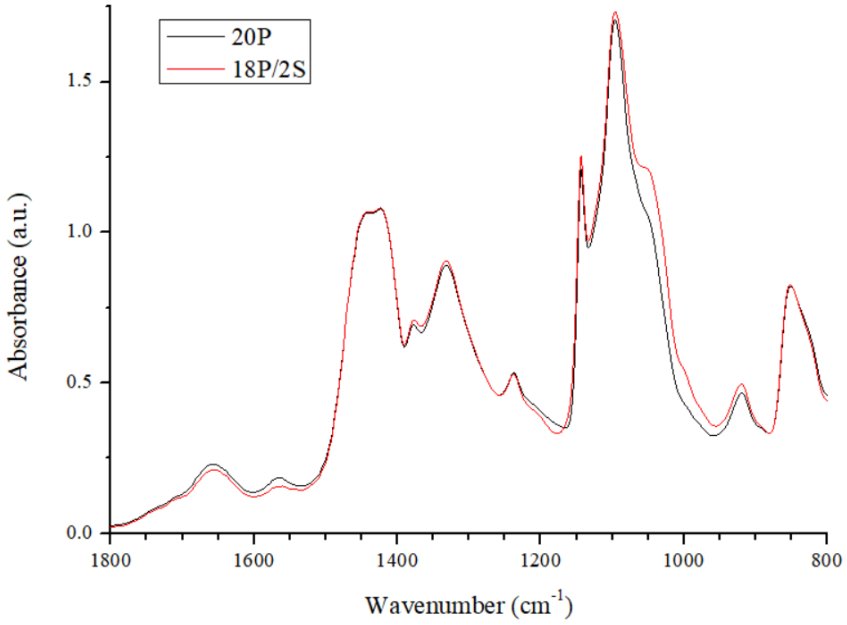

Figure 2.19. FTIR transmission spectra (fingerprint region) of 20P and 18P/2S films.

The magnitudes of the absorption bands observed indicate that the films are sufficiently thick to yield strong signals but not so thick as to completely saturate the detector. Focusing on the fingerprint region, there is no significant shift in the PVA-specific peak positions but just intensity modulations (as bands are now partly merged with starch signals). This suggests the little starch inclusion does not drastically alter PVA's bonding environment. Notably, a shoulder band at ~1020 cm^{-1} is now present in the blend, deriving from starch's C–O stretching vibrations in the glucose ring (anhydroglucose unit). Both PVA and starch have strong absorbances in the 1150–1080 cm^{-1} range, but their contributions differ. Starch extends the band above 1150 cm^{-1} (due to glucosidic C–O–C vibration) and also adds a shoulder contribution at the 1080 cm^{-1} region (C–O stretch of the polysaccharide). This indicates that the PVA's structural order is largely preserved even with starch added. Both spectra show a comparable O–H bending band of absorbed water around 1640–1650 cm^{-1}, since both PVA and starch are hygroscopic. It is worth noting that glycerol plasticizer has IR bands, but since its content is the same in both samples, it does not cause differences between the two spectra.

Before going further, it has to be discussed the reason why the same studies regarding additive dispersions were not carried out as well on the different 20P formulations. PVA formulations develop very high viscosity because of chain entanglement and hydrogen bonding. Starch, on the other hand, contributes less strongly per unit mass: it has branched or shorter chains, weaker entanglement, and lower intrinsic viscosity. Replacing part of the PVA with starch lowers the effective overlap and entanglement density, so the mixed system is less viscous even if the total polymer weight fraction is the same. Therefore, since it was evaluated that the 20P would be a little more viscous than the mixed 18P/2S, this would have been further beneficial for the homogeneity of the final zeolite dispersion.

3. Results and discussions

3.1 Pristine films' properties

Surface morphology

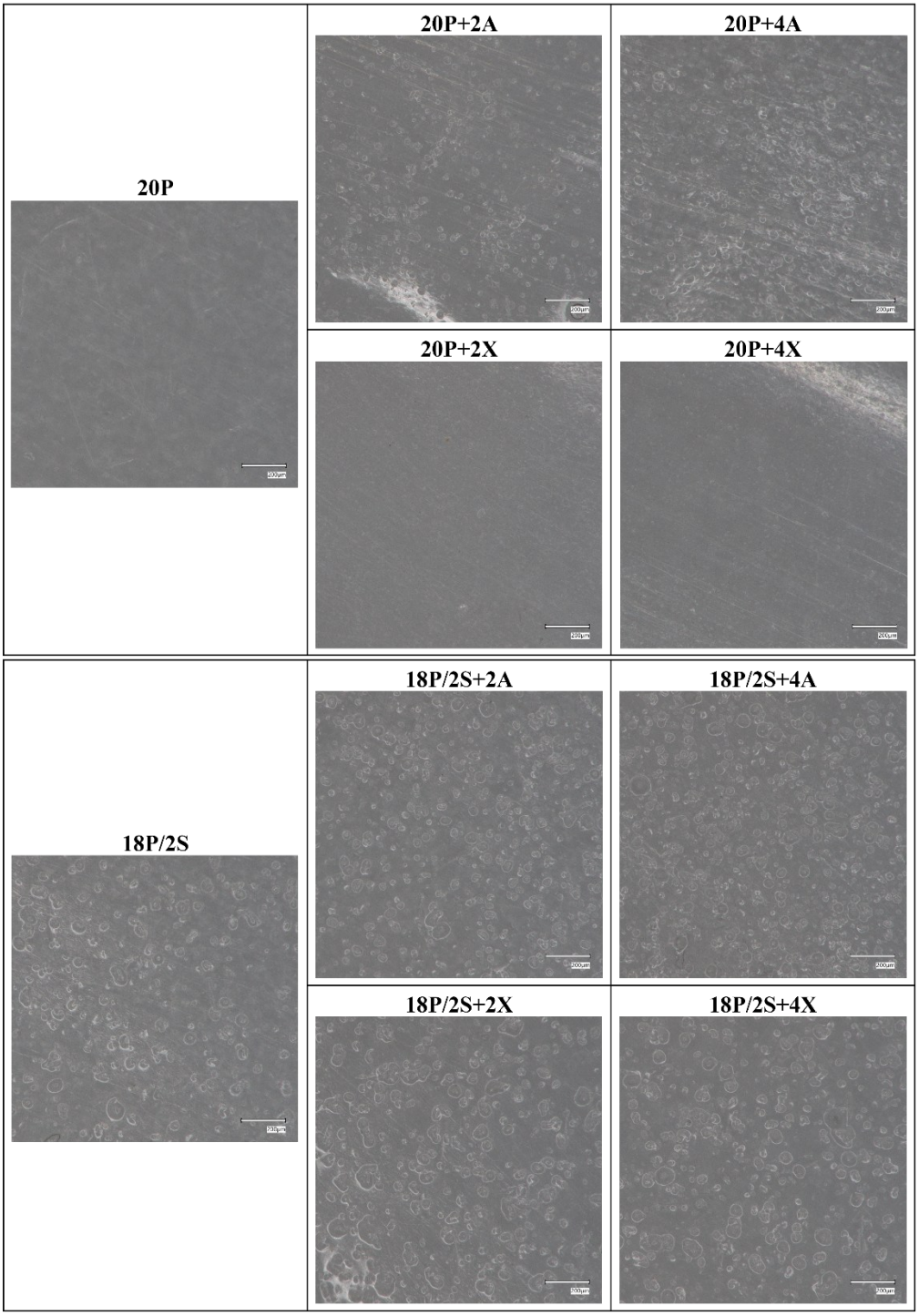

Figure 3.1. Optical micrographs (x200, scale bar 200μm) of the different pristine films.

All films are continuous and free of macroscopic defects, and they appear uniform either at visual inspection or optical microscopy at low magnification (50×, for which micrographs are not reported), with only faint casting artifacts (e.g., slight striations or glare) of the films. Instead, images at 200× magnification reveal clear differences in surface morphology depending on film composition (Figure 3.1).

The 20P film forms a smooth, homogeneous surface. Under optical microscopy, it appears essentially featureless – no visible particles or phase separation, just a continuous matrix. In contrast, introducing a small amount of starch as PVA replacement leads to a subtly less uniform morphology. Starch and PVA are not fully miscible at the microscopic scale: even in hot-water mixing, starch does not dissolve completely – small agglomerates can still persist, mainly if blending efficiency is limited by high formulation viscosity. These phenomena can cause local discontinuities or even trapping tiny moisture/air pockets that finally dry into more 'voids' or low-density halos with local shrinkage. After all, no large aggregates are evident (starch is well distributed, the film remains macroscopically uniform) [246]. Both films are otherwise continuous and free of cracks (glycerol plasticizer ensures flexibility), indicating good film formation in both cases.

Adding micro-zeolite particles changes the morphology as well, as it can be observed from optical micrographs. Particularly, in the 20P+Zeo A images, numerous ring-like features are clearly visible across the surface; by contrast, the 20P+Zeo X images have far fewer visible defects – their surface texture remains nearly as smooth as the base 20P film. The difference is especially obvious at the higher loading. During solvent casting of PVA-based films, water evaporation causes significant polymer shrinkage. In the vicinity of zeolite, which is very hydrophilic and can retain water and locally delay drying, the polymer may de-wet or pull away slightly due to shrinkage stress, leaving tiny halos. Still, a possible explanation for the different behaviour of A and X, which can only be observed clearly in 20P-series films, can be provided. Even with comparable particle size and film thickness, zeolite 13X interacts with PVA/glycerol more "continuously" (glycerol and water can access its larger FAU pores), desorbs faster, and presents less angular geometry, so interfaces remain better wetted and less stressed during

drying [321]. Zeolite 4A's tighter pores and specific morphology may favor interfacial stress and drying defects.

As concerns the 18P/2S-series films, the A-filled samples might exhibit a slightly higher density of defects compared to the X samples, but the contrast is not as pronounced as it was in the pure 20P series: starch addition in this case is mainly responsible for these surface defects. SEM micrographs were recorded, but only for 18P/2S+4X with four different magnifications (Figure 3.2), as this film formulation comprises both starch and zeolite (assuming similar behaviour for A and X) and already helps in understanding the expected morphological behaviour of the other films. The surface defects explained above are better visible in the x250 magnification SEM micrograph.

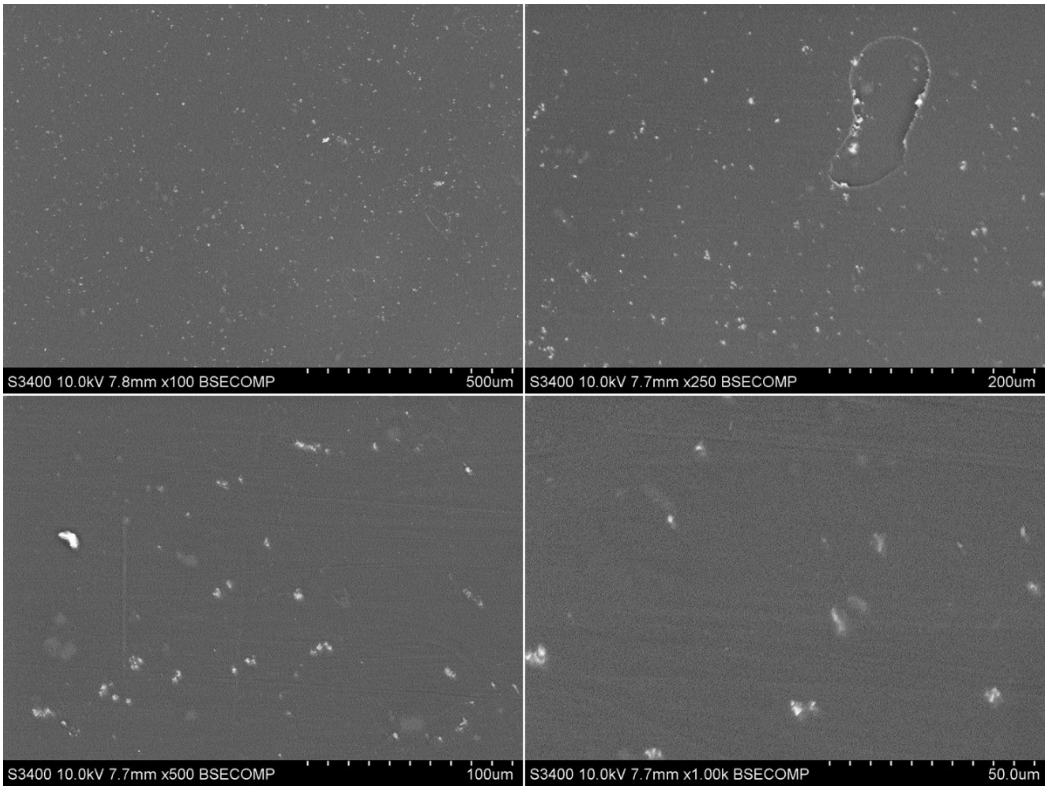

Figure 3.2. SEM micrographs of the pristine 18P/2S+4X film at different magnifications (up to x1000, scale bar 50 μm).

Notably, under optical microscopy, very small dots can be slightly observed in the 20P+zeoX films – they are present in the other films as well, but less visible with optical micrographs since they are covered by the polymer films' surface defects. These dots represent indeed the micro-inorganic additive [322].

Once again, the recorded SEM micrographs are a very powerful tool thanks to the provided contrast, even if just for 18P/2S+4X film. White dots can be seen at all magnifications on the grey surface, and their size (which can ultimately be better appreciated in the 1000x magnification) is consistent with zeolites' granulometry of 2–3 μm. Besides the zeolites, some light-grey regions can be observed: they possibly represent random little regions of agglomerated starch that may not have blended properly into the matrix, contributing to the overall surface defects [322].
A final and important consideration regarding the SEM micrographs is that zeolites are evenly distributed all over the surface of the 18P/2S+4X film (and reasonably so of the other zeolite-containing films). This beyond confirms the outcomes of the study in paragraph *2.3 Preparation of the films* (Chapter 2), in which zeolites' good dispersion through the film thickness was confirmed via ATR-FTIR on both sides of the films: SEM images (mainly x100 and x250 magnification) show that zeolites have not sedimented at the bottom, and a high dispersion was provided.

Thermal stability

A minor weight-loss step at low temperatures (~150 °C) is observed in all films, attributed to loss of residual moisture and initial decomposition of glycerol.
The reference 20P film shows a principal DTG peak at around 280–290 °C under N_2. This corresponds to the rapid decomposition of the PVA matrix (accompanied by glycerol's volatilization), and is relatively low for a fully hydrolyzed PVA due to the plasticizing effect of glycerol [323]. Particularly, this formulation shows a two-step degradation: initial chain scission/dehydration around 280 °C (which dominates the 20P film's decomposition), followed by a shoulder after 310 °C, then a smaller secondary weight-loss at higher temperature (above 400 °C) from charred residue breakdown. It is worth noting that the glycerol-plasticized PVA film exhibits a lower thermal stability than the pristine PVA powders, which – besides the little peak at 280 °C – showed its main degradation peak at 336 °C. This is the consequence of molecular-level changes that glycerol introduces in the PVA matrix. Glycerol sits between PVA chains, breaks hydrogen bonds, and lowers the apparent activation energy of the rate-determining dehydration/depolymerisation steps, leading to a peak at lower temperatures [244,323]. Anhydrous glycerol itself

decomposes at around 240°C (with onset at around 160 °C), as described earlier, and this may further slightly shift the degradation peak of the blend material to lower temperatures.

Introducing just a small amount of starch (sample 18P/2S, with PVA/starch=90:10) markedly increases the thermal stability of the film, as shown in Figure 3.3. The main DTG peak of the PVA–starch blend occurs at ≈340 °C, a significant shift (~+60 °C) to a higher temperature compared to 20P. The improved stability can be explained by strong intermolecular interactions, which in turn can "lock in" the polymer network and make thermal degradation more energy-demanding. In essence, starch reinforces the matrix through physical bonding, restricting the segmental motion of PVA chains and raising the decomposition threshold [324]. In the blend, the starch and PVA likely decompose in an overlapping process. Notably, no new distinct DTG peak appears for the starch (as its fraction is low); instead, the interactions yield the visible single broad peak around ~340 °C. Thus, even a small starch content in our films has a stabilizing effect for PVA/glycerol films, elevating the temperature at which maximum weight-loss occurs.

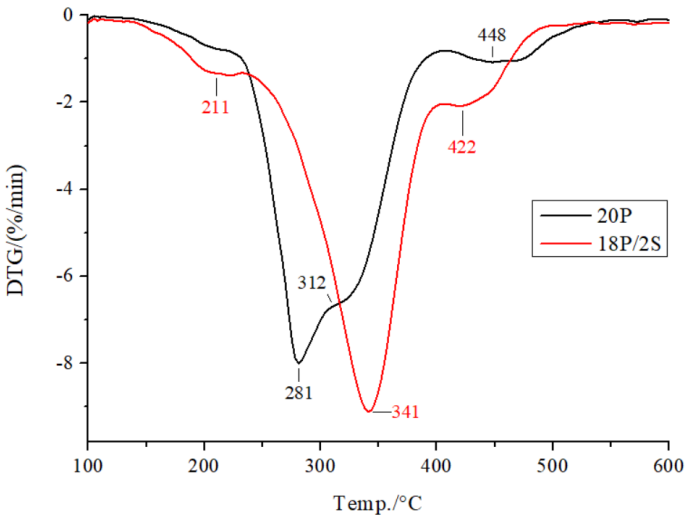

Figure 3.3. DTG analysis of 20P and 18P/2S films in N_2.

Adding microporous zeolites at 2–4 wt% in the 20P films also alters the thermal degradation behavior significantly, with the main DTG peak shifting to higher temperatures. For instance, with 4% zeolite 13X (20P+4X), the main degradation peak occurs around 340–345 °C, compared to ~280 °C in the neat film – an increase of over 60 °C. Even 2% of zeolite 4A or 13X raises the peak to the low-300 °C

range. This pronounced shift signifies that the polymer matrix becomes more thermally stable in the presence of the zeolites. Notably, the zeolites themselves do not decompose in this range: zeolites 4A and 13X are crystalline aluminosilicates that are stable well above the reported temperatures, as shown in paragraph *2.2 Components' analysis* (Chapter 2). Any minor weight loss from zeolites (i.e., release of adsorbed water in pores) occurs with a peak at ~180 °C (as shown earlier, excluding a minor contribution at ~340 °C for zeolite 4A) and is anyway too small at 2–4% filler loading to produce a visible DTG peak. Therefore, the changes in the DTG profile are effectively due to matrix–filler interactions and related thermal effects, rather than the zeolites' own degradation. In the zeolite-filled 20P films, a more complex two-step degradation can be observed: a small shoulder or secondary peak remains near ~270–280 °C, but a new dominant peak emerges at higher temperature (~320–340 °C). This suggests that a portion of PVA still degrades at the usual lower range (perhaps free chains or plasticizer-rich regions), but a substantial fraction is indeed stabilized until higher temperatures – likely those polymer segments in close contact with the zeolite. The inorganic filler acts as a thermal stabilizer in several ways. First, PVA chains can hydrogen-bond to the zeolites [324], anchoring the polymer and hindering rapid chain scission. Such filler–matrix bonding elevates the energy required for decomposition, as seen similarly with other nanofillers [325]. Second, the zeolite may absorb heat, slowing the breakdown of the polymer. An increase in degradation temperature upon adding zeolites is a known phenomenon in polymer composites [326]. So, both zeolite 4A and 13X enhance the thermal stability of the films, but zeolite 13X tends to impart a slightly greater effect than 4A at the same loading. For instance, at 4% filler in pure PVA films, 13X shifts the peak to ~344 °C, whereas 4A shifts it to ~330 °C (still a large increase over 280 °C, but ~10–15 °C lower than 13X's effect). This difference may be attributed to the intrinsic properties of the two zeolites. Zeolite 13X (FAU structure) has larger pore channels and higher adsorption capacity than 4A (LTA structure). It can host more small molecules (water, glycerol, volatile fragments) within its pores and on its internal surface. Thus, 13X might more effectively sequester plasticizer or early decomposition products and better interact with polymer chains, delaying the onset of rapid mass loss. Zeolite 4A, with smaller

pores, primarily adsorbs water; its impact on the polymer matrix is present but somewhat more limited.

A similar trend is seen in the starch-containing films. The 18P/2S base mainly degrades around 340 °C, as starch presence had already raised the degradation range. Adding 4% zeolite 13X pushes the peak to ~360 °C, whereas 4% 4A gives ~344 °C. Generally, 4A addition did not dramatically change the thermal behaviour, whereas 13X provided an additional upward shift, indicating a real though modest synergistic stabilization. Again, no new decomposition peaks relative to the inorganic additives were observed. All changes in the DTG profiles – peak temperature shifts or changes in peak shape – can therefore be interpreted as additional interaction effects rather than simple separate additive degradation.

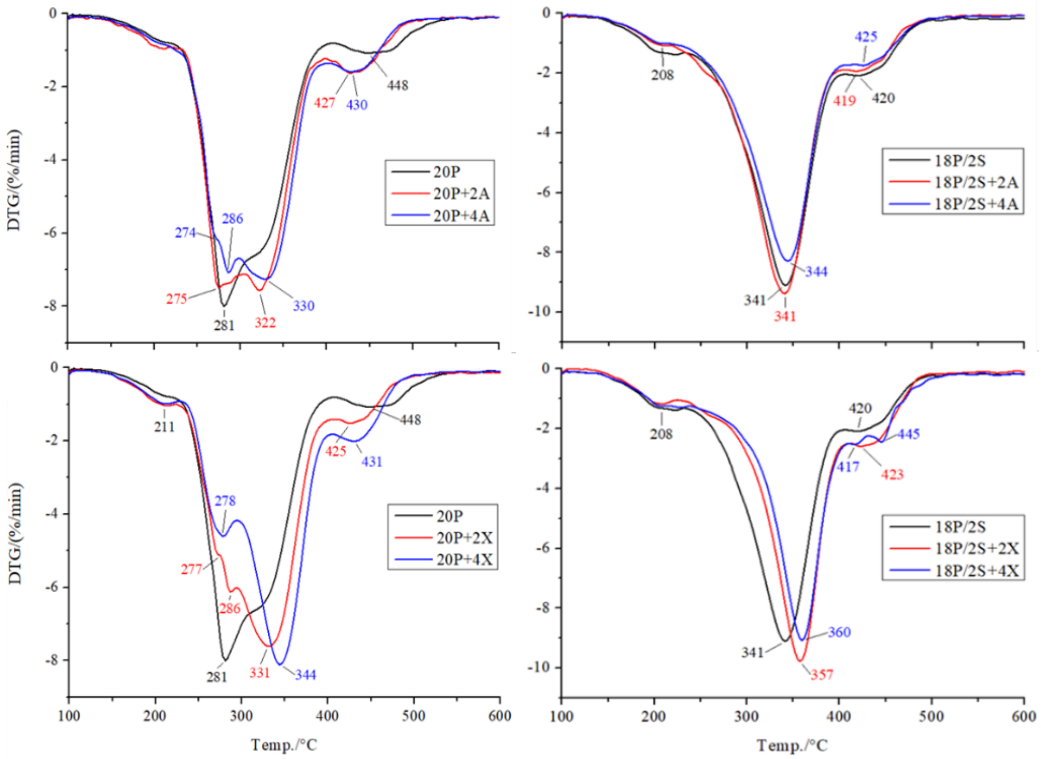

Figure 3.4. DTG analysis of the ten different films in N_2, particularly highlighting the contribution of a specific zeolite additive at different concentrations for a given matrix.

Degree of crystallinity

Processing history heavily affects peak visibility: if the same PVA granules are dissolved and recast, the crystals can be partially melted or reoriented, partially

changing the XRD peaks [327,328]. Also, glycerol plasticizer in all the films tends to reduce the overall crystallinity and contribute to these minor changes in peaks [329]. For instance, representative XRD patterns of the 20P and 18P/2S films are shown in Figure 3.5. Particularly for 20P (which is essentially just plasticized PVA), little peaks disappear from the pristine PVA powders' pattern (shown in Figure 2.5).

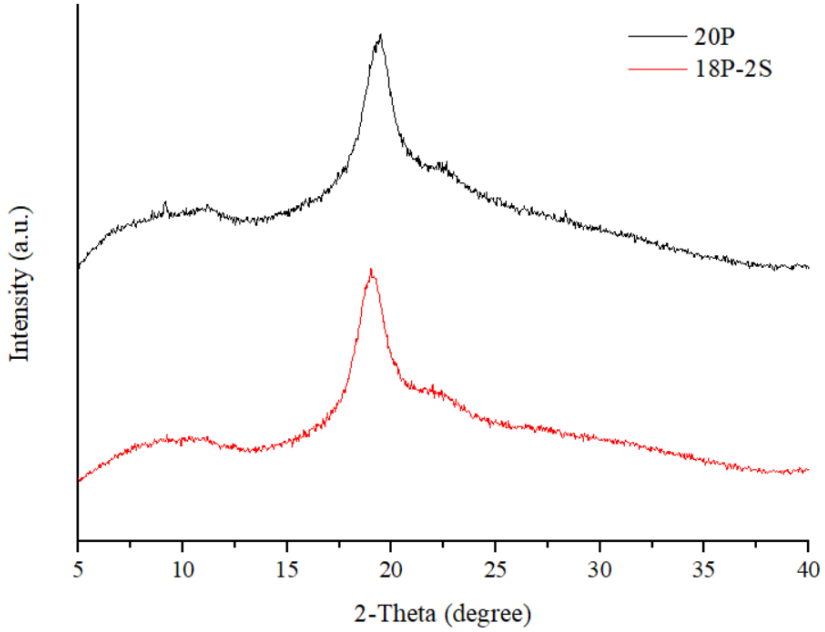

Figure 3.5. XRD patterns of the 20P and 18P/2S films.

The calculated XRD crystallinity indices of the ten different films (with relative margins of error over multiple calculations) are reported in Table 3.1.

Table 3.1. XRD crystallinity (X_c) of pristine PVA-based films (%)

20P	20P+2A	20P+4A	20P+2X	20P+4X
10.4 ± 1.8	8.0 ± 1.1	12.8 ± 2.0	8.8 ± 0.4	13.7 ± 1.1
18P/2S	18P/2S+2A	18P/2S+4A	18P/2S+2X	18P/2S+4X
10.4 ± 1.6	10.8 ± 1.9	8.6 ± 1.5	10.4 ± 1.0	10.8 ± 1.9

Incorporating a small fraction of starch into PVA had minimal impact on the overall crystallinity of the cast films. The 20P film showed a certain degree of semicrystallinity (~10%), similar to that of 18P/2S film (essentially no relevant changes within experimental error). This may be due to the low content of starch: when larger amounts of starch are blended, the crystallinity of the composite tends to decrease due to hydrogen-bond interactions in the blend that disrupt the regular

packing of each polymer's chains and therefore reduce crystallinity [330]. In the present study, the starch content was relatively low, so any reduction in PVA crystallinity was too subtle to rise above the margin of error.

Adding micro-zeolite particles into 20P films had a concentration-dependent effect on PVA crystallinity. In 20P+2A and 20P+2X, the crystallinity index actually decreased slightly compared to neat PVA (although a few percentage points lower). This suggests that a small amount of filler can hinder polymer chain packing – likely by introducing heterogeneities and restricting chain mobility – thus slightly reducing the crystalline fraction [331]. In contrast, for higher loading, 20P+4X and 20P+4A showed higher polymer crystallinity than the neat polymer. This trend is consistent with zeolite acting as a nucleating agent when present in sufficient quantity: the numerous particle surfaces can facilitate the nucleation of PVA crystallites during film drying, yielding enhanced overall crystallinity. So, 4% zeolite appears to cross the threshold where nucleation effects dominate over any mobility restriction, leading to modest crystallinity increases in 20P films. Notably, zeolite type made a difference: 13X-filled PVA film showed a slightly higher crystallinity index than 4A-filled PVA at equal loadings. Zeolite 13X, with its higher surface area, might induce more effective PVA crystal nucleation, whereas zeolite 4A might interfere a bit more with chain ordering at comparable loading [332].

As concerns the 18P/2S-series films, the crystallinity of the pristine films remained in the same general range (~8–11%) and showed no large deviations with filler addition. Adding 2–4% of either zeolite 13X or 4A resulted in crystallinity index changes that were within experimental uncertainty (except one case, discussed below), so these fillers did not significantly change the crystallinity of PVA/starch blends. The PVA–starch intermolecular interactions dominate the structure, and a small filler content does not dramatically reorganize the polymer microstructure. One outlier was observed: 18P/2S+4A showed a somewhat lower crystallinity than 18P/2S. This suggests that a higher loading of zeolite 4A may have disrupted crystallite formation in the blend more than 13X did. Overall, for the pristine starch-containing films, the presence of zeolite fillers had a relatively minor effect on crystallinity (small enough to be within the margin of error), especially compared to the more significant effects seen in pure PVA films.

Water uptake

The 1-hour water uptake results (with a 130–188% weight gain range depending on the film samples) that are reported in Figure 3.6 can be explained by considering parameters like polymers' hydrophilicity, filler interactions, and microstructure.
As described earlier, PVA 99%+ hydrolysis degree is not as water-sensible as starch; therefore, starch addition made the films much more hydrophilic. Also, the original 20P's crystalline structure may have been slightly disrupted [243,333]. Thus the 18P/2S film absorbed ~188% water, higher than ~156% for pure 20P. The base 20P's moderate crystallinity limited its swelling. Wherever crystallinity was higher (due to polymer composition or filler-induced), water uptake would have dropped. Adding 4% of either zeolite cut down the water gain (e.g., from 156% down to ~130–142% in PVA-only films, similar effects on starch-containing 18P/2S films). The zeolite fillers act as non-swellable diluents and could restrict polymer chain swelling, occupying volume. Comparable studies with nano-fillers show 30–50% reductions in water absorption with just a few weight-percent filler [243], thanks to these effects. Still, no differences between zeolite types were highlighted in water uptake. Although it may be contested that in this case the minor 'water uptake' is indeed the weight of some zeolite leaving the system after polymer swelling in the liquid medium, the differences in weight with 20P and 18P/2S films are too high with respect to the small zeolite concentrations.

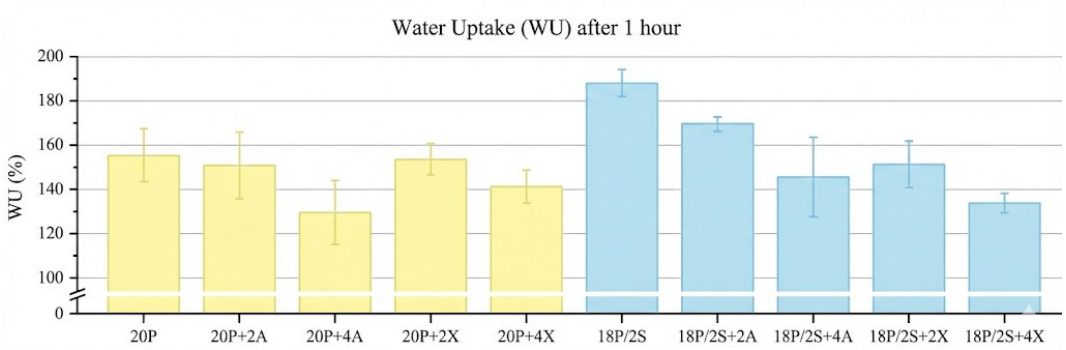

Figure 3.6. Water uptake after 1 hour of immersion in DI water for the 20P-series films (in yellow) and the 18P/2S-series films (in light blue).

Water vapor barrier

All the PVA-based films in this study showed very similar WVTR on the order of ~1000 g/m²·d at 40 °C and 40% RH (with only a few percent variation between formulations). In contrast, a non-polar PP reference film exhibited an order-of-magnitude lower WVTR (~136 g/m²·d), and an open cup (no film) showed extremely high evaporation (~4100 g/m²·d). These results are shown in Figure 3.7.

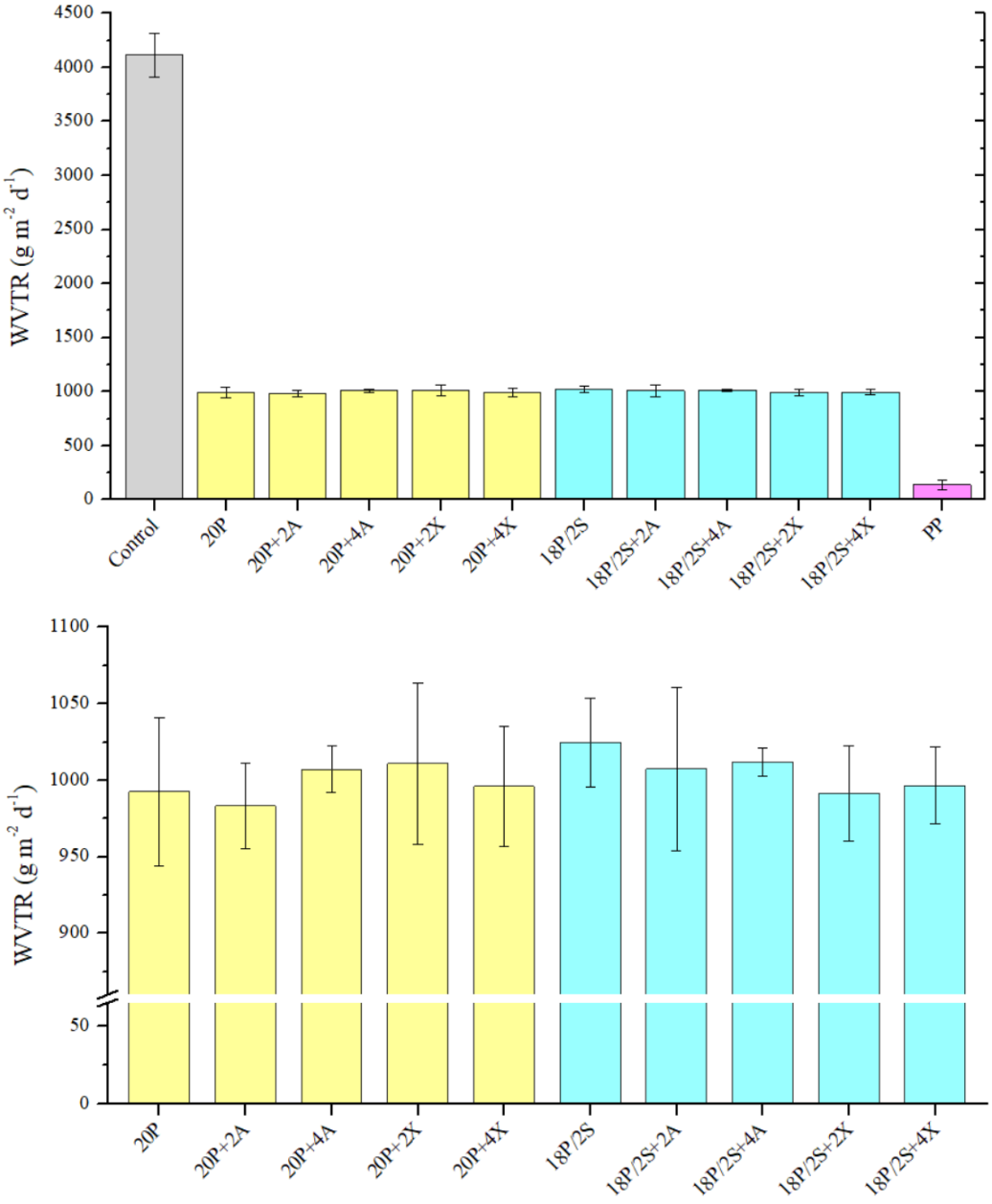

Figure 3.7. On top, WVTR (tested with the cup method at 40°C and 40% RH) for the ten PVA-based films, a commercial PP film, and the control cup with no film.
At the bottom, a focus on the results for PVA-based films only.

The minimal differences among the PVA films indicate that adding starch or zeolites did not dramatically alter the moisture barrier, which is largely governed by the PVA. Composition, crystallinity, and surface microstructure subtly influence WVTR, even if the effects in this case are slight.

Replacing a small fraction of PVA with starch (as from 20P to 18P/2S) introduces another hydrophilic component that tends to increase water affinity and permeability of the blend. Indeed, prior studies show that as starch content in PVA blends increases, water uptake and permeability rise correspondingly [334,335]. Starch disrupts the PVA matrix by interfering with PVA crystallinity, and this is important because crystalline regions are comparatively impermeable, forcing diffusing water to navigate around them [336]. Blending with starch slightly lowers the overall crystallinity of the films, as tested and shown earlier, thereby increasing the fraction of amorphous phase through which water can more easily diffuse. The net result is that an 18P/2S film shows a slightly higher WVTR than a 20P film, though the change is small (within experimental error), possibly due to the very low starch content.

Incorporating small amounts of zeolite particles into the PVA matrix was expected to influence WVTR, as they can increase the tortuosity of the diffusion path. In an ideal case of well-dispersed impermeable fillers, water molecules must travel around the particles, following a longer, more tortuous route to permeate the film [237,337]. However, in the present study, the improvements were minimal to non-significant, due to low filler loadings that may yield negligible barrier gains in a biopolymer film. Moreover, the zeolite geometry is not high-aspect-ratio platelets that create long tortuous paths, and this interrupts the polymer continuity less dramatically [337,338]. Notably, there was no consistent trend of zeolite type or amount improving the barrier. For instance, 20P+4A actually gave a slightly higher WVTR than 20P+2A (or than no 20P). Likewise, differences between 4A and 13X were negligible. At these low loadings, distinctions in zeolites' features did not translate into a measurable WVTR difference. Furthermore, the micro-defects in surface morphology – which were detected and discussed earlier with micrographs – shortcut the barrier. Although these films likely have no gross pinholes, each "dot" microscale imperfection is a site where the polymer continuity is disrupted. Still,

these morphological aspects may account only slightly on the final properties due to reduced defects size, with behaviours as predicted by compositions.

Overall, compared to the control cup, even a hydrophilic polymer like PVA can slow down water loss simply by adding a diffusion barrier. This is valid, in this study, regardless of zeolite addition – but filler granulometry may further change this aspect. On the other hand, the PP film had a WVTR of an order of magnitude lower than the PVA: this highlights the strong limitation of PVA-based films for moisture barrier applications.

3.2 Soil burial tests

Weight changes over time

All the PVA-based films showed a rapid initial weight loss in the first few weeks, followed by a much slower degradation rate in later weeks (Figure 3.8). This pattern is typical for biodegradable polymer systems: an easily leachable or digestible fraction is lost early, then the remaining polymer breaks down more gradually [339]. In the present soil burial test (30 °C, moist peat-based soil), the initial fast loss is attributed to the removal of low-molecular components (chiefly the ~2% w/v glycerol plasticizer present in all formulations, and starch in some films) and the onset of microbial colonization. Glycerol is very water-soluble and readily metabolized by microbes in the wet soil, so it likely leached out and was consumed within the first 2 weeks. After this initial phase, weight loss reflects mainly the biodegradation of the polymer matrix (PVA and any starch), which proceeds more slowly. Minor fluctuations (e.g., a slight decrease or plateau in recorded weight loss around 4–6 weeks for some samples) can be explained by experimental uncertainty and trace soil residues clinging to films. The residual soil adds a bit of weight (especially observed in starch-containing films), making the measured weight loss appear lower – but this effect is small and within the error margins.

Replacing a portion of PVA with 10% starch (sample 18P/2S) markedly increased the biodegradation of the films. At 2 weeks, the 20P film lost ~10.7% of its initial weight, whereas the 18P/2S film lost ~16.3%. By 16 weeks, 20P reached ~11% weight loss, versus ~18.7% for 18P/2S (almost 70% higher loss). This difference is largely due to the presence of starch, which soil microorganisms can easily digest, being broken down into sugars and providing a food source for microbes [243]. In the first couple of weeks, most of the starch in 18P/2S was likely consumed (in addition to glycerol loss), accounting for the higher initial weight reduction. Literature confirms that blending starch into PVA significantly accelerates its biodegradation, depending on starch content [83]. The added hydrophilicity from starch facilitates water uptake and rapid bacterial diffusion into the film.

Once the starch phase is exhausted (likely by ~4 weeks), the remaining material is predominantly the more recalcitrant PVA. Indeed, pure PVA (especially almost

fully-hydrolyzed grades) degrades slowly in soil because relatively few microbes have the specialized enzymes needed to metabolize it, as described in paragraph *1.3 Biodegradability in soil* (Chapter 1). As a result, the weight loss for 20P leveled off early – reaching ~11–11.5% by 4 weeks and not rising much thereafter (within error). That ~10–12% loss corresponds closely to the removal of glycerol (and perhaps a small amount of PVA surface erosion), with little further PVA mass loss over the next 3 months. Prior studies have reported poor biodegradability of pure PVA films in soil [339]. In these starch-blended films, however, PVA did undergo somewhat more degradation by 16 weeks – the 18P/2S film lost an extra ~2–3% beyond the starch and glycerol fraction. This suggests that the starch component not only contributes directly to weight loss but also indirectly enhances overall PVA degradation. The porous, roughened structure left behind after starch is digested, and the microbial communities established while consuming the starch, likely helped attack the PVA matrix (with either slow hydrolysis or enzymatic attack).

Across both 20P films and 18P/2S films, the incorporation of zeolite microparticle fillers led to higher weight loss compared to the unfilled counterparts. By the end of 16 weeks, the 20P films with 4% filler (20P+4X or 20P+4A) lost ~16% of their weight, versus ~11% for 20P (no filler). Similarly, in the starch-containing series, 18P/2S+4A and 18P/2S+4X reached ~22% weight loss, compared to ~18.7% with no filler. The effect was somewhat dose-dependent: 4% filler produced more loss than 2% filler in each case (e.g., 20P+2A ~14.1%, 20P+4A ~16.2% at 16 weeks). Notably, the type of zeolite (13X vs 4A) made little difference – their curves were very similar, with only negligible differences comprised within the margin of error. Ideally, both 4A and 13X zeolites in soil likely act as moisture reservoirs: they absorb water from the surrounding soil and retain it near the polymer matrix. This may help keep the films hydrated even in between soil wetting events, which is beneficial because moisture is crucial for microbial activity and for the hydrolytic enzymes that break down polymers. Another factor is that the dispersed inorganic particles introduce micro-scale heterogeneity in the film, as already observed in micrographs. Small fragments of polymer might break off or pathways for water ingress might open up along the filler sites, so that the films can be eroded more effectively. A study on PVA/Starch films with halloysite nanotube clay found that

increasing the clay content decreased the biodegradation rate by ~18% (at 5% filler) because the clay made the film less water-permeable [243]. In this case, zeolites had the opposite effect: their strong water affinity and porosity enhanced water ingress instead of impeding it [340]. Any small difference in pore size did not translate into a clear difference in biodegradation here; a 4% loading of either was enough to keep the films well-hydrated for microbial attack.

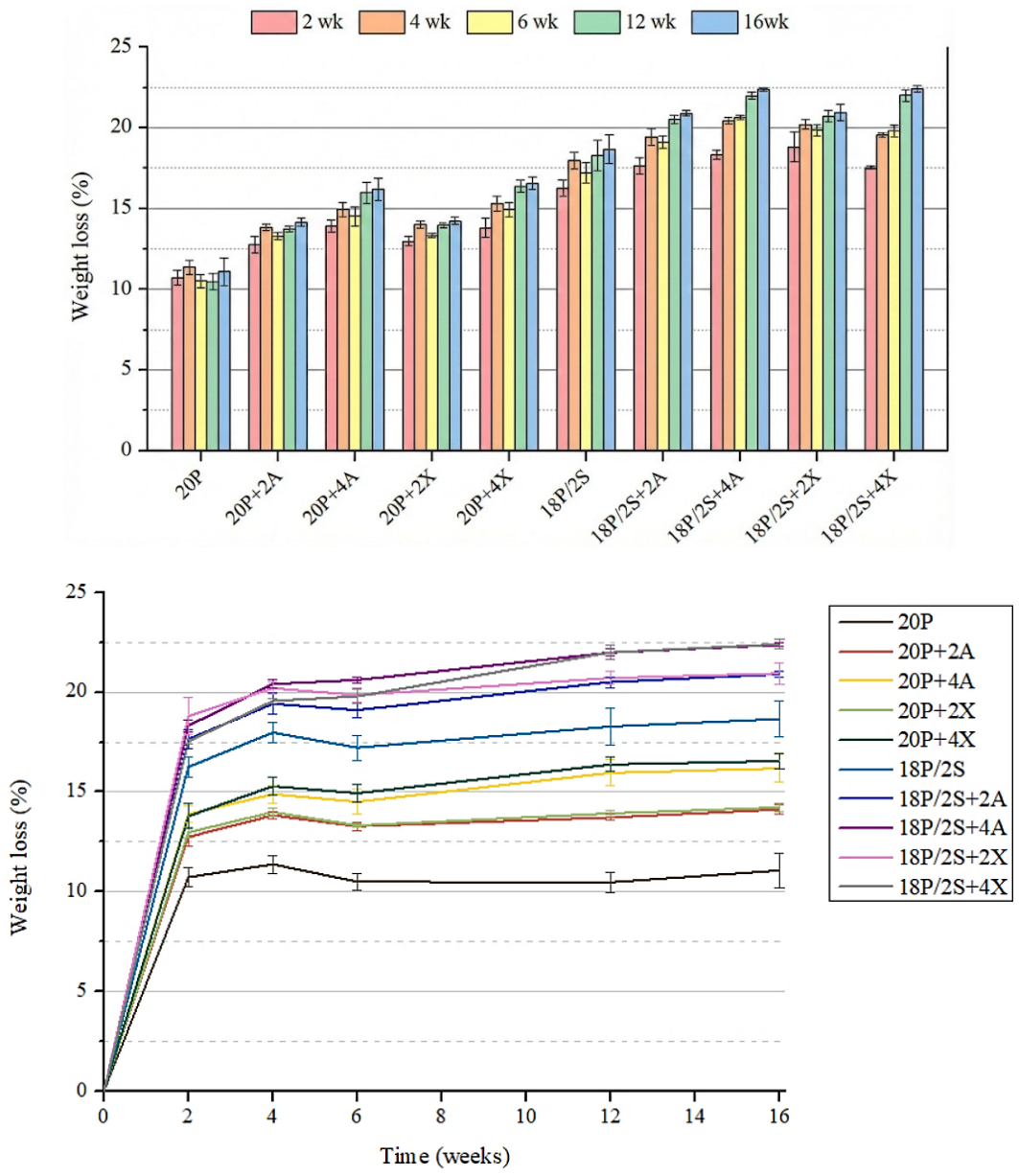

Figure 3.8. Graphical representations of the weight losses occurred in films as a function of soil burial weeks (wk): the difference between the 20P- and 18P/2S-series is evident.

Finally, it is worth noting that the inorganic fillers themselves cannot biodegrade, so the increased weight loss for the zeolite-including films is not due to their vanishing but due to the organic portion. As observed by SEM micrographs, zeolites are still present on the surface at the end of the 16-week soil burial tests, although it is possible that some filler particles (closer to the outside of the films) became detached easily after water swelling and erosion in soil, contributing slightly to weight loss. However, some considerations need to be made.

Slight soil residues actually reduce the measured loss of zeolite-filled films – so the true polymer-loss advantage is, if anything, larger than the one actually measured. Additionally, given the zeolite contents of 4 or 2 %w/w on polymer basis but then considering the effective percentage in final dried solid films, even in a worst-case where all zeolites were lost from a +4A/+4X sample, it could at most add ~3.5% to the apparent weight loss (and ~1.7% for +2A/4A). Since the zeolite-filled films actually exceed the organic-only films by much more than those numbers, the extra loss cannot be explained purely by zeolite shedding (even imagining that all zeolites were removed from the films, and it does not even happen): it must be additional polymer that was either removed or degraded (hydrolysis or microbial action).

Effects on surface defects

After 16 weeks of soil burial, the films' surfaces – which optical micrographs are reported in Figure 3.9 – exhibit notable changes in topography and appearance, depending on composition, and mostly following the trends observed for the pristine non-buried film surfaces. The qualitative optical changes indicate that starch content is the dominant factor in surface morphology degradation. The 18P/2S series consistently shows far more defects than the 20P series. In the starch-containing films, microbial action on starch created a huge number of voids in the PVA matrix – a clear sign of erosion facilitated by the biodegradable starch. These films also trapped some soil particles in their rough surfaces, leading to a dirty, speckled look. In contrast, the starch-free 20P films remained comparatively smooth and clean, with only minor surface defects.

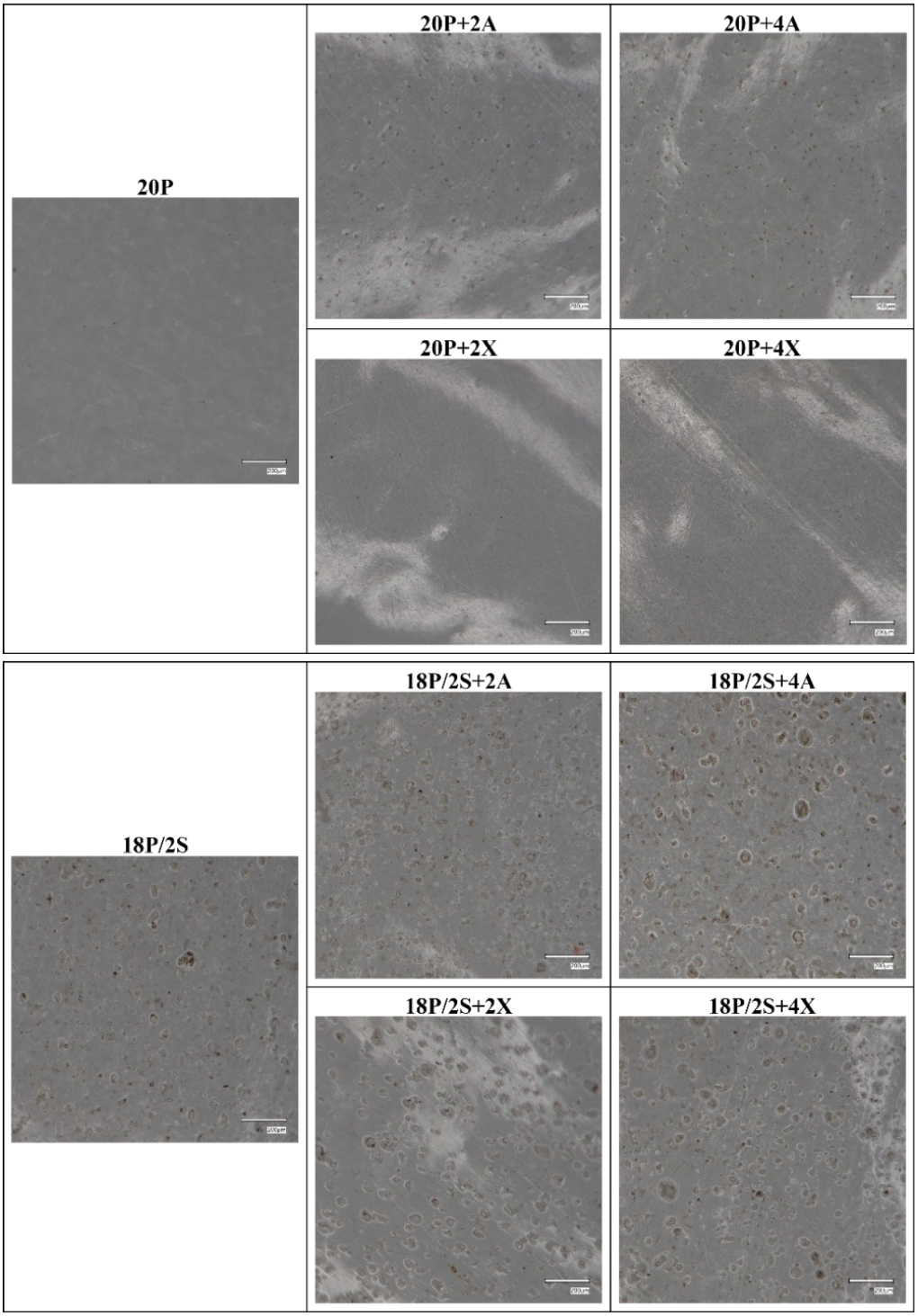

Figure 3.9. Optical micrographs (x200, scale bar 200µm) of the different films after the 16th week of soil burial biodegradation tests.

Considering the role of zeolites in the absence of starch, X addition leads to considerably fewer defects in 20P films than A does, which is linked to a more

diffuse roughening and a more uniformly etched surface. In the 18P/2S series, the distinction between X and A effects is much less pronounced because starch degradation dominates. At 4% zeolite loading, there were more sites for potential defects, leading to more pits or more widespread polymer-filler interfacial erosion; anyway, the effect of the inorganic filler is subtle relative to the large impact of starch. Nonetheless, both these outcomes for zeolites are consistent with the pristine morphology that was already observed and discussed in the previous paragraph.

Soil particulate adhesion was much more significant when the surface was pitted (as it provides anchoring points for dirt). The cleaning step removed loose soil (being almost the entirety), as it was possible to see with the naked eye, but fine light particles were lodged in crevices. Finally, while microbes cannot be seen directly in these images, the patterns observed (selective erosion of starch zones, deposits in holes, etc.) are suggestive of biological activity.

So, as predicted, the smoother PVA regions (more recalcitrant) show far less change, implying that microbes primarily attacked the starch (and glycerol). Any possible erosion after 16 weeks is likely a combination of very slow PVA abiotic hydrolysis and surface defects due to zeolite presence. So, microbial forces have selectively etched away the more biodegradable components (glycerol and starch), leaving inert components (zeolite, unless partially eroded away depending on their distance from the surface) and overall the more recalcitrant PVA matrix with holes. These trends are further confirmed by the SEM micrographs of 18P/2S+4X films after the 16 weeks of soil-burial tests, observable in Figure 3.10, with the highest magnifications (particularly the x1500 one) showing both zeolite particles – still on the film – and voids due to starch.

It is important to note that only prior to these last micrographs, the mentioned film was cleaned with an alcohol/water mixture (and dried) to remove essentially all the soil residues from the surface. This is why the SEM images do not show soil.

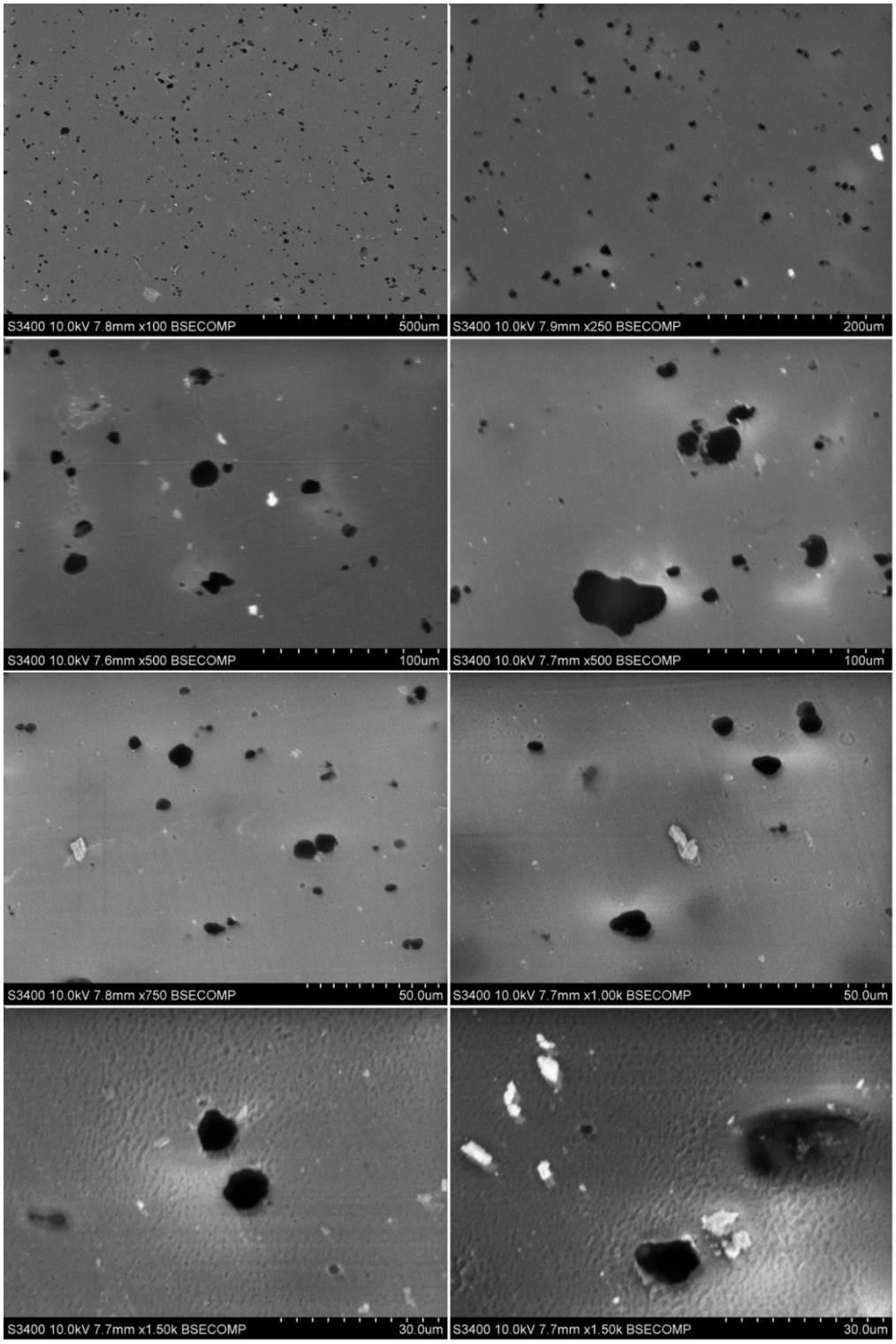

Figure 3.10. SEM micrographs of the 18P/2S+4X film at different magnifications (up to x1500, scale bar 30 μm) after the 16th week of soil burial biodegradation tests.

Chemical-structural changes

ATR-FTIR spectra of the films were collected at every unburial stage, though only the 4- and 16-week data are discussed here, as they best capture the main structural changes observed after the burial period – to be observed in Figure 3.11.

A dominant change in all films upon soil burial is the disappearance of spectral features associated with glycerol (and starch, in starch-containing samples). Initially, the as-cast films show a pronounced band in the C–O stretching region around 1040-1050 cm^{-1} (characteristic of the glycerol plasticizer) which diminishes markedly after the first weeks, indicating leaching and/or microbial consumption of glycerol. Literature on PVA/starch blends confirms that glycerol is preferentially removed in early degradation: after only several days of soil burial, FTIR bands from glycerol disappear entirely [341]. This aligns with the weight loss data, where an initial rapid mass loss corresponds to the loss of glycerol (~10% of film mass). After 4 weeks, indeed, the intensity around 1020–1050 cm^{-1} drops substantially; by 16 weeks, starch-related bands are essentially gone as well, consistent with starch (and glycerol) being the most labile components.

After the removal of glycerol and starch, the residual PVA matrix dominates the IR spectra, and its structural bands become comparatively more prominent. Notably, the broad O–H stretching band of PVA (~3275 cm^{-1}) undergoes subtle changes. Initially, with glycerol present, the O–H band may be centered slightly higher (due to glycerol disrupting PVA–PVA hydrogen bonding). Once glycerol is gone, the O–H band shifts to a lower wavenumber (~3255 cm^{-1}), possibly due to restored intermolecular hydrogen-bonding between PVA chains. Importantly, no new functional groups appear in the PVA spectra after 16 weeks, indicating that the polymer's chemical structure remains largely intact aside from the loss of additives. In particular, there is no emergent carbonyl peak in the soil-buried samples, suggesting essentially no oxidative degradation of PVA in these conditions [65]. Overall, the core PVA fingerprint bands (i.e., the C–O stretch at ~1088 cm^{-1}, the CH_2 at 1327 cm^{-1} and 1417 cm^{-1}) remain observable and do not change significantly – confirming that chemically the PVA remains intact throughout the burial period.

FTIR transmission spectra of 20P and 18P/2S films, both pristine and after the 16th week of tests, further confirm these trends for the organic compounds (Figure 3.12).

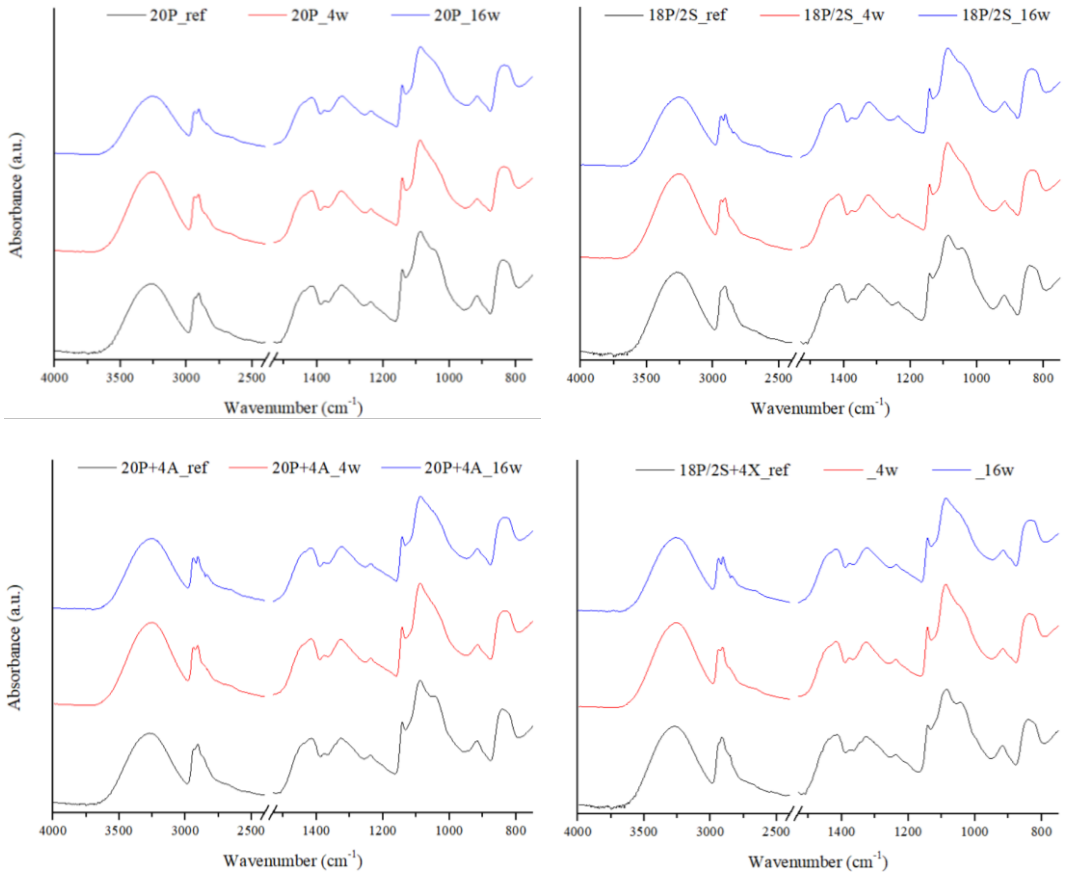

Figure 3.11. ATR-FTIR spectra of the pristine (ref) films and after 4 weeks (4w) and 16 weeks (16w) of soil burial tests. For conciseness, only 4 representative formulations are reported to observe just the main differences depending on the additive concentrations.

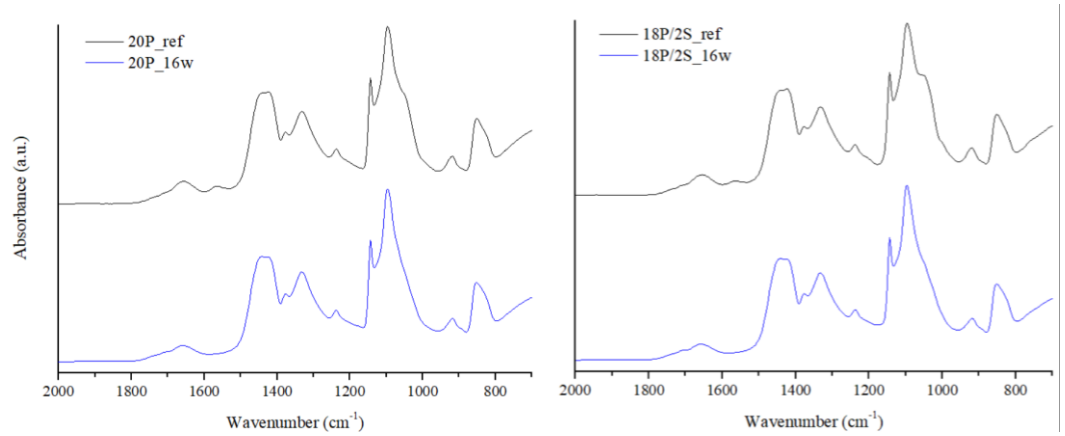

Figure 3.12. FTIR transmission spectra of the pristine (ref) films and after 16 weeks (16w) of soil burial tests, to highlight changes related to the films' organic components.

Changes in crystallinity

After 16 weeks of burial in moist soils, all films showed changes in crystallinity, with trends depending on their composition, as shown in Table 3.2 and Figure 3.13. 20P films showed only a slight decrease in crystallinity after soil burial. Within experimental error, this change is modest, suggesting that fully hydrolyzed PVA (in this study, the most recalcitrant organic compound to biodegrade) did not undergo extensive crystallite breakdown in 16 weeks. Instead, a small loss of crystallinity might indicate some erosion of PVA's crystalline domains due to environmental moisture (hydrolysis) and also to glycerol leaving voids in the system.

PVA/starch blend films (18P/2S) experienced a pronounced decrease in crystallinity upon soil burial. The crystallinity index roughly halved in these samples after 16 weeks, indicating significant structural changes. Starch, being easily attacked by soil microorganisms and effectively enzymatically hydrolyzed and metabolized over the burial period, was likely almost entirely consumed by week 16. The PVA itself possibly underwent greater microbial attack than it would have alone, possibly because the starch degradation created a porous structure that contributed to the resulting crystallinity.

The two types of zeolite had markedly different effects on how the films' crystallinity evolved during soil burial. In the 20P films, a higher filler loading corresponded to a greater drop in polymer crystallinity after burial. For instance, the 20P+4X and 20P+4A samples (which initially had the highest crystallinity among pristine films due to nucleation) showed large decreases in crystallinity index post-burial – falling even below the neat 20P value. Meanwhile, the low-filler samples (20P+2X, 20P+2A) exhibited only minor decreases similar to neat PVA. This suggests that having more zeolite in the plasticized only-PVA film made the polymer more susceptible to crystallinity loss in soil. One likely reason is moisture dynamics. In a wet soil environment, the zeolite particles in the film would rapidly take up water, creating local regions of concentrated moisture and thus possibly promoting polymer swelling, hydrolysis, and finally microbial penetration around those particles. Particularly, the 20P+4A sample lost roughly half its crystallinity, a very pronounced change. On the other hand, zeolite 13X (20P+4X) also caused a significant crystallinity drop, though slightly less drastic. This may confirm the

trend (with possible local fluctuations) that more filler means more sites for water accumulation and relatively less polymer matrix holding everything together.

In the presence of X, the starch-containing films (18P/2S +2X and +4X) maintained nearly the same crystallinity index after burial as they had initially – a visible contrast to the large drop seen in the 18P/2S film without zeolite filler. It is possible that X adsorbed some of the water or acidic byproducts from starch biodegradation, thereby moderating the environment around zeolites and slowing PVA hydrolysis locally. In contrast, the 18P/2S + 2A and +4A films still showed major drops in crystallinity after burial (comparable to or even exceeding the drop in the no-filler case). Ideally, this would indicate that most of the PVA either degraded or lost its ordered structure. However, in general, it is crucial to remember that defects and voids left on the films after the tests can impact the detected crystallinity. Additionally, random local fluctuations of films' composition can further lead to less precise measurements and calculations. Therefore, the results just have to be interpreted as predictable trends.

Table 3.2. XRD crystallinity (X_c) of PVA-based films after 16 weeks of soil burial.

20P	20P+2A	20P+4A	20P+2X	20P+4X
9.4 ± 1.2	7.5 ± 1.5	6.4 ± 1.7	8.2 ± 1.6	8.6 ± 1.0
18P/2S	18P/2S+2A	18P/2S+4A	18P/2S+2X	18P/2S+4X
5.2 ± 0.5	4.5 ± 1.4	3.3 ± 0.6	9.3 ± 0.9	9.8 ± 1.5

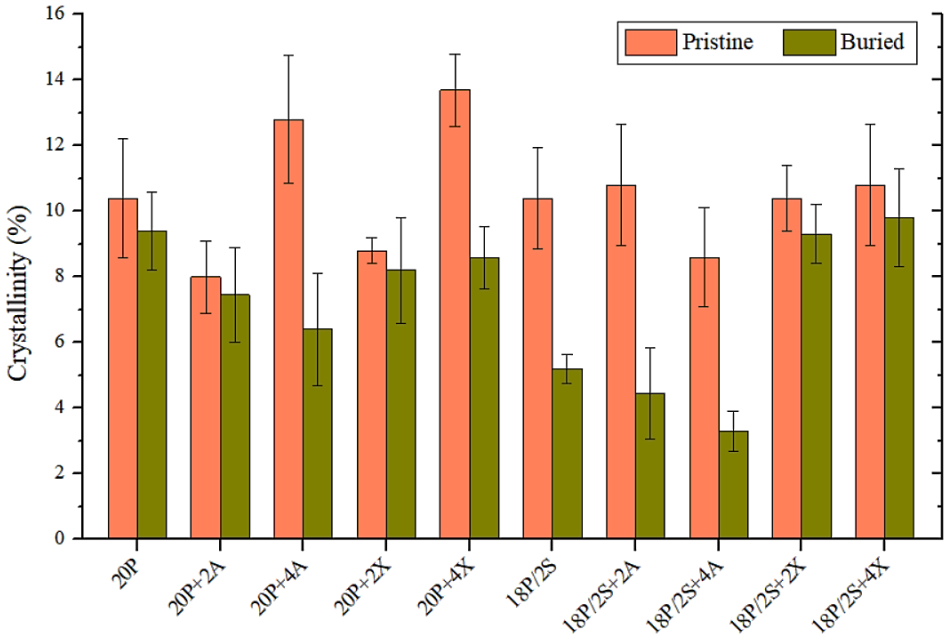

Figure 3.13. Comparison of X_c calculated for pristine films and after soil burial tests.

Soil response and bacterial activity

The bar chart in Figure 3.14 shows the relative fluorescence (RFU) as a proxy for microbial activity in soil samples treated with various polymer formulations, compared to reference soils without any added films, and to soils enriched with just either zeolite 4A or 13X powders (10%w/w of soil).

First, the reference soil exhibits the lowest RFU, indicating the least microbial activity, whereas all biodegradability test soils showed somewhat higher RFU values. This suggests that adding the films generally stimulates microbial metabolism in soil compared to no addition. It is important to note that all the polymer formulations contained the same amount of glycerol (2% w/v) as a plasticizer, and it is easily metabolized by soil microorganisms, so its presence likely boosted microbial activity across every test soil sample. This explains why all the polymer-containing soils have higher RFU than the reference soils. However, the key observation is that the differences among the various biodegradability test soils themselves are not very large, especially when considering the error bars. One expects starch to boost microbial activity, but the data do not show any dramatic increase for starch-containing samples. Indeed, the soil with 20P has an RFU around the same level as the soil with 18P/2S. Their averages are very close, and their error bars overlap. This may simply be due to the very low starch content in the films, making any beneficial effect subtle considering the margins of error. Also, when either zeolite 4A or 13X was included at any concentration, all samples showed relatively similar RFU values. Indeed, as for starch, the zeolite effect on soil is negligible due to the even lower concentration in the films, which translates to a $<10^{-2}$ wt% concentration in the final test soils (overestimating, as most zeolites are still present in the films and not directly into the soil). The small differences are within the error range and cannot be considered significant.

Interestingly, a certain effect of zeolites on bacterial activity was observed only in the reference soils with the significant 10wt% zeolite addition – specially prepared to test the effects of only zeolite at significant concentrations (compared to soil amounts). Particularly, in this case, a modest microbial activity was stimulated. It was shown in literature that zeolites' microporous structure provides more surface for bacteria to attach and form microcolonies [342]. Possibly, zeolites could also

buffer the pH of their environment through ion exchange, increasing the overall metabolic activity of the bacteria – as a near-neutral pH is optimal for many soil bacteria [268,343]. Additionally, the pH of the test soils – measured throughout the experimental campaign – showed a slight increase (up to 6.5) after the campaign. These outcomes may be interesting for future applications by modulating the filler concentration in the matrix.

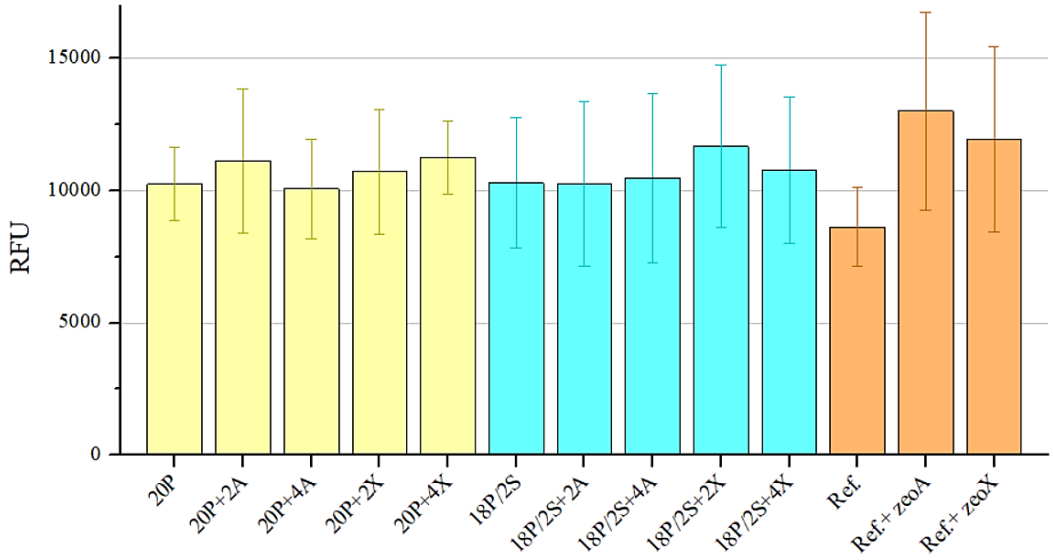

Figure 3.14. RFU values of Alamar Blue assays for the ten different test soils, the neat reference soil, and the zeolites-enriched reference soils (after PBS buffer). Despite the margins of error being too high to appreciate differences, the reference soils clearly appear to have the lowest bacterial metabolic activity.

4. Conclusions and perspectives

This work investigated thin PVA-based films containing starch and synthetic zeolites as model systems for water-based functional coatings intended for sustainable packaging applications. The study combined initial formulation and processing development, multi-technique characterisation of pristine films, and an extended soil burial campaign, in order to link composition and microstructure to functional performance and environmental behaviour.

A first outcome of the thesis concerns the formulation and processing strategy. Fully hydrolysed (99+%) PVA of relatively high molar mass was selected as the main matrix to grant high technological and functional properties of the final films; PVA was plasticised with glycerol and, in some formulations, blended with a small fraction of soluble starch, replacing part of the PVA. Aqueous film-forming formulations were prepared at overall polymer concentrations up to 20% w/v and applied by rod coating on PTFE-coated substrates. Therefore, by systematically varying polymer concentration and drying temperature, and monitoring the distribution of zeolite microfillers through ATR-FTIR spectra collected on both sides of the films, it was possible to identify an operating window in which sedimentation of the inorganic phase during drying is effectively suppressed. In particular, an 18P/2S (PVA 18%w/v and starch 2%w/v) aqueous formulation, rod-coated and dried in a ventilated oven at 105 °C, provided sufficiently high viscosity for coating, good spreading and, crucially, nearly identical FT-IR signatures for the “air side” and the “plate side” in the spectral region dominated by zeolite bands. This simple spectroscopic protocol is a methodological contribution of the work, as it offers a rapid way to assess filler dispersion in the thin, solvent-processed films without requiring destructive cross-sectional analyses.

A second set of conclusions relates to the structure and properties of the pristine films. All PVA-based formulations, with and without starch and zeolites, yielded continuous, highly transparent films with an average dry thickness of about 20 μm. Optical microscopy revealed that the reference plasticized PVA film (20P, with PVA 20%w/v to compare the same polymeric contents) exhibits a smooth, almost featureless surface, while the introduction of starch leads to a more heterogeneous

morphology, with small domains or halos attributed to incomplete dissolution or local agglomeration of starch and to differential drying. The addition of zeolite particles introduces further microstructural features: especially in the 20P+zeolite A series, where ring-like defects were observed around particles, consistent with local stress and dewetting during solvent evaporation. SEM images, recorded on representative starch- and zeolite-containing films, confirmed that zeolite particles with nominal sizes of 2–3 μm are well distributed across the surface and, by extension, throughout the thickness of the optimised films.

Thermogravimetric analysis provided quantitative insight into thermal stability. Glycerol-plasticised PVA (20P) films exhibit a main mass-loss event around 280–290 °C under nitrogen, at a significantly lower temperature than the pristine PVA powder due to the plasticising effect of glycerol on the polymer network. Incorporating a small amount of starch (18P/2S) unexpectedly increased thermal stability, shifting the main degradation peak up to approximately 340 °C. This behaviour points to strong intermolecular interactions between PVA and starch, which stiffen the network and raise the activation energy for thermal degradation. The presence of zeolite fillers further modifies the degradation pattern. At loadings of 2–4 wt%, both zeolite 4A and 13X acted as effective thermal stabilisers, with the most pronounced effect observed for 13X at 4 wt%, for which the main DTG peak shifted by more than 60 °C compared with the neat PVA film. The zeolites themselves did not decompose in the investigated temperature range, so the observed changes are fully attributable to matrix–filler interactions, heat-sink effects, and possible adsorption of volatile degradation products. Overall, the combined use of starch and zeolites allows tuning of the thermal response of PVA films in a favourable direction, which is relevant for processing and for applications involving moderate heat exposure.

X-ray diffraction analyses showed that the solvent-processed, plasticised PVA films are semi-crystalline, with a crystallinity index around 10%, lower than that of the starting PVA powder due to the thermal/processing history and the presence of glycerol. The inclusion of 10 wt% starch in the 18P/2S films did not significantly alter the overall crystallinity within experimental error, consistent with the low starch content and with partial miscibility between the two polymers. At low zeolite

loading (2 wt%), crystallinity tended to decrease slightly, suggesting that dispersed particles hindered the regular packing of chains. At 4 wt%, instead, both zeolite types acted as nucleating agents in the 20P films, leading to a modest increase in crystallinity. In the PVA/starch blend films, the effect of zeolites on crystallinity was less clear and, in some cases, zeolite 4A at higher loading seemed to disrupt crystalline order, emphasising that the interplay between polymer blend structure and filler is more complex than in the single-polymer matrix.

The moisture-related properties confirmed the intrinsically hydrophilic nature of the systems. All films absorbed large amounts of water during 1 h immersion tests, with weight increase values between about 130 and 190%, depending on composition. Starch-containing films displayed higher water uptake than PVA-only films, in line with the strong hydrophilicity of starch. The addition of zeolites slightly reduced water uptake, likely by diluting the polymer fraction and restricting swelling in their vicinity, but the effect remained modest at the tested loadings. Water vapour transmission rates measured by the cup method at 40 °C and 40% RH were on the order of 10^3 g m^{-2} d^{-2} for all PVA-based films, with only minor variations among formulations. In contrast, a reference PP film of comparable thickness exhibited a WVTR roughly one order of magnitude lower. These findings confirm that, while PVA and PVA/starch films provide excellent oxygen barrier in the dry state, they are not suited to act as stand-alone moisture barriers and, in packaging architectures, would have to be combined with more hydrophobic layers.

The soil burial tests carried out at 30 °C in a highly moist peat-based soil over 16 weeks provided a dynamic picture of biodegradation phenomena. For all formulations, a rapid initial weight loss was observed in the first weeks, followed by a much slower decrease or plateau. The early loss is attributed mainly to leaching and microbial consumption of glycerol and, where present, starch. The neat PVA film (20P) reached a weight loss of about 10–12% and then stabilised, indicating that the fully hydrolysed, high-molar-mass PVA phase degrades only slowly under the selected soil conditions. In contrast, the PVA/starch blend film (18P/2S) exhibited a substantially higher final weight loss (around 19%), consistent with the almost complete removal of starch and with a modest additional degradation of the

PVA matrix, likely facilitated by the porous structure left after starch consumption and by the microflora established while metabolising starch.

Zeolite-containing films consistently showed higher weight losses than their zeolite-free counterparts. At equal polymer composition, increasing zeolite loading from 2 to 4 wt% led to higher total weight loss after 16 weeks, with only minor differences between zeolite 4A and 13X. This trend indicates that the inorganic fillers do not act as barriers to biodegradation; instead, they appear to promote it slightly, probably by enhancing local water retention and creating micro-heterogeneities that favour erosion. Optical microscopy and SEM on buried films confirmed that starch-containing and zeolite-filled formulations developed more pronounced surface defects and voids than the neat PVA film. These features are consistent with the selective removal of the more labile components (glycerol and starch) and with micro-erosion around filler particles, while zeolites themselves remained as bright, undissolved domains embedded in the residual PVA.

ATR- and transmission FT-IR spectra collected during the burial campaign corroborated the weight-loss and morphological observations. With increasing burial time, bands associated with glycerol and starch in the C–O stretching region gradually disappeared, while the main PVA backbone bands remained essentially unchanged, and no new strong carbonyl peaks associated with oxidative degradation were detected. XRD patterns acquired after 16 weeks showed composition-dependent changes in crystallinity. For the neat PVA films, the crystallinity index decreased only slightly, whereas for the PVA/starch films, a significant reduction was observed, reflecting both the removal of starch and structural rearrangements in the PVA phase. In highly filled (4% zeolite) systems, the initial crystallinity increase induced by zeolite nucleation was largely lost after burial, suggesting that crystalline domains are not immune to the combined effect of moisture and microbial activity over the investigated timescale.

Finally, AlamarBlue® assays performed on the test soils showed that microbial metabolic activity in soils containing the different films was comparable across formulations and consistently higher than in the reference soil without added films. This result confirms that the presence of PVA, starch, and zeolites at the amounts considered does not inhibit soil bacteria and, if anything, provides additional readily

metabolizable carbon (mainly glycerol and starch). Only when zeolites were added directly to the soil at a much higher concentration (10 wt% on soil) was a noticeable further increase in RFU observed, suggesting that zeolites can also act as benign, micro-structured supports for bacterial colonisation.

Taken together, these results demonstrate that thin PVA-based films containing moderate amounts of starch and synthetic zeolites can be produced by a scalable wet-coating process, exhibit improved thermal stability and controlled microstructure, and are capable of undergoing partial biodegradation in moist soil without adverse effects on soil microbial activity. At the same time, the study highlights the persistent limitations of PVA-based films in terms of moisture barrier and the relatively slow mineralisation of fully hydrolysed PVA under the tested conditions, issues that must be taken into account when designing packaging structures in line with PPWR requirements.

Future research directions

The present work has deliberately focused on free-standing films as simplified model systems. Several avenues can now be pursued to bridge the gap between these laboratory-scale results and real packaging applications.

The first, natural development is the translation of the optimised PVA/starch/zeolite formulations into thin coatings deposited on industrially relevant substrates. Polyolefin films (e.g., PE and PP) and paperboard for folding cartons represent the most obvious targets, in line with the predominance of these materials in the current packaging market. Applying the water-based formulations by Mayer-bar or other roll-to-roll coating techniques on such substrates would allow evaluation of adhesion, coat weight control, drying behaviour, and defect formation under more realistic constraints. Mechanical performance of the coated structures (tensile properties, bending resistance, sealability, and heat-seal window) should be assessed, together with their oxygen and water vapour barrier at the laminate level. Equally important, recyclability tests—such as repulpability for coated paperboard and reprocessing trials for coated polyolefin films—would be needed to verify that the thin PVA-based layers do not impair the existing recycling streams and can so be accommodated within the mono-material criteria supported by the PPWR.

A second line of research concerns the design of the zeolite phase itself. In this thesis, commercially available micro-sized 4A and 13X zeolites were used as model fillers. Future work could explore natural zeolites such as clinoptilolite, which are abundant, inexpensive, and already employed in contact with animals and humans, as well as nano-structured synthetic zeolites. Nano-zeolites, thanks to their smaller size and higher external surface area, could be more easily dispersed in very thin coating layers and might provide more pronounced improvements in gas barrier and thermal stability at lower loadings, while keeping the total coating mass well below the thresholds that affect recyclability. At the same time, zeolites can be exploited as carriers for antimicrobial cations (Ag^{+}, Zn^{2+}, Cu^{2+}) or other active species, enabling truly "active" PVA-based coatings that can extend food shelf life by modulating the package atmosphere or inhibiting microbial growth. In such developments, careful migration studies and compliance with food-contact regulations will be essential.

Further efforts are also warranted to deepen the understanding of biodegradation mechanisms for PVA-based films and coatings. Extending the soil burial tests to longer times and to different environments (e.g., industrial and home compost, wastewater treatment conditions, freshwater and marine scenarios) would provide a more complete picture of the environmental fate of these materials. Coupling weight-loss and spectroscopy with respirometric measurements and molecular-weight analysis of residual PVA could help quantify actual mineralisation versus mere disintegration. The influence of film thickness and of the presence of a non-degradable substrate on biodegradation kinetics should be addressed explicitly, since real coatings will be much thinner and partially confined compared with the free-standing films studied here.

As concerns the soil burial tests, considering that PVA is the most recalcitrant polymeric component of the films (and also the main and most abundant), it was decided to prolong the experimental campaign for up to 1 year. Basically, the test soils are going to be kept moist for the next several months in order to possibly observe further weight losses (if any), supposing more time is required than the 3-month burial achieved up to now – and that the commercial test soils comprise such a bacterial culture to achieve the effective and complete PVA biodegradation.

Finally, from a broader perspective, integrating the present materials-oriented results within a life-cycle and techno-economic assessment framework would be highly valuable. Comparative studies between conventional multi-material laminates and proposed structures based on recyclable substrates plus thin PVA/zeolite coatings could quantify potential benefits in terms of material efficiency, greenhouse-gas emissions, and end-of-life performance. Such analyses, combined with further experimental work on coating scale-up and on active functionalities, would help identify the conditions under which PVA-based, starch- and zeolite-containing coatings can become a realistic option for industry in the evolving landscape defined by the PPWR and by future circular-economy policies.

Acknowledgements

This study was carried out within the MICS (Made in Italy – Circular and Sustainable) Extended Partnership and received funding from the European Union – NextGenerationEU (PIANO NAZIONALE DI RIPRESA E RESILIENZA (PNRR) – MISSIONE 4 COMPONENTE 2, INVESTIMENTO 1.3 – D.D. 1551.11-10-2022, PE00000004). This manuscript reflects only the authors' views and opinions, neither the European Union nor the European Commission can be considered responsible for them.

The activities described within the section *3.2 Soil burial tests*, along with some activities reported in the section *3.1 Pristine films' properties*, have been carried out during a research stay at the Poznań University of Technology (Politechnika Poznańska), under the supervision of Dr. Wojciech Smułek. Important contributions also came by Dr. Aleksandra Grząbka - Zasadzińska and Dr. Krzysztof Knofczyński (from the same research institute), who helped to conduct respectively the XRD measurements and the SEM investigations.

The final acknowledgements, respectively for the support in carrying out the TGA tests and for general research advice, are owed to Dr. Assunta Campanile and Prof. Veronica Ambrogi (Università degli Studi di Napoli Federico II).

Bibliography

[1] European Parliament and Council, Directive 94/62/EC, 2018.
[2] Grand View Research, (2023).
[3] Grand View Research, (2023).
[4] J. Alves, P.D. Gaspar, T.M. Lima, P.D. Silva, J. Sci. Food Agric. 103 (2023) 1004–1020.
[5] M. Ozdemir, J.D. Floros, Crit. Rev. Food Sci. Nutr. 44 (2004) 185–193.
[6] G.K. Deshwal, N.R. Panjagari, T. Alam, J. Food Sci. Technol. 56 (2019) 4391–4403.
[7] V.G. Martins, V.P. Romani, in: A.K. Shukla (Ed.), Food Packag. Smarter Way, Springer Nature Singapore, Singapore, 2022, pp. 1–9.
[8] R. Geyer, J.R. Jambeck, K.L. Law, Sci. Adv. 3 (2017) e1700782.
[9] A. Pettinari, P.L. Bradley, B. Burgmeier, H. Chan, S. Goldstein, P.J. Juvekar, R. Toth, T.P. Wrigglesworth, O. Yee, Citi GPS Glob. Perspect. Solut. (2018).
[10] PlasticEurope, Plastics – the Facts 2022, PlasticsEurope - Association of Plastics Manufacturers, Brussels, Belgium, 2022.
[11] C.O. Mohan, S. Remya, K.R. Sreelakshmi, C.N. Ravishankar, in: A.K. Shukla (Ed.), Food Packag. Smarter Way, Springer Nature Singapore, Singapore, 2022, pp. 165–186.
[12] M. Al-Ali AlMa'adeed, I. Krupa, in: Polyolefin Compd. Mater., Springer International Publishing, Cham, 2016.
[13] A. Chamas, H. Moon, J. Zheng, Y. Qiu, T. Tabassum, J.H. Jang, M. Abu-Omar, S.L. Scott, S. Suh, ACS Sustain. Chem. Eng. 8 (2020) 3494–3511.
[14] I. Novák, A. Popelka, Z. Špitalský, I. Krupa, S. Tavman, in: M. Al-Ali AlMa'adeed, I. Krupa (Eds.), Polyolefin Compd. Mater., Springer International Publishing, Cham, 2016, pp. 181–199.
[15] B. Bamps, M. Buntinx, R. Peeters, Packag. Technol. Sci. 36 (2023) 507–532.
[16] L. Piergiovanni, S. Limbo, Food Packaging Materials, Springer International Publishing, Cham, 2016.
[17] P.S. Sari, T. Sharika, K. Bicy, S. Thomas, in: M. Al-Ali AlMa'adeed, I. Krupa (Eds.), Polyolefin Compd. Mater., Springer International Publishing, Cham, 2016, pp. 315–339.
[18] P. Galli, S. Danesi, T. Simonazzi, Polym. Eng. Sci. 24 (1984) 544–554.
[19] H.G. Karian, Handbook of Polypropylene and Polypropylene Composites, Marcel Dekker, New York, 1999.
[20] H.A. Maddah, Am. J. Polym. Sci. 6 (2016) 1–11.
[21] Y. Tokiwa, B.P. Calabia, C.U. Ugwu, S. Aiba, Int. J. Mol. Sci. 10 (2009) 3722–3742.
[22] European Bioplastics, nova-Institute, (2023).
[23] V.M. Pathak, Navneet, Bioresour. Bioprocess. 4 (2017) 15.
[24] P.R. Sutkar, S.M. Pore, V.P. Dhulap, Curr. World Environ. 17 (2022) 289–305.
[25] C.Y. Barlow, D.C. Morgan, Resour. Conserv. Recycl. 78 (2013) 74–80.
[26] M. Guerritore, F. Olivieri, R. Castaldo, R. Avolio, M. Cocca, M.E. Errico, M.R. Galdi, C. Carfagna, G. Gentile, Resour. Conserv. Recycl. 179 (2022) 106126.

[27] M.K. Eriksen, J.D. Christiansen, A.E. Daugaard, T.F. Astrup, Waste Manag. 96 (2019) 75–85.
[28] ASTM-D5209, (2017).
[29] ASTM-D5338, (2021).
[30] ASTM-D5988, (2018).
[31] ASTM-D6691, (2018).
[32] ASTM-D6400, (2022).
[33] J. A. Glaser, in: A. Gomiero (Ed.), Plast. Environ., IntechOpen, 2019.
[34] V. Goel, P. Luthra, G.S. Kapur, S.S.V. Ramakumar, J. Polym. Environ. 29 (2021) 3079–3104.
[35] A. Nazrin, S.M. Sapuan, M.Y.M. Zuhri, R.A. Ilyas, R. Syafiq, S.F.K. Sherwani, Front. Chem. 8 (2020) 213.
[36] X. Shi, L. Cui, C. Xu, S. Wu, Materials 18 (2025) 2919.
[37] A.K. Sugih, F. Picchioni, L.P.B.M. Janssen, H.J. Heeres, Carbohydr. Polym. 77 (2009) 267–275.
[38] V. Voet, J. Jager, R. Folkersma, Plastics in the Circular Economy, De Gruyter, 2021.
[39] R.P. Veregin, C.A. Fyfe, R.H. Marchessault, M.G. Taylor, Macromolecules 19 (1986) 1030–1034.
[40] B. Pfister, S.C. Zeeman, Cell. Mol. Life Sci. 73 (2016) 2781–2807.
[41] L. Averous, Polymer 41 (2000) 4157–4167.
[42] W. Ning, Y. Jiugao, M. Xiaofei, W. Ying, Carbohydr. Polym. 67 (2007) 446–453.
[43] R.F.T. Stepto, Macromol. Symp. 201 (2003) 203–212.
[44] E. Basiak, A. Lenart, F. Debeaufort, Polymers 10 (2018) 412.
[45] A. Heydari, I. Alemzadeh, M. Vossoughi, Mater. Des. 50 (2013) 954–961.
[46] P.J. Andersen, S. Ong, B.J. Christensen, S.K. Hodson, Sheets Having a Starch-Based Binding Matrix, US6083586A, 2000.
[47] G.F. Fanta, F.C. Felker, R.L. Shogren, J.H. Salch, J. Appl. Polym. Sci. 84 (2002) 1781–1788.
[48] B. Khan, M. Bilal Khan Niazi, G. Samin, Z. Jahan, J. Food Process Eng. 40 (2017) e12447.
[49] S. Kim, A. Biswas, M. Singh, S.C. Peterson, S. Liu, J. Cereal Sci. 56 (2012) 720–725.
[50] R. Auras, B. Harte, S. Selke, Macromol. Biosci. 4 (2004) 835–864.
[51] J.R. Dorgan, B. Braun, J.R. Wegner, D.M. Knauss, ACS Symp. Ser. (2006) 102–125.
[52] R. Bhardwaj, A.K. Mohanty, Biomacromolecules 8 (2007) 2476–2484.
[53] I.S.M.A. Tawakkal, M.J. Cran, J. Miltz, S.W. Bigger, J. Food Sci. 79 (2014) R1477–R1490.
[54] N. Ljungberg, B. Wesslén, J. Appl. Polym. Sci. 86 (2002) 1227–1234.
[55] N. Ljungberg, B. Wesslén, Biomacromolecules 6 (2005) 1789–1796.
[56] M. Murariu, A. Da Silva Ferreira, M. Alexandre, P. Dubois, Polym. Adv. Technol. 19 (2008) 636–646.
[57] K.M. Kim, J.H. Son, S.-K. Kim, C.L. Weller, M.A. Hanna, J. Food Sci. 71 (2006) E119–E124.
[58] M.N.V.R. Kumar, R.A.A. Muzzarelli, C. Muzzarelli, H. Sashiwa, A.J. Domb, Chem. Rev. 104 (2004) 6017–6084.

[59] E.I. Rabea, M.E.-T. Badawy, C.V. Stevens, G. Smagghe, W. Steurbaut, Biomacromolecules 4 (2003) 1457–1465.
[60] Z. Ma, A. Garrido-Maestu, K.C. Jeong, Carbohydr. Polym. 176 (2017) 257–265.
[61] I. Aranaz, A.R. Alcántara, M.C. Civera, C. Arias, B. Elorza, A. Heras Caballero, N. Acosta, Polymers 13 (2021) 3256.
[62] B.L. Butler, P.J. Vergano, R.F. Testin, J.M. Bunn, J.L. Wiles, J. Food Sci. 61 (1996) 953–956.
[63] P. Cazón, M. Vázquez, Environ. Chem. Lett. 18 (2020) 257–267.
[64] European Bioplastics, nova-Institute, (2023).
[65] E. Chiellini, A. Corti, S. D'Antone, R. Solaro, Prog. Polym. Sci. 28 (2003) 963–1014.
[66] J.O. Dennis, M.F. Shukur, O.A. Aldaghri, K.H. Ibnaouf, A.A. Adam, F. Usman, Y.M. Hassan, A. Alsadig, W.L. Danbature, B.A. Abdulkadir, Molecules 28 (2023) 1781.
[67] A.S. Elgharbawy, A.-G.M. El Demerdash, W.A. Sadik, M.A. Kasaby, A.H. Lotfy, A.I. Osman, Polymers 16 (2024) 1356.
[68] L. Rahman, J. Goswami, J. Packag. Technol. Res. 7 (2023) 1–10.
[69] C. Rolsky, V. Kelkar, Int. J. Environ. Res. Public. Health 18 (2021) 6027.
[70] A. Idris, A. Muntean, B. Mesic, M. Lestelius, A. Javed, Coatings 11 (2021) 1253.
[71] I.A. Channa, J. Ashfaq, S.J. Gilani, A.D. Chandio, S. Yousuf, M.A. Makhdoom, M.N.B. Jumah, Membranes 12 (2022) 701.
[72] FAO, (2007).
[73] N. Ben Halima, RSC Adv. 6 (2016) 39823–39832.
[74] A. Filimon, A.M. Dobos, M.D. Onofrei, D. Serbezeanu, Polymers 17 (2025) 1016.
[75] S. Farris, L. Piergiovanni, in: Emerg. Food Packag. Technol., Elsevier, 2012, pp. 274–302.
[76] M. Bercea, Polymers 16 (2024) 2021.
[77] N. Couți, A. Porfire, R. Iovanov, A.G. Crișan, S. Iurian, T. Casian, I. Tomuță, Polymers 16 (2024) 517.
[78] Kurarai POVAL™, (2024).
[79] J. Zanela, M. Casagrande, M.O. Reis, M.V.E. Grossmann, F. Yamashita, Waste Biomass Valorization 10 (2019) 319–326.
[80] F. Liu, Y. Zhang, X. Xiao, Y. Cao, W. Jiao, H. Bai, L. Yu, Q. Duan, Chem. Eng. J. 472 (2023) 144959.
[81] FDA, (2018).
[82] Z.W. Abdullah, Y. Dong, I.J. Davies, S. Barbhuiya, Polym.-Plast. Technol. Eng. 56 (2017) 1307–1344.
[83] E. Negim, R. Rakhmetullayeva, G. Yeligbayeva, P. Urkimbaeva, S. Primzharova, D. Kaldybekov, J. Khatib, G. Mun, C. W, Int. J. Basic Appl. Sci. 3 (2014) 263–273.
[84] R. Solaro, A. Corti, E. Chiellini, Polym. Adv. Technol. 11 (2000) 873–878.
[85] T. Ikejima, N. Yoshie, Y. Inoue, Polym. Degrad. Stab. 66 (1999) 263–270.
[86] I. Restrepo, C. Medina, V. Meruane, A. Akbari-Fakhrabadi, P. Flores, S. Rodríguez-Llamazares, Polímeros 28 (2018) 169–177.

[87] J. Zanela, A.P. Bilck, M. Casagrande, M.V.E. Grossmann, F. Yamashita, Polímeros 28 (2018) 256–265.
[88] R. Fong, A. Robertson, P. Mallon, R. Thompson, Polymers 10 (2018) 1036.
[89] Y. Wei, J. Fu, J. Wu, X. Jia, Y. Zhou, C. Li, M. Dong, S. Wang, J. Zhang, F. Chen, Appl. Environ. Microbiol. 84 (2018) e01898-17.
[90] P. Alexy, D. Káchová, M. Kršiak, D. Bakoš, B. Šimková, Polym. Degrad. Stab. 78 (2002) 413–421.
[91] C.C. DeMerlis, D.R. Schoneker, Food Chem. Toxicol. 41 (2003) 319–326.
[92] European Food Safety Authority, EFSA J. 12 (2014).
[93] State Intellectual Property Office of China, Stretched PVA (Polyvinyl Alcohol) Film and Preparation Method for Same, CN102604294A, n.d.
[94] A. Apicella, A. Barbato, E. Garofalo, L. Incarnato, P. Scarfato, Polymers 14 (2022) 935.
[95] A. Barbato, A. Apicella, F. Malvano, P. Scarfato, L. Incarnato, Polymers 15 (2023) 4002.
[96] P. Tyagi, K.S. Salem, M.A. Hubbe, L. Pal, Trends Food Sci. Technol. 115 (2021) 461–485.
[97] S. Weng, I. Marcet, M. Rendueles, M. Díaz, Food Bioprocess Technol. 18 (2025) 3245–3271.
[98] H. Christophliemk, E. Bohlin, P. Emilsson, L. Järnström, Coatings 13 (2023) 1489.
[99] S.S. Hamdani, Z. Li, P. Ruoqi, E. Rollend, M. Rabnawaz, J. Appl. Polym. Sci. 139 (2022) 51707.
[100] F.V. Borbolla-Jiménez, S.I. Peña-Corona, S.J. Farah, M.T. Jiménez-Valdés, E. Pineda-Pérez, A. Romero-Montero, M.L. Del Prado-Audelo, S.A. Bernal-Chávez, J.J. Magaña, G. Leyva-Gómez, Pharmaceutics 15 (2023) 1914.
[101] S.F. Kistler, P.M. Schweizer, eds., Liquid Film Coating, Springer Netherlands, Dordrecht, 1997.
[102] L.A. Felton, Int. J. Pharm. 457 (2013) 423–427.
[103] A. Kramar, I. Rodríguez Ortega, G. González-Gaitano, J. González-Benito, Cellulose 30 (2023) 2037–2052.
[104] A.A. Sapalidis, Symmetry 12 (2020) 960.
[105] A.F. Routh, Rep. Prog. Phys. 76 (2013) 046603.
[106] M.A. Butt, Coatings 12 (2022) 1115.
[107] K.B. Singh, L.R. Bhosale, M.S. Tirumkudulu, Langmuir 25 (2009) 4284–4287.
[108] J. Laven, JCT CoatingsTech 73 (2001) 49–58.
[109] B.A. Miller-Chou, J.L. Koenig, Prog. Polym. Sci. 28 (2003) 1223–1270.
[110] R. Hussain, S.A. Batool, A. Aizaz, M. Abbas, M.A. Ur Rehman, ACS Omega 8 (2023) 42301–42310.
[111] S. Sultana, S. Imran, A. Naveed, S. Hussain, R. Khattak, L.A. Shah, K. Rehan, I. Rehan, M.U. Rehman, U. Hashmat, F. Haider, Heliyon 10 (2024) e28290.
[112] D.E. Bornside, C.W. Macosko, L.E. Scriven, J. Appl. Phys. 66 (1989) 5185–5193.
[113] E.D. Cohen, E.B. Gutoff, Modern coating and drying technology, John Wiley & Sons, 1992.
[114] L.E. Scriven, MRS Proc. 121 (1988) 717.

[115] T. Carey, C. Jones, F. Le Moal, D. Deganello, F. Torrisi, ACS Appl. Mater. Interfaces 10 (2018) 19948–19956.
[116] F. Aziz, A.F. Ismail, Mater. Sci. Semicond. Process. 39 (2015) 416–425.
[117] A. Berni, in: Thick Film Mater. Process., Saarland University, 2004, pp. 39–51.
[118] E.B. Gutoff, E.D. Cohen, Coating and Drying Defects: Troubleshooting Operating Problems, 1st ed., Wiley, 2006.
[119] Z. Shen, A. Rajabi-Abhari, K. Oh, G. Yang, H.J. Youn, H.L. Lee, Polymers 13 (2021) 1334.
[120] X. Tang, S. Alavi, Carbohydr. Polym. 85 (2011) 7–16.
[121] P. Alexy, I. Lacík, B. Šimková, D. Bakoš, N. Prónayová, T. Liptaj, S. Hanzelová, M. Várošová, Polym. Degrad. Stab. 85 (2004) 823–830.
[122] Aonghus Heatley, Fieldfisher (2025).
[123] Off. J. Eur. Union 40 (2025).
[124] European Commission, EU Comm. - Environ. (2025).
[125] Wolfgang Trunk, Maja Desgrées du Loû, Louise Tang Pedersen, David Buhé, Daniele Ape, Ioannis Antonopoulos, Eur. Comm. (2024).
[126] Keller & Heckman LLP, (2025).
[127] Verpact, (2025).
[128] FINAT, FINAT (2025).
[129] AF&PA, Am. For. Pap. Assoc. (2021).
[130] FDF, Food Drink Fed. (2024).
[131] USDA FAS, USDA Foreign Agric. Serv. (2024).
[132] César Aliaga, ITENE (2024).
[133] Edith M. Flanigen, in: Stud. Surf. Sci. Catal., Elsevier, 1991, pp. 13–34.
[134] E. Pérez-Botella, S. Valencia, F. Rey, Chem. Rev. 122 (2022) 17647–17695.
[135] C. Baerlocher, Atlas of Zeolite Framework Types, 6th ed, Elsevier Science & Technology, Oxford, 2007.
[136] M.E. Davis, Ind. Eng. Chem. Res. 30 (1991) 1675–1683.
[137] H. Kim, H.J. Cho, S. Narayanan, S. Yang, H. Furukawa, S. Schiffres, X. Li, Y.-B. Zhang, J. Jiang, O.M. Yaghi, E.N. Wang, Sci. Rep. 6 (2016) 19097.
[138] A. Corma, Chem. Rev. 97 (1997) 2373–2420.
[139] S. Kulprathipanja, Zeolites in Industrial Separation and Catalysis, 1st ed, John Wiley & Sons, Incorporated, Weinheim, 2010.
[140] B. Jha, D.N. Singh, ChemInform 43 (2012).
[141] USGS, US Geol. Surv. Natl. Miner. Inf. Cent. (2025).
[142] M. Yoldi, E.G. Fuentes-Ordoñez, S.A. Korili, A. Gil, Microporous Mesoporous Mater. 287 (2019) 183–191.
[143] M. Dusselier, M.E. Davis, Chem. Rev. 118 (2018) 5265–5329.
[144] E.T.C. Vogt, B.M. Weckhuysen, Chem. Soc. Rev. 44 (2015) 7342–7370.
[145] C. Baerlocher, D. Brouwer, M. Bernd, L.B. McCusker, Int. Zeolite Assoc. IZA (2017).
[146] R. Bai, X. Song, W. Yan, J. Yu, Natl. Sci. Rev. 9 (2022) nwac064.
[147] P.R. Pujadó, J.A. Rabó, G.J. Antos, S.A. Gembicki, Catal. Today 13 (1992) 113–141.
[148] J. Li, M. Gao, W. Yan, J. Yu, Chem. Sci. 14 (2023) 1935–1959.
[149] B. Liguori, P. Aprea, B.D. Gennaro, F. Iucolano, A. Colella, D. Caputo, Materials 12 (2019) 4231.

[150] G. Calleja, J. Pau, J.A. Calles, J. Chem. Eng. Data 43 (1998) 994–1003.
[151] M. Munthali, M. Elsheikh, E. Johan, N. Matsue, Molecules 19 (2014) 20468–20481.
[152] T. Xue, L. Yang, Front. Chem. 9 (2021) 751581.
[153] M. Mancinelli, A. Martucci, Sustain. Chem. 6 (2025) 9.
[154] E. Davarpanah, M. Armandi, S. Hernández, D. Fino, R. Arletti, S. Bensaid, M. Piumetti, J. Environ. Manage. 275 (2020) 111229.
[155] M.E. Davis, Acc. Chem. Res. 26 (1993) 111–115.
[156] A. Julbe, M. Drobek, in: E. Drioli, L. Giorno (Eds.), Encycl. Membr., Springer Berlin Heidelberg, Berlin, Heidelberg, 2016, pp. 2055–2056.
[157] A. Julbe, M. Drobek, in: E. Drioli, L. Giorno (Eds.), Encycl. Membr., Springer Berlin Heidelberg, Berlin, Heidelberg, 2014, pp. 1–2.
[158] D.G. Boer, Z. Asgar Pour, J. Langerak, B. Bakker, P.P. Pescarmona, Molecules 28 (2023) 2198.
[159] R. Arletti, L. Gigli, F. Di Renzo, S. Quartieri, Microporous Mesoporous Mater. 228 (2016) 248–255.
[160] F. Raganati, F. Miccio, P. Ammendola, Energy Fuels 35 (2021) 12845–12868.
[161] F.G. Cirujano, A. Nowacka, in: V. Blay, L.F. Bobadilla, A. Cabrera García (Eds.), Zeolites Met.-Org. Framew., Amsterdam University Press, 2018, pp. 289–306.
[162] D. Fu, M.E. Davis, Chem. Soc. Rev. 51 (2022) 9340–9370.
[163] S.U. Rege, R.T. Yang, Ind. Eng. Chem. Res. 36 (1997) 5358–5365.
[164] V.K. Yadav, N. Choudhary, G.K. Inwati, A. Rai, B. Singh, B. Solanki, B. Paital, D.K. Sahoo, Front. Med. 10 (2023) 1147373.
[165] A. Hedström, J. Environ. Eng. 127 (2001) 673–681.
[166] L. Velarde, M.S. Nabavi, E. Escalera, M.-L. Antti, F. Akhtar, Chemosphere 328 (2023) 138508.
[167] U. Wingenfelder, C. Hansen, G. Furrer, R. Schulin, Environ. Sci. Technol. 39 (2005) 4606–4613.
[168] N. Grifasi, M. Fornaro, M. Piumetti, B. Liguori, D. Caputo, in: Adv. Technol. Wastewater Treat., Elsevier, 2025, pp. 243–261.
[169] N. Lucas, C. Bienaime, C. Belloy, M. Queneudec, F. Silvestre, J.-E. Nava-Saucedo, Chemosphere 73 (2008) 429–442.
[170] T.P. Haider, C. Völker, J. Kramm, K. Landfester, F.R. Wurm, Angew. Chem. Int. Ed. 58 (2019) 50–62.
[171] T. Sang, C.J. Wallis, G. Hill, G.J.P. Britovsek, Eur. Polym. J. 136 (2020) 109873.
[172] J. Kim, N.S. Gupta, L.B. Bezek, J. Linn, K.K. Bejagam, S. Banerjee, J.H. Dumont, S.Y. Nam, H.W. Kang, C.H. Park, G. Pilania, C.N. Iverson, B.L. Marrone, K.-S. Lee, Int. J. Mol. Sci. 24 (2023) 7638.
[173] K.W. Meereboer, M. Misra, A.K. Mohanty, Green Chem. 22 (2020) 5519–5558.
[174] F. Kawai, T. Kawabata, M. Oda, Appl. Microbiol. Biotechnol. 103 (2019) 4253–4268.
[175] ISO 17556:2019, (2019).
[176] M. Tosin, A. Pischedda, F. Degli-Innocenti, Polym. Degrad. Stab. 166 (2019) 213–218.

[177] J.R.A. Pires, V.G.L. Souza, P. Fuciños, L. Pastrana, A.L. Fernando, Polymers 14 (2022) 1359.
[178] N. Fierer, R.B. Jackson, Proc. Natl. Acad. Sci. 103 (2006) 626–631.
[179] V. Torsvik, L. Øvreås, Curr. Opin. Microbiol. 5 (2002) 240–245.
[180] J. O'Brien, I. Wilson, T. Orton, F. Pognan, Eur. J. Biochem. 267 (2000) 5421–5426.
[181] S.N. Rampersad, Sensors 12 (2012) 12347–12360.
[182] P. Costa, A.T.P.C. Gomes, M. Braz, C. Pereira, A. Almeida, Antibiotics 10 (2021) 974.
[183] R.R.A. Silva, C.S. Marques, T.R. Arruda, S.C. Teixeira, T.V. De Oliveira, Macromol 3 (2023) 371–399.
[184] S.M. Emadian, T.T. Onay, B. Demirel, Waste Manag. 59 (2017) 526–536.
[185] A.A. Shah, F. Hasan, A. Hameed, S. Ahmed, Biotechnol. Adv. 26 (2008) 246–265.
[186] M. Shimao, H. Saimoto, N. Kato, C. Sakazawa, Appl. Environ. Microbiol. 46 (1983) 605–610.
[187] F. Kawai, X. Hu, Appl. Microbiol. Biotechnol. 84 (2009) 227–237.
[188] P.A. Withana, X. Yuan, D. Im, Y. Choi, M.S. Bank, C.S.K. Lin, S.Y. Hwang, Y.S. Ok, Environ. Sci. Process. Impacts (2025) 10.1039.D4EM00754A.
[189] T. Vaclavkova, J. Ruzicka, M. Julinova, R. Vicha, M. Koutny, Appl. Microbiol. Biotechnol. 76 (2007) 911–917.
[190] S. Matsumura, H. Kurita, H. Shimokobe, Biotechnol. Lett. 15 (1993) 749–754.
[191] A. Corti, P. Cinelli, S. D'Antone, E.-R. Kenawy, R. Solaro, Macromol. Chem. Phys. 203 (2002) 1526–1531.
[192] A. Corti, R. Solaro, E. Chiellini, Polym. Degrad. Stab. 75 (2002) 447–458.
[193] K. Qiu, A.N. Netravali, J. Polym. Environ. 21 (2013) 658–674.
[194] O. Alonso-López, S. López-Ibáñez, R. Beiras, Polymers 13 (2021) 3742.
[195] D. Byrne, G. Boeije, I. Croft, G. Hüttmann, G. Luijkx, F. Meier, Y. Parulekar, G. Stijntjes, Tenside Surfactants Deterg. 58 (2021) 88–96.
[196] U.S. EPA, US Environ. Prot. Agency (2025).
[197] ECHA, Eur. Chem. Agency (2023).
[198] Y. Zhang, Q. Wang, J. Yuan, in: Adv. Text. Biotechnol., Elsevier, 2019, pp. 21–36.
[199] H. Bian, M. Cao, H. Wen, Z. Tan, S. Jia, J. Cui, Int. J. Biol. Macromol. 124 (2019) 10–16.
[200] M. Shimao, T. Tamogami, S. Kishida, S. Harayama, Microbiology 146 (2000) 649–657.
[201] M. Ullah, H. Li, S.-W. Sun, C.-H. Weng, H. Zhang, H. Zhu, 3 Biotech 9 (2019) 350.
[202] Y. Liu, Y. Deng, P. Chen, M. Duan, X. Lin, Y. Zhang, J. Basic Microbiol. 59 (2019) 368–374.
[203] V. Marturano, P. Cerruti, V. Ambrogi, Phys. Sci. Rev. 2 (2017).
[204] P. Singh, S. Saengerlaub, A. Abas Wani, H. Langowski, Pigment Resin Technol. 41 (2012) 368–379.
[205] S.-Y. Fu, X.-Q. Feng, B. Lauke, Y.-W. Mai, Compos. Part B Eng. 39 (2008) 933–961.

[206] H.P.S. Abdul Khalil, E.W.N. Chong, F.A.T. Owolabi, M. Asniza, Y.Y. Tye, S. Rizal, M.R. Nurul Fazita, M.K. Mohamad Haafiz, Z. Nurmiati, M.T. Paridah, J. Appl. Polym. Sci. 136 (2019) 47251.
[207] V. Siracusa, Int. J. Polym. Sci. 2012 (2012) 1–11.
[208] J. Lange, Y. Wyser, Packag. Technol. Sci. 16 (2003) 149–158.
[209] Canada Plastics Pact, (2021).
[210] A.E. Giannakas, C.E. Salmas, D. Moschovas, M. Baikousi, E. Kollia, V. Tsigkou, A. Karakassides, A. Leontiou, G. Kehayias, A. Avgeropoulos, C. Proestos, Nanomaterials 12 (2022) 1843.
[211] A.S. More, C. Sen, M. Das, J. Appl. Packag. Res. 9 (2017).
[212] C. López-de-Dicastillo, G. López-Carballo, P. Vázquez, F. Schwager, A. Aragón-Gutiérrez, J.M. Alonso, P. Hernández-Muñoz, R. Gavara, Polymers 15 (2023) 3899.
[213] A. Nesic, S. Meseldzija, G. Cabrera-Barjas, A. Onjia, Foods 11 (2022) 360.
[214] S.D. Do Nascimento Sousa, R.G. Santiago, D.A. Soares Maia, E. De Oliveira Silva, R.S. Vieira, M. Bastos-Neto, Food Packag. Shelf Life 26 (2020) 100584.
[215] T.R.P. Soares, A.F. Reis, J.W.S. Dos Santos, E.G.L. Chagas, A.C. Venturini, R.G. Santiago, M. Bastos-Neto, R.S. Vieira, R.A. Carvalho, C.F. Da Silva, C.M.P. Yoshida, Food Bioprocess Technol. 16 (2023) 1101–1115.
[216] A.M. Pereyra, M.S. Moreno, C.M. Piqueras, J.A. Ávila Ramírez, Microporous Mesoporous Mater. 395 (2025) 113702.
[217] A. Coloma, F.J. Rodríguez, J.E. Bruna, A. Guarda, M.J. Galotto, J. Chil. Chem. Soc. 59 (2014) 2409–2414.
[218] J. De Bruijn, A. Gómez, C. Loyola, P. Melín, V. Solar, N. Abreu, F. Azzolina-Jury, H. Valdés, Crystals 10 (2020) 471.
[219] N. Kumar, K.R. Tiwari, Km. Meenu, A. Sharma, A. Jain, S. Singh, R. Tomar, Int. J. Nonferrous Metall. 08 (2019) 35–71.
[220] E. Oheix, T.J. Daou, L. Pieuchot, Mater. Horiz. 11 (2024) 6222–6256.
[221] L.O. De Araújo, K. Anaya, S.B.C. Pergher, Coatings 9 (2019) 786.
[222] P. Upadhyay, M. Zubair, M.S. Roopesh, A. Ullah, Polymers 16 (2024) 2007.
[223] S. Sharma, P. Sudhakara, M. Petru, J. Singh, S. Rajkumar, Nanotechnol. Rev. 11 (2022) 2366–2432.
[224] S.S. Belkhair, Antimicrobial Properties of Ag Zeolites and Ag Zeolite Containing Polymers, Manchester Metropolitan University, 2016.
[225] H. Park, H. Lim, Curr. Green Chem. 2 (2015) 354–361.
[226] V.H. Ramos-Martinez, E. Ramirez-Vargas, F.J. Medellin-Rodriguez, C.A. Ávila-Orta, C.A. Gallardo-Vega, A.B. Jasso-Salcedo, M.L. Andrade-Guel, Microporous Mesoporous Mater. 295 (2020) 109941.
[227] J. Jiang, G. Li, Q. Ding, K. Mai, Polym. Degrad. Stab. 97 (2012) 833–838.
[228] G. Zhang, Y. Xiao, J. Yan, N. Xie, R. Liu, Y. Zhang, Polymers 11 (2019) 1841.
[229] Z. Abbasi, J. Taiwan Inst. Chem. Eng. 43 (2012) 264–268.
[230] H. Ismail, N.F. Zaaba, J. Elastomers Plast. 46 (2014) 96–109.
[231] M. Jurca, M. Julinová, R. Slavik, Sci. Eng. Compos. Mater. 26 (2019) 97–103.
[232] L.M. Jurkić, I. Cepanec, S.K. Pavelić, K. Pavelić, Nutr. Metab. 10 (2013) 2.

[233] S. Kraljević Pavelić, V. Micek, A. Filošević, D. Gumbarević, P. Žurga, A. Bulog, T. Orct, Y. Yamamoto, T. Preočanin, J. Plavec, R. Peter, M. Petravić, D. Vikić-Topić, K. Pavelić, Microporous Mesoporous Mater. 249 (2017) 146–156.
[234] N. Eroglu, M. Emekci, C.G. Athanassiou, J. Sci. Food Agric. 97 (2017) 3487–3499.
[235] S.C. Hodgson, R.J. Casey, S.W. Bigger, Polym.-Plast. Technol. Eng. 41 (2002) 795–818.
[236] M. Hosseinnia, R. Alaee, P. Tabarzadi, A. Masoumi, H. Farrokhzad, A. Poorkhalil, J. Vinyl Addit. Technol. 30 (2024) 363–382.
[237] M. Fornaro, B. Liguori, V. Ambrogi, D. Caputo, Polymers 16 (2024) 3399.
[238] D. Metın, F. Tihminlioğlu, D. Balköse, S. Ülkü, Compos. Part Appl. Sci. Manuf. 35 (2004) 23–32.
[239] Kishwar Zehra, Anjum Nawab, Feroz Alam, Alina Hadi, Mohib Reza, J. Pet. Environ. Biotechnol. 13 (2022) 1000491.
[240] H. Deng, J. Su, W. Zhang, A. Khan, M.A. Sani, G. Goksen, P. Kashyap, P. Ezati, J.-W. Rhim, Int. J. Biol. Macromol. 273 (2024) 132926.
[241] A. Dirpan, A.F. Ainani, M. Djalal, Polymers 15 (2023) 2781.
[242] R. Abedi-Firoozjah, N. Chabook, O. Rostami, M. Heydari, A. Kolahdouz-Nasiri, F. Javanmardi, K. Abdolmaleki, A. Mousavi Khaneghah, Polym. Test. 118 (2023) 107903.
[243] Z.W. Abdullah, Y. Dong, Front. Mater. 6 (2019) 58.
[244] A.A. Aydın, V. Ilberg, Carbohydr. Polym. 136 (2016) 441–448.
[245] B. Sreedhar, M. Sairam, D.K. Chattopadhyay, P.A.S. Rathnam, D.V.M. Rao, J. Appl. Polym. Sci. 96 (2005) 1313–1322.
[246] B.H. Musa, N.J. Hameed, Mater. Today Proc. 20 (2020) 439–442.
[247] X.-Y. Zhou, D.-M. Jia, Y.-F. Cui, D. Xie, J. Reinf. Plast. Compos. 28 (2009) 2771–2780.
[248] N. A. Azahari, N. Othman, H. Ismail, J. Phys. Sci. 22 (2011) 15–31.
[249] K. Chi, H. Wang, J.M. Catchmark, Food Hydrocoll. 103 (2020) 105696.
[250] V. Guazzotti, S. Limbo, L. Piergiovanni, R. Fengler, D. Fiedler, L. Gruber, Food Packag. Shelf Life 3 (2015) 9–18.
[251] S. Huang, X. Wang, Y. Zhang, Y. Meng, F. Hua, X. Xia, Sci. Rep. 13 (2023) 12292.
[252] Y. Jia, T.-A. Asoh, Y.-I. Hsu, H. Uyama, Polym. Degrad. Stab. 177 (2020) 109197.
[253] Z. Guohua, L. Ya, F. Cuilan, Z. Min, Z. Caiqiong, C. Zongdao, Polym. Degrad. Stab. 91 (2006) 703–711.
[254] B.H. Stuart, Infrared Spectroscopy: Fundamentals and Applications, 1st ed., Wiley, 2004.
[255] P.R. Griffiths, J.A. De Haseth, Fourier Transform Infrared Spectrometry, 1st ed., Wiley, 2007.
[256] M. Milosevic, Appl. Spectrosc. Rev. 39 (2004) 365–384.
[257] R.M. Silverstein, F.X. Webster, D.J. Kiemle, D.L. Bryce, Spectrometric Identification of Organic Compounds, Eighth edition, Wiley, Hoboken, NJ, 2015.
[258] N.J. Harrick, Internal Reflection Spectroscopy, Interscience, New York, 1967.

[259] L. Reimer, Meas. Sci. Technol. 11 (2000) 1826–1826.
[260] H. Chen, F. Chen, H. Chen, H. Liu, L. Chen, L. Yu, Waste Manag. Res. J. Sustain. Circ. Econ. 41 (2023) 431–441.
[261] M.E. Brown, ed., Introduction to Thermal Analysis: Techniques and Applications, Kluwer Academic Publishers, Dordrecht, 2004.
[262] S. Vyazovkin, in: E.N. Kaufmann (Ed.), Charact. Mater., 1st ed., Wiley, 2012, pp. 1–12.
[263] S. Zeng, L. Li, Q. Wang, Polym. Test. 126 (2023) 108143.
[264] L. Segal, J.J. Creely, A.E. Martin, C.M. Conrad, Text. Res. J. 29 (1959) 786–794.
[265] W. Ruland, Acta Crystallogr. 14 (1961) 1180–1185.
[266] ASTM-E96, (2017).
[267] O. Braissant, M. Astasov-Frauenhoffer, T. Waltimo, G. Bonkat, Front. Microbiol. 11 (2020) 547458.
[268] J. Rousk, P.C. Brookes, E. Bååth, Soil Biol. Biochem. 42 (2010) 926–934.
[269] N. Jamil, H. Husin, A.W. Alfida, Z. Aman, Z. Hassan, Int. J. Curr. Res. Sci. Eng. Technol. 1 (2018) 578.
[270] D.M. Nerkar, V.P. Jadhav, C.T. Chakraborty, Int. J. Sci. Res. Rev. 7 (2018) 136–147.
[271] Z. Peng, L.X. Kong, Polym. Degrad. Stab. 92 (2007) 1061–1071.
[272] B.J. Holland, J.N. Hay, Polymer 42 (2001) 6775–6783.
[273] Z.A. Alhulaybi, I. Dubdub, Polymers 16 (2024) 629.
[274] T.M. Ejara, S. Balakrishnan, J.C. Kim, SPE Polym. 2 (2021) 288–296.
[275] I. Erol, Ö. Hazman, F. Yılmaz, G. Khamidov, J. Polym. Environ. 33 (2025) 2173–2192.
[276] E. Ojogbo, R. Blanchard, T. Mekonnen, J. Polym. Sci. Part Polym. Chem. 56 (2018) 2611–2622.
[277] Z. Kamaruddin, R. Jumaidin, R. Ilyas, M. Selamat, R. Alamjuri, F. Yusof, Polymers 14 (2022) 514.
[278] M. Pigłowska, B. Kurc, Ł. Rymaniak, P. Lijewski, P. Fuć, Polymers 12 (2020) 357.
[279] P. Dony, F. Berzin, Molecules 28 (2023) 4519.
[280] D. Gonçalves, L. Bozzi Barbeiro, P. Tonon De Souza, E.A. Caldas Batista, A.J. De Almeida Meirelles, J. Therm. Anal. Calorim. 147 (2022) 11857–11874.
[281] M. Almazrouei, I. Adeyemi, I. Janajreh, Biomass Convers. Biorefinery 12 (2022) 4403–4417.
[282] M.L. Castelló, J. Dweck, D.A.G. Aranda, J. Therm. Anal. Calorim. 105 (2011) 737–746.
[283] P. Azhagapillai, M. Khaleel, F. Zoghieb, G. Luckachan, L. Jacob, D. Reinalda, ACS Omega 7 (2022) 6463–6471.
[284] M.K. Król, P. Jeleń, Materials 14 (2021) 4642.
[285] Y. Youn, S. Yoon, T.W. Kim, S.K. Hong, K. Cho, J. Energy Storage 89 (2024) 111805.
[286] P. Tabero, E. Gabruś, Chem. Process Eng. New Front. (2023) 38–38.
[287] A. Lobo-Guerrero, Mater. Lett. 265 (2020) 127434.
[288] F. Rashid, S.S. Soshi, Md.A. Gafur, Mater. Sci. Appl. 15 (2024) 336–349.

[289] C. Tsioptsias, D. Fardis, X. Ntampou, I. Tsivintzelis, C. Panayiotou, Polymers 15 (2023) 1843.
[290] M. Todica, E.M. Nagy, C. Niculaescu, O. Stan, N. Cioica, C.V. Pop, J. Spectrosc. 2016 (2016) 1–6.
[291] P. Pineda-Gómez, N.C. Angel-Gil, C. Valencia-Muñoz, A. Rosales-Rivera, M.E. Rodríguez-García, Starch - Stärke 66 (2014) 691–699.
[292] K. Dome, E. Podgorbunskikh, A. Bychkov, O. Lomovsky, Polymers 12 (2020) 641.
[293] M. Paluch, J. Ostrowska, P. Tyński, W. Sadurski, M. Konkol, J. Polym. Environ. 30 (2022) 728–740.
[294] S. Wang, L. Copeland, Crit. Rev. Food Sci. Nutr. 55 (2015) 1081–1097.
[295] A.R. Sowunmi, C.O. Folayan, F.O. Anafi, O.A. Ajayi, N.O. Omisanya, D.O. Obada, D. Dodoo-Arhin, Data Brief 20 (2018) 90–95.
[296] S. Hashemian, S.H. Hosseini, H. Salehifar, K. Salari, Am. J. Anal. Chem. 04 (2013) 123–126.
[297] E. Khoramzadeh, M. Mofarahi, C.-H. Lee, J. Chem. Eng. Data 64 (2019) 5648–5664.
[298] Q. Touloumet, G. Postole, L. Massin, C. Lorentz, A. Auroux, J. Mater. Chem. A 11 (2023) 2737–2753.
[299] N.S. Alghunaim, Results Phys. 6 (2016) 456–460.
[300] I. Jipa, A. Stoica, M. Stroescu, L.-M. Dobre, T. Dobre, S. Jinga, C. Tardei, Chem. Pap. 66 (2012).
[301] J.J. Cael, J.L. Koenig, J. Blackwell, Biopolymers 14 (1975) 1885–1903.
[302] J. Pu-you, B. Cai-ying, H. Li-hong, Z. Yong-hong, J. For. Prod. Ind. 3 (2014) 151–153.
[303] C. Pozo, S. Rodríguez-Llamazares, R. Bouza, L. Barral, J. Castaño, N. Müller, I. Restrepo, J. Polym. Res. 25 (2018) 266.
[304] J.J.G. Van Soest, H. Tournois, D. De Wit, J.F.G. Vliegenthart, Carbohydr. Res. 279 (1995) 201–214.
[305] M. Król, A. Koleżyński, A. Mikuła, W. Mozgawa, in: A. Koleżyński, M. Król (Eds.), Mol. Spectrosc. Theory, Springer International Publishing, Cham, 2019, pp. 301–332.
[306] M. Król, W. Mozgawa, W. Jastrzębski, K. Barczyk, Microporous Mesoporous Mater. 156 (2012) 181–188.
[307] J.D. Monzón, M.R. Gonzalez, M. Muñoz, A.M. Pereyra, E.I. Basaldella, Clays Clay Miner. 69 (2021) 735–745.
[308] J.H. Jacobs, C.E. Deering, R. Sui, A.P. Cann, K.L. Lesage, R.A. Marriott, New J. Chem. 47 (2023) 5249–5261.
[309] A.R. Jamali, A.A. Shaikh, A. Dad Chandio, Mater. Res. Express 11 (2024) 045102.
[310] P. Boonsuk, A. Sukolrat, S. Chantarak, A. Kelarakis, C. Chaibundit, J. Appl. Polym. Sci. 139 (2022) 52362.
[311] K. Zehra, A. Nawab, F. Alam, A. Hadi, M. Raza, J. Food Process. Preserv. 46 (2022).
[312] S. Siraj, A.H. Al-Marzouqi, M.Z. Iqbal, W. Ahmed, Polymers 14 (2022) 4830.
[313] Ege University, Faculty of Engineering, L. Altay, M. Sarikanat, Ege University, Faculty of Engineering, M. Sağlam, İzmir Eğitim Sağlık Sanayi

Yatırım A.Ş., T. Uysalman, İzmir Eğitim Sağlık Sanayi Yatırım A.Ş., Y. Seki, 3Dokuz Eylul University, Faculty of Sciences, Res. Eng. Struct. Mater. (2021).
[314] A. Idris, A. Muntean, B. Mesic, J. Coat. Technol. Res. 19 (2022) 699–716.
[315] S.H. Chang, R.K. Gupta, M.E. Ryan, J. Rheol. 36 (1992) 273–287.
[316] J.F. Richardson, W.N. Zaki, Chem. Eng. Res. Des. 75 (1997) S82–S100.
[317] W.B. Russel, D.A. Saville, W.R. Schowalter, Colloidal Dispersions, 1st ed., Cambridge University Press, 1989.
[318] P. Xu, A.S. Mujumdar, B. Yu, Dry. Technol. 27 (2009) 636–652.
[319] A. Al-Harrasi, S. Bhatia, M.S. Al-Azri, S. Ullah, A. Najmi, M. Albratty, A.M. Meraya, S. Mohan, M.F. Aldawsari, Membranes 12 (2022) 862.
[320] B. Schönfeld, U. Westedt, K.G. Wagner, Int. J. Pharm. 596 (2021) 120233.
[321] Y.C. Yin, X. Sang, X.F. Xu, L.R. Ma, Y. Tian, S.Z. Wen, J.B. Luo, Microporous Mesoporous Mater. 294 (2020) 109919.
[322] S. Radoor, J. Karayil, J. Parameswaranpillai, S. Siengchin, J. Polym. Environ. 28 (2020) 2631–2643.
[323] G. Kovtun, T. Cuberes, Polymers 17 (2025) 2095.
[324] Esmat Sedaghat, Abbas Ali Rostami, Mousa Ghaemy, Ali Rostami, Int. J. Appl. Chem. 13 (2017) 855–877.
[325] A. Usman, Z. Hussain, A. Riaz, A.N. Khan, Carbohydr. Polym. 153 (2016) 592–599.
[326] Y. Kwon, S. Chaudhari, C. Kim, D. Son, J. Park, M. Moon, M. Shon, Y. Park, S. Nam, RSC Adv. 8 (2018) 20669–20678.
[327] M. Abazari, S.M. Badeleh, S. Barkhordari, S.S. Mohammed, M.M. Ahmed, M.S. Mohammed Ameen, H. Abdollahi, Heliyon 11 (2025) e43604.
[328] S. Gupta, A.K. Pramanik, A. Kailath, T. Mishra, A. Guha, S. Nayar, A. Sinha, Colloids Surf. B Biointerfaces 74 (2009) 186–190.
[329] P.A. Sreekumar, M.A. Al-Harthi, S.K. De, J. Appl. Polym. Sci. 123 (2012) 135–142.
[330] S. Naderizadeh, A. Shakeri, H. Mahdavi, N. Nikfarjam, N. Taheri Qazvini, Starch - Stärke 71 (2019) 1800027.
[331] A. Bozdoğan, J. Appl. Polym. Sci. 142 (2025) e56405.
[332] Z. Lv, K. Wang, Z. Qiao, W. Wang, Mater. Des. 31 (2010) 3804–3809.
[333] N. Jain, V.K. Singh, S. Chauhan, J. Mech. Behav. Mater. 26 (2017) 213–222.
[334] G.-X. Zou, P.-Q. Jin, L.-Z. Xin, J. Elastomers Plast. 40 (2008) 303–316.
[335] B.A. Omoike, F.E. Okieimen, C. Imoisi, Trends Appl. Sci. Res. 19 (2024) 225–232.
[336] M. Hedenqvist, Prog. Polym. Sci. 21 (1996) 299–333.
[337] H.M.C. De Azeredo, L.H. Capparelli Mattoso, T. Habig, in: B. Reddy (Ed.), Adv. Diverse Ind. Appl. Nanocomposites, InTech, 2011.
[338] D. Adame, G. Beall, Appl. Clay Sci. 42 (2009) 545–552.
[339] T. Ishigaki, Y. Kawagoshi, M. Ike, M. Fujita, World J. Microbiol. Biotechnol. 15 (1999) 321–327.
[340] H. Sun, T. Lei, X. Guo, J. Liu, X. Sun, J. Ma, Pol. J. Environ. Stud. 33 (2024) 4355–4364.
[341] P. Boonsuk, A. Sukolrat, K. Kaewtatip, S. Chantarak, A. Kelarakis, C. Chaibundit, J. Appl. Polym. Sci. 137 (2020) 48848.

[342] N. Laothamteep, K. Naloka, O. Pinyakong, Environ. Pollut. 292 (2022) 118309.
[343] M. Mondal, B. Biswas, S. Garai, S. Sarkar, H. Banerjee, K. Brahmachari, P.K. Bandyopadhyay, S. Maitra, M. Brestic, M. Skalicky, P. Ondrisik, A. Hossain, Agronomy 11 (2021) 448.